The Feasibility of Acoustic Emission as a Proof Test Method for Silicon Carbide Tubes

by

Brent William Wenger, B.S.C.E.

Thesis

Presented to the Faculty of the Graduate School of

The University of Texas at Austin

in Partial Fulfillment

of the Requirements

for the Degree of

Master of Science in Engineering

The University of Texas at Austin

May 2000

The Feasibility of Acoustic Emission as a Proof Test Method for Silicon Carbide Tubes

Approved by
Supervising Committee:

Timothy J. Fowler

Michael D. Engelhardt

Dedication

To my parents, Gregory and Jane, and my brother, Bryan, for their constant love and support, and for shaping the way I live.

To my grandparents, William and Alice Chase, and Walter and Ruth Wenger, for always being such a big part of my life

Acknowledgements

I would like to express my sincere thanks to my supervisor, Dr. Timothy J. Fowler, for his guidance and for giving me the opportunity to work on this project. His knowledge and assistance were instrumental to this research. I would also like to thank Dr. Michael D. Engelhardt for his suggestions.

This project would not have been possible without the funding provided by MEMC. I would like to express my appreciation to Mr. Dick Williams and Dr. Jameel Ibrahim and their associates at MEMC for their technical support and helpful contributions. For donating their time and efforts in machining ceramic parts used for this research, my thanks goes to Mr. Peter Mangan and his staff at LTD Ceramics. Mr. Russell Austin's assistance with the literature search at Texas Research Institute is also appreciated.

Thanks to the Ferguson Laboratory staff for all of their help with many of the finer details related to this work. A special thanks goes to Wayne Fontenot for fabricating two of the test frames that were essential for the test program.

For opening me up to your diverse backgrounds, my sincere thanks goes to all of my friends in the Structural Engineering Department. Your friendship and the times that we shared will always be remembered. Most of all, I would like to thank my family for their support and encouragement. I truly feel lucky to be part of such a wonderful group of loving people.

May 5, 2000

Abstract

The Feasibility of Acoustic Emission as a Proof Test Method for Silicon Carbide Tubes

Brent William Wenger, M.S.E.

The University of Texas at Austin, 2000

Co-Supervisors: Timothy J. Fowler
Michael D. Engelhardt

The feasibility of using acoustic emission as a nondestructive method for proof testing silicon carbide tubes was investigated. Silicon carbide maintains its structural integrity at very high temperatures making it a very beneficial material for certain applications. However, this material has inherent flaws in its microstructure and is very brittle. Therefore, the prospect of determining in a nondestructive manner which tubes are excessively flawed is very attractive.

Various specimen sizes and shapes were tested under different loading conditions for this research. The following conclusions were made based on these experiments and a comprehensive literature search. Additional research and development work to establish an acoustic emission based proof test for silicon carbide tubes is not recommended. Acoustic emission can identify the development or growth of a new crack, but does not necessarily detect the presence of an existing one. However, acoustic emission monitoring of SiC can be a valuable tool in understanding the response of the material to applied stress.

Table of Contents

List of Tables

List of Figures

List of Illustrations

Chapter 1: Introduction

Silicon carbide (SiC) is used in the electronics industry because it retains its structural integrity, is chemically stable at high temperatures, and can withstand radical temperature transients. Figure 1.1 below displays a tube made of SiC. In actual service, the inside of the tube is regularly heated to temperatures of near 2000° F, while the outside is at significantly lower temperatures. The thermal gradient and thermal shock created by this process imparts very high stresses on the tubes. Although SiC has been the material of choice for this type of application, it is very susceptible to brittle fracture and has inherent flaws in its microstructure resulting from its production. The amount, size, and distribution

(a) (b)

Figure 1.1 An example of a silicon carbide tube (a) side view (b) looking at the cross-section

of these flaws can cause a wide variation of properties within a batch of silicon carbide. The possibility of having structurally significant flaws within a specimen, along with the brittle nature of the material, can cause some tubes to fail unexpectedly either at stress levels below that which they are expected to handle or after only very short service lives. Failure of these tubes is extremely costly due to resulting equipment repairs and the accompanying loss of production.

In recent years there has been a tremendous effort not only to improve the material properties of SiC, but to also improve the consistency of those properties within a batch of SiC components. These efforts have realized a reasonable amount of success, however, SiC specimen will always have a range of properties. The prospect of being able to distinguish, in a noninvasive manner, which tubes have poor mechanical properties and or those that are excessively flawed is very attractive.

The primary goal of this research is to evaluate acoustic emission testing methods as a potential proof test for silicon carbide tubes. This test could possibly be used to establish the adequacy of a particular tube for the anticipated service load conditions. Acoustic emission is defined as the "phenomenon whereby transient elastic waves are generated by the rapid release of energy from localized sources within a material" (ASTM 1993). AE is a global test that has had proven success in the testing of tanks, railroad tank cars, and pressure vessels made of steel and fiber-reinforced plastics (FRP). The theory behind acoustic emission

and how it can be used for SiC and similar materials will be presented in much more detail in Chapter 2.

By conducting a series of mechanical tests on SiC samples while monitoring for acoustic emission data, comparisons between the AE data resulting from “good” silicon carbide components and that resulting from “bad” ones will be investigated. The condition of each component is determined through inspections of the sample both before the test and after failure, as well as evaluating that maximum load and stress required to cause that specimen to fail.

If there are any differences observed in the AE parameters from those specimens that are considered to be in poor condition, they will be used to establish evaluation criteria for testing SiC tubes of unknown condition. These criteria would be used to determine the condition of each individual tube in the proof test and ultimately detect those tubes that may not perform up to the expected standards. During the proposed proof test, the SiC tubes would only be stressed to a level that is below the maximum that they endure during normal use. The results, analysis, and conclusions from the tests used to try to establish the evaluation criteria are presented in the following chapters.

Chapter 2: Acoustic Emission and Its Application to Ceramic Materials

2.1 ACOUSTIC EMISSION

Acoustic emission (AE) is a well-established nondestructive testing method that has been in existence for many years. AE is defined in Chapter 1 as a localized release of energy that causes elastic waves to radiate outward within the body of the specimen being stressed. The localized sources can be a wide variety of phenomena such as crack initiation and growth, and yielding or plastic deformation in metals. Also, delamination, fiber debonding, and fiber breakage can be sources in fiber-reinforced plastics. The elastic waves from these sources travel throughout the body of the material and can be detected by the use of sensors attached to the body's surface. The sensor contains a piezoelectric crystal that can detect a change in pressure along its face caused by the elastic wave and then converts that pressure change into a voltage signal.

2.1.1 Detailed Explanation and Successful Applications of Acoustic Emission

Acoustic emission has been used effectively to either study the failure mechanics and process of a material or to detect the presence of defects within a structure. The material must be stressed to a certain level in order to create the mechanism (yielding, crack growth, etc.) that causes the emission. Since these mechanisms are essentially damage within the structure, there are those who say

that AE is not a nondestructive method. However, in AE tests, the specimen is stressed only to its service load level. An AE test on a structure in good condition will not produce any emission and thus no damage. Generally, any damage that is detected is miniscule and microscopic in scale rather that macroscopic.

Up to this point, AE has been used primarily on two classes of materials: metals and fiber-reinforced plastics (FRP). This is because the behaviors of these materials lend themselves well to acoustic emission testing. For AE to be effective, it is desired that any defects in a material generate significant emission at relatively low stress levels. In metals, emission is generated from local yielding at crack tips or other stress concentrations while the rest of the body of the sample is at a stress level well below yielding. AE testing can be used effectively for FRP because of the many mechanisms that can generate emission in this material such as matrix cracking, fiber pullout, delamination, and fiber breakage. These types of damage can be distinguished from each other by close examination of the properties of the AE data. Therefore, the condition of an FRP specimen can be accurately estimated. If little or no emission is generated, then the specimen is known to be in good condition. If a significant amount of emission occurs, then the data can be analyzed to determine which mechanisms are occurring and how far along in the failure process the sample has progressed.

For the most part, acoustic emission has had its greatest use by the chemical, petroleum, and process industries. These industries use AE to test and inspect pressure vessels, tanks, and railroad tank cars. Organizations that work with these industries have created and published standards for testing by acoustic

emission. The Association of American Railroads Procedure for Acoustic Emission Evaluation of Tank Cars and IM101 Tanks (AAR 1999), the American Society for Nondestructive Testing CARP Recommended Practice for AE Evaluation of FRP Tanks and Pressure Vessels (ASNT 1999), and Article 12 of Section V of the American Society of Mechanical Engineers Code (ASME 1998) are all examples of standard procedures for using AE in various applications. There has been a great deal of research into using AE in a variety of other applications including civil uses such as bridges, cranes, and even man-lifts. The following sections will present in detail what acoustic emission is and how it is detected and analyzed.

2.1.2 Wave Propagation and Attenuation

Once the AE stress wave is emitted from a source, it radiates in a spherical pattern within the body of the specimen being tested. At this point, the emission consists of P-waves and S-waves and loses energy at a rate of the distance it has traveled squared (Lenain 1979). Actually the energy is not really lost at this stage, but the wave is spread out as it emanates from the source. After some time, the wave reaches the surface of the body and is converted to a surface wave. If the structure being tested is a plate, then the surface wave usually takes the form of a Lamb wave. After the wave has traveled through or along a body for some time, it loses energy and amplitude. This loss in energy is usually referred to as attenuation of the signal and is caused by absorption, geometric factors, and scattering. The factors that affect the amount of attenuation are not only the

material microstructure and thickness, but also how the specimen is supported and whether or not there are any surface coatings (Bray and Stanley 1997). Higher frequency components of the wave are more attenuated than the lower frequency ones. Therefore, as the wave travels, the higher frequency components die out and the wave spreads out (lower frequencies dominate). Understanding the basic behavior of wave propagation and attenuation is important. These factors affect the location and spacing of sensors on a structure for a particular test and also should be considered in the analysis of the data after the test.

2.1.3 Acoustic Emission Sensors and Detection of the Stress Wave

Piezoelectric sensors that are attached to the surface of a body are used to detect the stress waves as they move past the sensor. A piezoelectric crystal within the sensors converts a change in pressure on its surface, which is caused by the AE stress waves, into a high impedance electric signal. The electric signal is recorded and then analyzed for its significance. These sensors have the ability to detect particle motion that is both perpendicular and parallel to the surface that the sensor is attached to. However, the sensors are more sensitive to the motion that is perpendicular to the plate. In other words, for an equal amount of movement parallel and perpendicular to the surface, the perpendicular movement will generate larger signal amplitudes.

These sensors can be manufactured such that they are broadband or are resonant at a particular frequency. Using a broadband sensor ensures that the entire AE signal will be recorded, however sensitivity to the signals is lost

because a broadband sensor is basically just a resonant sensor that is heavily damped. Therefore, resonant sensors are desired for sensitivity reasons and the problem then becomes deciding what resonant frequency should be used. As mentioned previously, the higher frequencies are attenuated more. Therefore, as low a frequency as possible should be employed. However, the low frequency sensors are very susceptible to background noise, including air born noises if the frequency is too low. Therefore, the frequency is chosen so that it is as low as possible, but still just above the background noise level. For most of the process industry structures (tanks, vessels, etc.), it has been found that a 150 kHz resonant sensor works well. For aircraft, which have a great deal of wind and engine noise, a 300 kHz sensor is chosen. In concrete structures, there is a great deal of damping of the background noise within the structure itself, so a 60 kHz sensor can be used. The most common sensors are resonant at 150 kHz.

Figure 2.1 shows a diagram of a typical sensor. The sensor is connected to the surface of the specimen that is being tested with a couplant in order to ensure good contact between the sensor face and the body's surface. The couplant is usually either vacuum grease or hot melt glue. If vacuum grease is used, duct tape, rubber bands, or a mechanical hold-down device are used to attach the sensor. These sensors typically have a wear plate at their base to protect the piezoelectric crystal and to transmit the pressure. Behind the wear plate is the crystal, to which the electrodes that create the electric signal are attached. Damping material is placed behind the crystal, which is used to prevent it from ringing continuously. An internal pre-amplifier is also housed within some

sensors. The preamplifier usually adds 40 dB gain to the signal. Other sensors have an external pre-amplifier, which tend to be more susceptible to electromagnetic interference than the internal ones. Sensors are manufactured in many different shapes and sizes in order to accommodate different sized specimen and testing geometries.

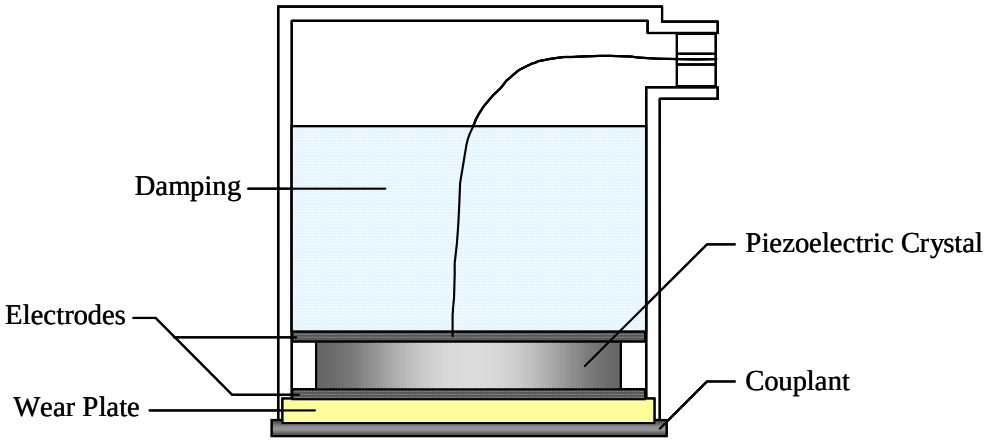

Figure 2.1 Cross-section of a typical sensor

2.1.4 Recording the Data

After the sensor generates the electric signal of the acoustic emission, that signal is amplified in a pre-amplifier near the sensor. This amplification assists in transferring the signal over long distances. As mentioned in the previous section, this pre-amplifier can be either inside of the sensor or external to it. A filter is usually included with the pre-amplifier. The filter helps to eliminate unwanted noise and allows for the choice of a frequency range to work within.

Filters typically allow only frequencies somewhere between 20 kHz and 1 MHz, but are made with many different ranges within that larger span. After the AE signal passes through the filter, it is usually taken to an acoustic emission data acquisition instrument. Within this system, the signal is amplified further up to 100 dB, but a typical amplification is 23 dB. The data acquisition instrument can be programmed to record various characteristics of the AE signal itself. The signal parameters that usually recorded are explained in the following section.

2.1.5 The Acoustic Emission Signal and Its Parameters

Figure 2.2 is a diagram of a typical acoustic emission signal output from a resonant sensor. The parameters that are shown in the figure are defined below. These definitions are as printed in ASTM E 1316 – 93b-Standard Terminology for Nondestructive Examinations (ASTM 1993).

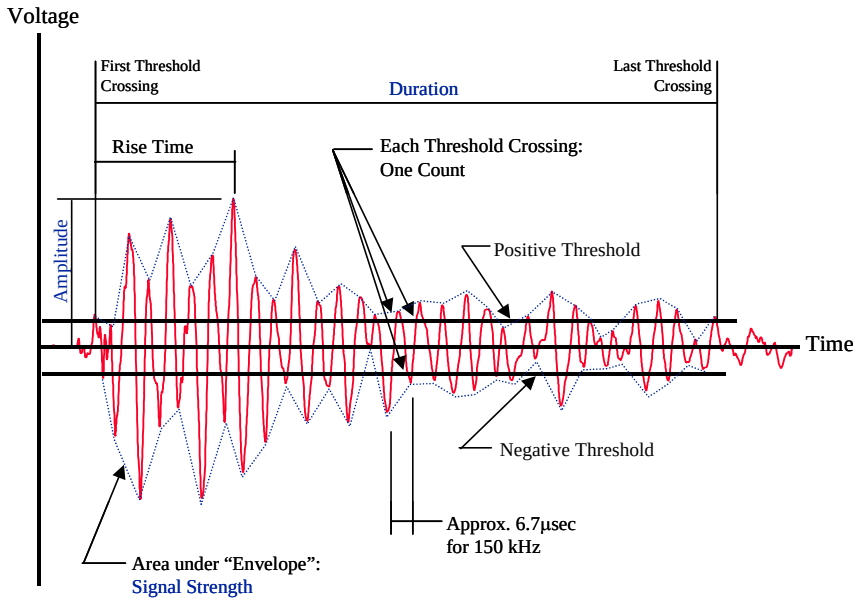

Figure 2.2 A typical acoustic emission hit and the measured parameters

Threshold – a threshold value used for analysis of the examination data.

Peak Amplitude – the peak voltage of the largest excursion attained by the signal waveform from an emission event.

Duration – the time between AE signal start and AE signal end.

Counts – the number of times the acoustic emission signal exceeds a preset threshold during any selected portion of a test.

Rise Time – the time between AE signal start and the peak amplitude of that AE signal.

Hit – any signal that exceeds the threshold and causes a system channel to accumulate data

Two important terms that are not defined by ASTM are signal strength and MARSE. Signal strength is defined in the draft version of the American Society

for Nondestructive Testing Recommended Practice for AE Evaluation of FRP Tanks and Pressure Vessels (ASNT 1999). The definition of MARSE can be found in the ASME Code, Section V, Article 12 (ASME 1998).

Signal Strength – The area under the envelope of the linear voltage time signal from the sensor.

MARSE – a measurement of the area under the envelope of the rectified linear voltage time signal from the sensor.

The MARSE is a special case of the signal strength of a hit and is what was measured during this research. The MARSE value will be referred to as the signal strength for the remainder of this paper.

No data is recorded in the AE data acquisition instrument until the signal crosses the threshold. The threshold is used to define a significant AE signal, which should be recorded. After the threshold is crossed, the instrument begins recording data. This marks the beginning of an AE hit. The hit ends at the last threshold crossing before a period of time during which the threshold is not crossed again. This time period is referred to as the Hit Definition Time (HDT) and is usually about 400 microseconds. After there are no threshold crossings and the HDT is over, there is a time period called the Rearm Time in which the computer clears itself, does not record any data, and prepares for the next hit. The rearm time is usually 200 microseconds. The AE signal is therefore set off as a

series of hits and the parameters defined above are recorded for each individual hit.

2.2 AE DATA ANALYSIS AND PRESENTATION

A tremendous amount of data is usually generated during an AE examination of a structure. Thousands of hits will often be recorded and each hit has numerous characteristics associated with it. There are many different graphs that can be used to assist with the AE data analysis. Once experience with a particular material and specimen type is gained, an understanding of the plots that are most useful for that test will be achieved. This section will present some of the more common ways of analyzing and presenting AE data.

2.2.1 Correlation Plots for Data Quality Analysis

One of the first matters to be accomplished after a test is to check the quality of the emission data. Through the examination of the emission signal parameters, an interpretation of the genuineness and relevance of a hit may be made. Sometimes emission from background noise or other nonstructural sources is recorded during a test. Filtering of the spurious, non-genuine emission can be conducted to prevent it from altering the test results. More information regarding data quality analysis can be obtained by referring to Chapter 12 of the ASNT CARP Procedure (ASNT 1999).

One of the ways to inspect the quality of the data is through the use of correlation plots. The most commonly used correlation plot is the log duration versus amplitude graph. An example of one of these plots is shown in Figure 2.3. The data shown is this graph is from an actual test on a short cylinder of SiC that was stressed by applying internal pressure. This test was completed for this research and is discussed in detail later in Chapter 5.

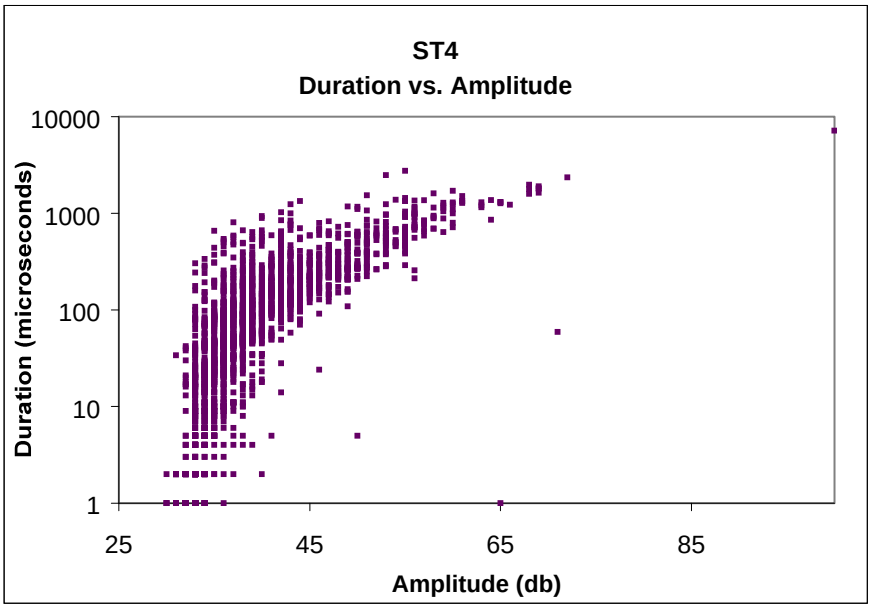

Figure 2.3 Typical log duration versus amplitude plot

What is desired from this plot is that all hits fit within a good band as shown in the figure and there are not many hits outside of the band. Graphing this information helps to distinguish events that may not have been caused by material changes in the specimen being tested. Mechanical rubbing or sliding and

electromagnetic interference (EMI) are events that cause unwanted noise that can be detected using this plot. Mechanical rubbing produces hits of very long duration with low amplitudes, while EMI causes hits of extremely short duration with high amplitude. These hits will lie outside of the normal band in the log duration versus amplitude plot. A similar graph that can be used in the same manner is the signal strength versus amplitude plot. Some of the time history plots, discussed in the next section, are also used to judge the data quality.

2.2.2 Time History Plots

One of the primary time history plots used for AE data analysis is cumulative signal strength versus time. An increase in the slope of this plot signifies that the damage has started to increase more rapidly and is often referred to as the "knee" in the curve. This slope increase usually acts as a warning of failure as additional load is applied. Figure 2.4 shows a representative cumulative signal strength versus time plot and also shows the increasing slope of the curve as failure is approached. The data in this plot comes a C-ring sample of SiC tested under a compressive force at the top and bottom of the specimen. These tests are described further in Chapter 4. Depending on what loading schedule is used, the same information may also be obtained by plotting the cumulative signal strength versus load or strain instead of time.

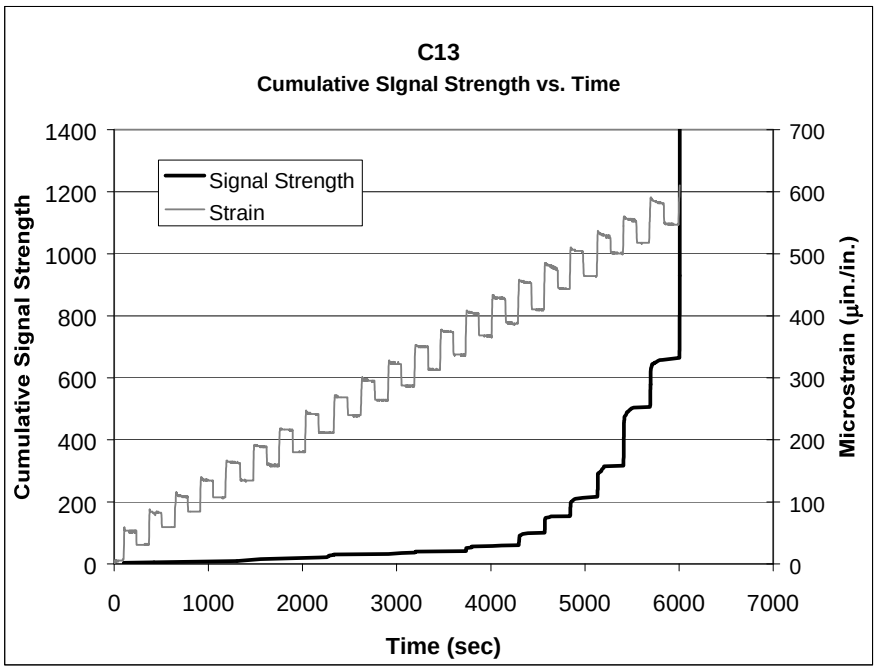

Figure 2.4 Typical cumulative signal strength versus time graph

Other time history plots include graphing the values of the amplitude, signal strength, or duration, of each individual hit against time. An example of one of these graphs from another C-ring test is shown in Figure 2.5. These plots are used to find trends such as increasing amplitude or signal strength as the specimen approaches failure or to locate when high values of these parameters took place. They can also be used to judge the quality of the data and to look for spurious groups of hits that do not belong. Seeing significant amounts of emission during load holds is also very important. Load hold emission indicates that damage is taking place under constant load, which usually signifies the specimen is under distress.

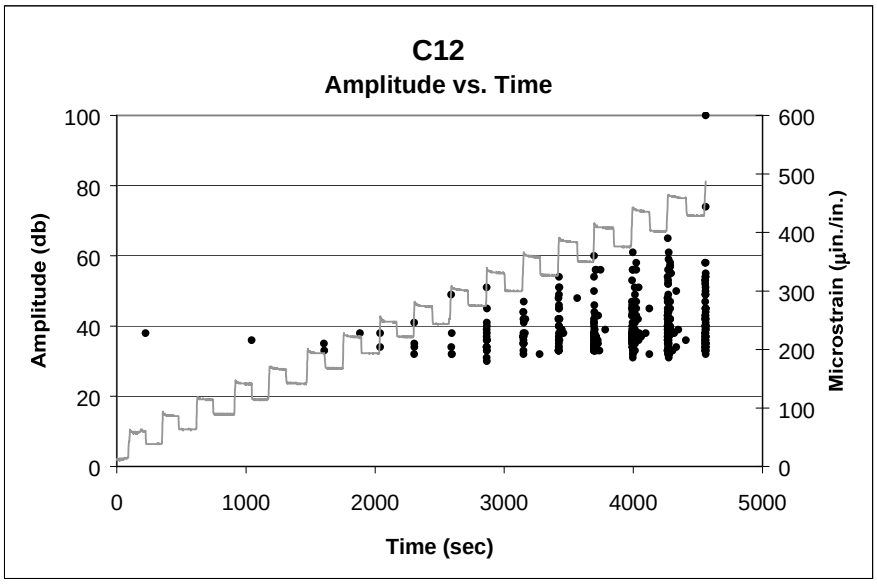

Figure 2.5 Typical amplitude versus time graph

2.2.3 Kaiser and Felicity Effects

A very important theory in acoustic emission testing is that emission should not occur up to the previous maximum stress. This idea is called the Kaiser Effect and it holds true as long as the structure is in good condition and not damaged. The breakdown of the Kaiser Effect is when a significant amount of emission occurs at a stress that is lower than the specimen has seen recently. This is called the Felicity Effect. It signifies that a previous loading did enough damage such that more damage is taking place at a lower load during the current test. The Felicity Ratio is calculated by dividing the load or strain at which significant emission occurs during the present loading by the previous maximum

load or strain that the specimen has undergone recently. Observing the Felicity Effect or a Felicity Ratio of less than one is usually a very good indicator that the structure is significantly defected or damaged. The Kaiser and Felicity Effects can be studied in a test using many different types of plots. One common way is to plot cumulative signal strength versus load or strain for a test that includes unloads and reloads. Figure 2.6 below is an example of one of those graphs.

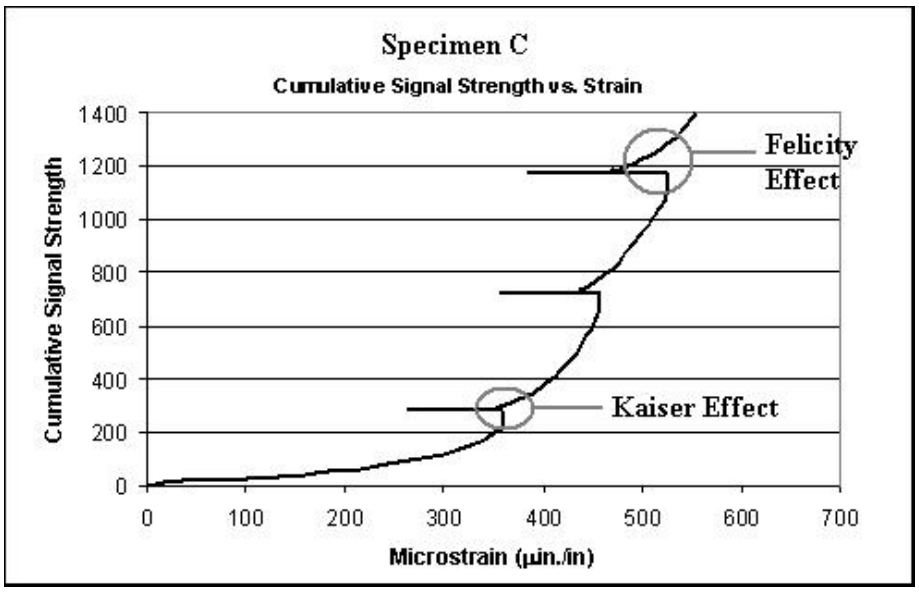

Figure 2.6 Kaiser and Felicity Effects displayed in a cumulative signal strength versus strain graph

While the Kaiser effect is still holding true, little increase in the emission will be seen until the previous maximum load or strain is surpassed. Once damage has occurred, the cumulative signal strength will increase significantly at a load or strain below the previous maximum (the Felicity Effect) and a "gap" opens up in the plot. For tests utilizing multiple load steps, the reload emission can be plotted

for each load step on a bar chart. The load step when a significant amount of reload emission occurs can then be detected and this will also indicate the Felicity Effect.

2.2.4 Intensity Analysis

There is one final method that is often used to study and analyze AE data and it is called intensity analysis. Intensity is a combination of two indicators called the historic index and the severity. Historic index compares the energy of the most recent hits to all of the previous hits of the test. Severity is the average of the signal strength of the ten largest signal strength hits of a test (Fowler et al. 1989). The significance of these values is very empirical and specific to each test. They are judged in relation to results from previous similar tests. A zonal intensity plot of the historic index and the severity values can be created, which is based on earlier recorded results. The zonal intensity plot will rate the significance of the test results and provide insight as to the condition of the structure being tested. Figure 2.7 shows an example of a zonal intensity plot used for metal pressure vessels.

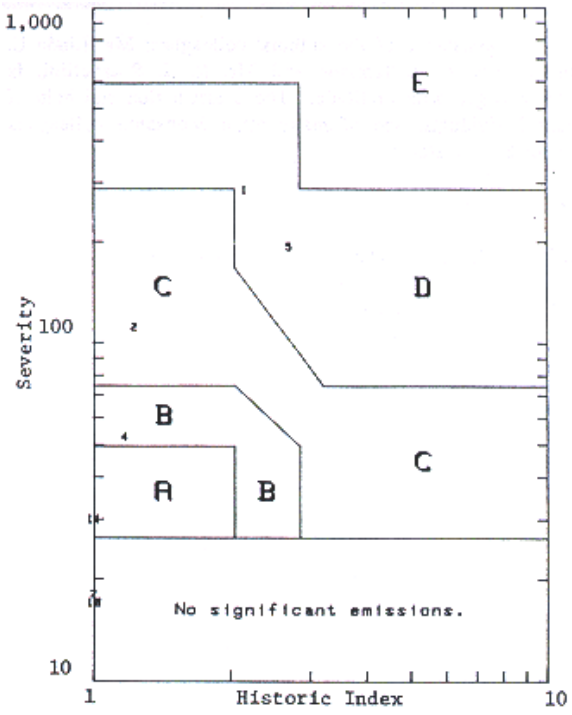

Zone Intensity	Recommended Action
A	Minor defect, note for reference in future tests.
B	Note for reference in future tests and check for surface defects such as corrosion, pitting, gouges and cracked attachment welds.
C	Defects requiring immediate follow-up inspection. Evaluation may be based on further data analysis, retest, or complimentary nondestructive examination.
D	Significant defects requiring immediate follow-up inspection using complimentary nondestructive examination.methods.
E.	Major defect requiring immediate shutdown and follow-up nondestructive examination.

Figure 2.7 A zonal intensity plot for metal vessels (Fowler et al. 1989)

2.3 LITERATURE REVIEW ON ACOUSTIC EMISSION TESTING OF CERAMICS

A search for any literature related to acoustic emission testing of silicon carbide or even similar ceramic materials was undertaken at the beginning of this project. The main goals of the literature search were to become familiar with any acoustic emission testing of ceramics, including the latest advances, and to determine who is working in this field and why. Any helpful studies and information obtained in this search would then be used to aid this research program.

The primary search was carried out at the Nondestructive Testing Information Analysis Center (NTIAC), which is a Department of Defense center operated by Texas Research Institute. NTIAC is the most extensive nondestructive test database in the world. It contains references from overseas and from many of the smaller conferences. In addition, it includes an English translation of many of the papers from foreign sources. A keyword search of this large database yielded 115 papers. Based on the abstracts, about 25 of them were relevant to this project. As many of these articles as could be found, were then obtained and read. Additional searches were carried out at the engineering libraries of the University of Texas at Austin and the University of Wisconsin – Madison. These searches provided some additional information to supplement the NTIAC search. The important aspects of the literature, as it relates to this research program, are summarized in the following sections.

2.4 ACOUSTIC EMISSION TESTING OF CERAMICS

As was discussed earlier, acoustic emission testing has been applied mostly to metals and FRP because there is a need and an economic benefit from it and the behaviors of these materials are conducive to it. In this research, the application of AE testing to defect detection and existing strength determination in ceramics (especially silicon carbide) will be studied. Although there are differences and variations in the characteristics among the different types of ceramics or even within a single type of ceramic, related information from any type of ceramic was studied. This was done because all ceramics are brittle materials and understanding the AE patterns and microfracture processes for one type of ceramic can provide good insight for the behavior in other types. Also, there has not been a great deal of work done in this area, so any information is helpful.

AE for brittle materials, in general, is difficult because there is no plastic zone to be detected as in steel or the large number of easily detectable mechanisms as in FRP. The failure of brittle materials essentially comes from the initiation of a crack and then propagation of that crack to complete fracture. Therefore, AE for brittle materials is basically centered on microcracking and cracking. The AE mechanisms that could possibly be detected in brittle materials are microcrack initiation and propagation, maincrack formation, crack closure/rubbing, and crushing of pores. The key to using acoustic emission successfully for ceramics will depend on whether or not the microcracking and coalescence can be detected as a warning of a crack before it extends to cause

failure. Also, whether or not there is a difference in the acoustic emission patterns from a specimen that is significantly flawed compared to one that is not is very important to using AE effectively for ceramics.

2.4.1 Understanding the Microfracture Process of Ceramics using AE

Extensive testing and statistics (such as the Weibull distribution) have traditionally been used to determine the strength and reliability of ceramic structures. Although this method has been successful, it really neglects the fracture process that leads to failure in this material. Understanding the microfracture process is the key to understanding if and how acoustic emission testing could be applied to improve the reliability assessment of ceramic structures (Wakayama et al. 1990). Four-point bending tests with AE monitoring of small alumina beams were carried out by Wakayama et al in order to try to gain better information regarding the microfracture process of this material. The specimens were 3 x 3 x 40 mm, 4 x 4 x 40 mm, or 5 x 5 x 40 mm with a span between supports of 24 mm and an 8 mm constant moment region. The tests were carried out on a loading machine at a constant strain rate of 4×10^{-6} /sec. A sensor was used at each end of the specimen and a Physical Acoustics Corporation (PAC) LOCAN instrument measured the AE signals with various threshold values.

The researchers used the dye penetrant method to observe microcracking and coalescence, so those phenomena could be related to the acoustic emission results. It was concluded from these tests that there is a critical stress value, σ_c, at

which the rate of emission increases rapidly. Figure 2.8 shows the results of some of the four-point bending test with different thresholds and an increase in AE can be observed at the same stress level (σ_c) for each. The value of σ_c appears to be a second knee in the cumulative signal strength plot. An initial knee occurs in these tests at a stress of approximately 20-30 MPa. This graph shows a similar AE pattern as was shown in Figure 2.4

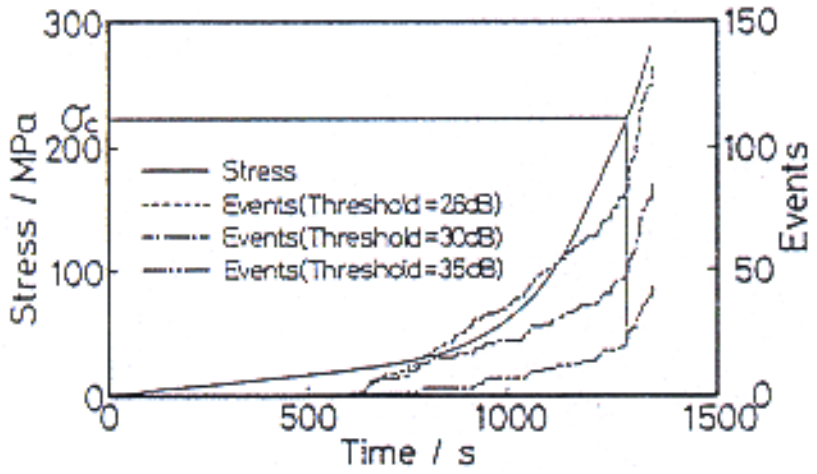

Figure 2.8 AE data showing σ_c is independent of threshold (Wakayama et al. 1990)

The initial knee or onset of the emission that occurs much earlier in the test seems to be somewhat threshold dependant. This emission is probably due to microcracking. The value of σ_c is claimed to be independent of the threshold and through observations with the fluorescent dye penetrant is shown to correlate well with the coalescence of a microcrack into a maincrack. Beyond σ_c, emission

occurs rapidly and the specimen is on its way to failure. A qualitative view of what is happening in the specimen is shown in Figure 2.9.

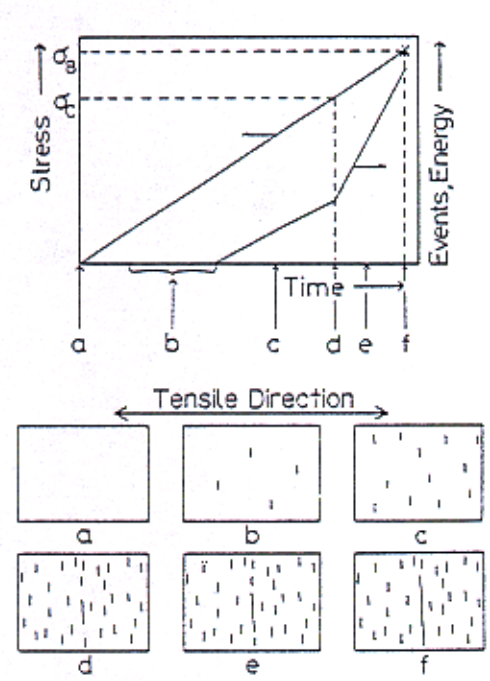

Figure 2.9 Failure process of alumina and related AE pattern (Wakayama et al. 1990)

During the time interval (b) in Figure 2.9, the AE from a small amount of microcracking is detected in the sample. The initial knee shown in the cumulative signal strength plots correlates with time (c), in which significant microcracking is occurring. The change in the slope of the AE curve at point (d) is caused by the microcracks coming together to form a larger crack, as was stated. The failure stress is defined as σ_B in the figure and the time between σ_c and σ_B is probably very short. In other words, once the specimen reaches σ_c it is in a critical state and on its way to failure. The key to using AE from this information is what can

be detected before the value of σ_c is reached. Detecting the microcracking may serve as a warning of failure. The factor that is missing in this research is the effect of the initial flaw size. If the specimen is already essentially at point (d) before the test because of an initial defect, it is important to determine what the AE pattern would be like early in the test.

2.4.2 Investigating the AE Results from a Known Defect Size in Ceramics

Knowing the initial flaw size of a specimen would be very beneficial so that comparison in the AE patterns from specimens with varying initial flaw sizes could be made. One way to achieve that is to impart an artificial flaw into the specimen before testing. Mori et al (1988) did that for four-point bending tests of hot-pressed Si_3N_4 bars. The bars were 3 x 4 x 40 mm and the types of flaws that were induced are shown in Figure 2.10. These flaws included a perpendicular slit made with a diamond cutter, Knoop indentations from a hardness tester, and internal defects of a wire or ball made of Tungsten. These specimens were tested in a loading frame with a constant crosshead speed of 0.1 mm/min to 0.5 mm/min. The supports and the loading configuration in the test provided a 30 mm span and a 10 mm constant moment region. The acoustic emission equipment consisted of two PAC Pico sensors, which are resonant at 500 kHz and a PAC model 3400 AE data acquisition instrument. A threshold of 100 μV at the sensor output was chosen and a total gain of 90 dB was applied to the signals.

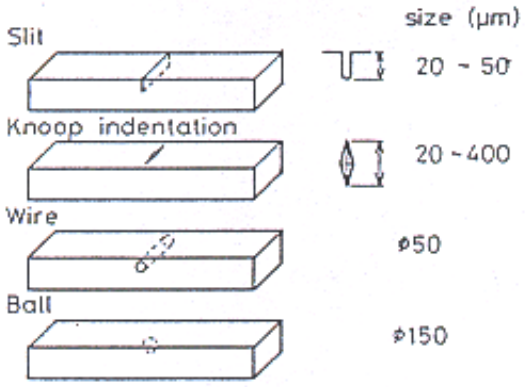

Figure 2.10 Artificial flaws induced for Si_3N_4 tests (Mori et al. 1988)

The results of the tests yield two types of behavior for the acoustic emission. The specimens that are grouped in Type A in Figure 2.11 only had emission right as the failure occurred (σ_B is the failure stress in the graph). The onset of emission, σ_{AE}, for specimens of Type B occurred at a stress of 50% or below of the final failure stress. The solid circles are those specimens that failed at the artificial flaw location and the open circles are those that did not. It appears as though the specimens that did not fail at the induced flaw or that had small initial flaws fall mostly within category B.

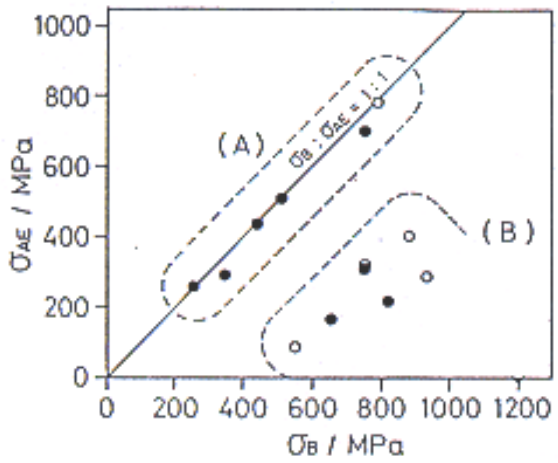

Figure 2.11 Onset of AE stress versus failure stress showing two different behaviors (Mori et al. 1988)

Figure 2.12 shows a plot of the ratio of the stress at the onset of AE (σ_{AE}) to the failure stress (σ_B) against the equivalent crack length. The distinction for the two categories of AE behavior lies at an equivalent crack length of 25 μm. The specimens that had the early acoustic emission (Type B emission) contained equivalent cracks less than 25 μm. The early emission was due to microscopic fracture events including the interaction and coalescence of microscopic inherent flaws. Also of interest was that the fracture surfaces of those specimens that fell under category A were very smooth while the fracture surfaces for category B specimens were quite rough.

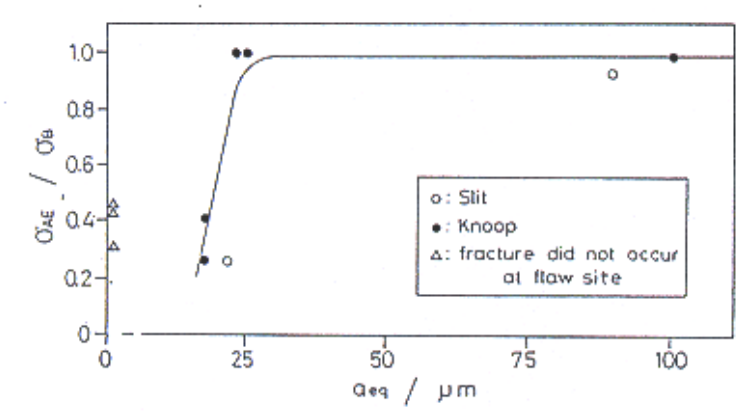

Figure 2.12 Ratio of onset of AE stress to failure stress versus equivalent crack length (Mori et al. 1988)

The results of these tests are somewhat discouraging in that acoustic emission could not predict the failure of the specimens with the larger flaws. On the other hand, the microscopic fractures in the specimens with small initial flaws were detected. It should also be noted that the critical value of 25 μm that was determined in these tests is very specific to the specimen size and the method of loading.

Shinke et al (1988) achieved similar results on three-point bending tests of sintered alumina with artificial defects. Their specimens were 10 x 25 x 100 mm bars that spanned 90 mm in the test frame. A loading frame was used to apply force with a crosshead speed of 0.05 mm/min. These researchers also used a hardness tester to cause the initial flaws on the specimens. These flaws were between 50 and 272 μm and were orientated at various angles to the direction of the applied stress. Two 200 kHz resonant sensors were used for these tests (one at each end of the specimen). The signals from these sensors were amplified 40 dB

in a pre-amplifier and another 40 dB in the main AE data acquisition instrument, which was a SIMADZU SAE-1000.

Figure 2.13 displays results from these tests that are similar to results shown previously from the experiments conducted by Mori et al. These graphs show three lines of data plotted against time. Line 1 is the total AE energy measured during the test. AE cumulative event count is displayed as Line 2 and Line 3 shows a constantly increasing load until failure is reached. The specimen with no induced defect (a_o = 0 μm) started generating emission just after the beginning of the test while the specimen with the 272 μm artificial flaw only produced emission shortly before failure. As in the previous paper, σ_{AE} is defined as the stress at which the onset of acoustic emission occurs.

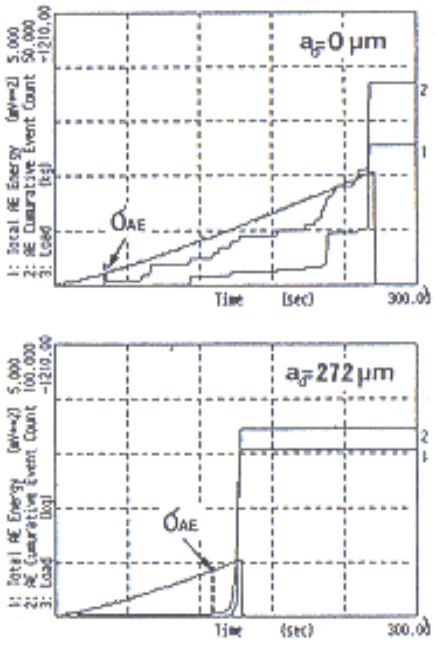

Figure 2.13 AE data from bending tests of alumina from two initial flaw sizes (Shinke et al. 1988)

Again there seems to be two categories for the type of emission that is detected, as was the case for Mori et al. Some specimens generate AE only right before failure, while others create emission at a very low stress. This trend is shown in Figure 2.14.

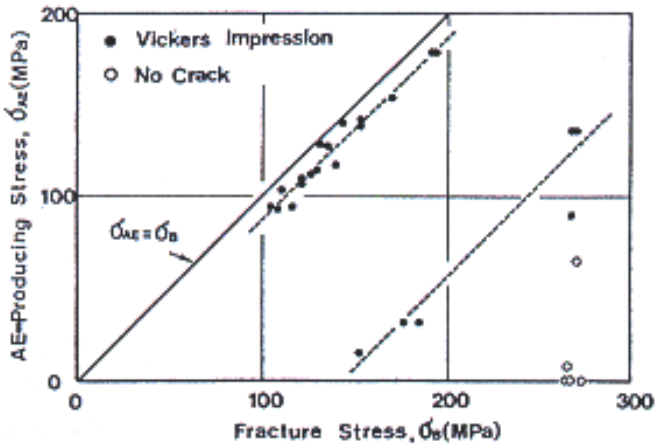

Figure 2.14 Onset of AE stress versus failure stress again showing two different behaviors (Shinke et al. 1988)

It was also determined in these tests that the final fracture stress in unaffected by initial cracks lengths that were less than 60 μm (Shinke et al. 1988). Specimens that had initial flaw sizes larger than 60 μm had decreasing fracture strengths. Also, the values of AE cumulative event count and total energy increase significantly with increasing initial crack size. Figure 2.15 shows the data from these tests that lead to those conclusions.

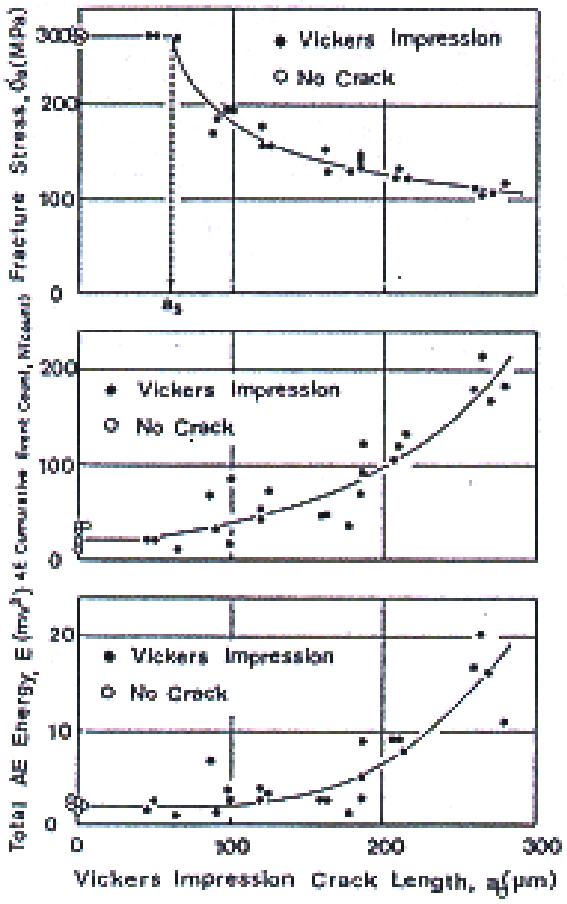

Figure 2.15 Data from bending tests of alumina showing the fracture stress and total AE values versus the initial crack length (Shinke et al. 1988)

The increasing amount of total emission with increasing initial flaw size shown in the data from these tests is the type of trend that would be very beneficial in determining the condition of specimens with unknown flaw sizes. However, the problem appears to be that the emission was not generated until shortly before failure in the specimens with the larger flaws and insufficient warning from the AE was provided in these tests. The specimens would have to

be stressed to a level that is too close to a critical level in order to be able to obtain an indication of its condition.

As in the previous set of tests, there were two categories of emission observed. One where emission started near the beginning of the test and another where emission was only detected right before failure. It was the specimens that had small initial flaws that produced emission throughout the test, which goes against traditional acoustic emission behavior of other materials. The problem with imparting an artificial defect in a specimen is that it is not known how well this would approximate the real flaws within a specimen. In general, artificially induced defects are not the same and behave very differently from natural defects. This has been found to be particularly important in steel specimens and a number of improper tests have been reported where artificial defects have been used. It is not known if the same is true for ceramics, but it is reasonable to be cautious in assuming that data from artificial defects will be the same from specimens without such defects. It is also not known whether or not the acoustic emission events came from the controlling flaw or from other flaws in the sample.

2.4.3 Using Source Location to Aid in Improving the AE Results

Studying the AE behavior from events that are only generated from the controlling flaw through source location techniques may provide better insight as to how AE relates to the fracture process of ceramics. Thus, source location could improve the feasibility for applying acoustic emission as a non-destructive test method to ceramics. Real time effects of increasing stress on the fracture process

at the controlling flaw could be observed. Also, the AE response from the controlling flaw could be isolated from other AE events and then correlated to the failure strength (Hamstad et al. 1986).

Source location techniques were attempted during four-point bending tests of alumina carried out by Hamstad et al. The specimens were again bar samples with dimensions of 7.62 x 10.16 x 127.0 mm. They had a span length of 80.0 mm and a constant moment region of 40.0 mm. Again, a test apparatus that operated at a constant crosshead rate of 0.05 mm/min was used. A Dunegan 8000 AE data acquisition system was implemented in these tests with a signal threshold of 27 dB. Two PAC μ30 sensors (resonant at 250 kHz) were used to carry out the source location; one sensor was placed at each end of the specimen.

By comparing the calculated source location from the AE data to the actual location of the artificial flaws or pencil lead breaks, the source location techniques for this system were developed. The actual flaw location was predicted within about 1.3 mm by the center of the AE location distribution. AE events that were only a few dB above the threshold of the system were able to be located as well as larger amplitude hits. From the results of these tests, it is observed that the AE data from the controlling flaw can be distinguished in multi-flaw samples.

Jadaan et al (1993) also carried out the source location techniques in fatigue evaluation tests. There were three materials tested in this set of tests and they were alumina (Al_2O_3), silicon nitride (Si_3N_4), and silicon carbide whisker-reinforced composites (SiC_w/Al_2O_3). The samples used were buttonhead tensile

specimens that were tested in fatigue cycles of tensile mechanical loading. They had a 6.3 mm gage diameter and a 25.4 mm gage length. PAC model D9215 sensors, which have a resonant peak at 450 – 500 kHz, were placed at each end of the gage section. The signal threshold of these tests was set between 39 and 45 dB for the two sensors and a PAC LOCAN AT main processor unit was used to record the AE data.

Many concepts were studied in this group of tests, but one of the successful aspects was source location. For the alumina specimen, the AE data was able to predict the fracture within 2 mm of the actual fracture site. Figure 2.16 shows a plot of counts versus the calculated position during the last half an hour of a fatigue test on a silicon nitride specimen. There is a large peak of emission at position x = 15 mm. That position coincided with the actual failure site for this specimen.

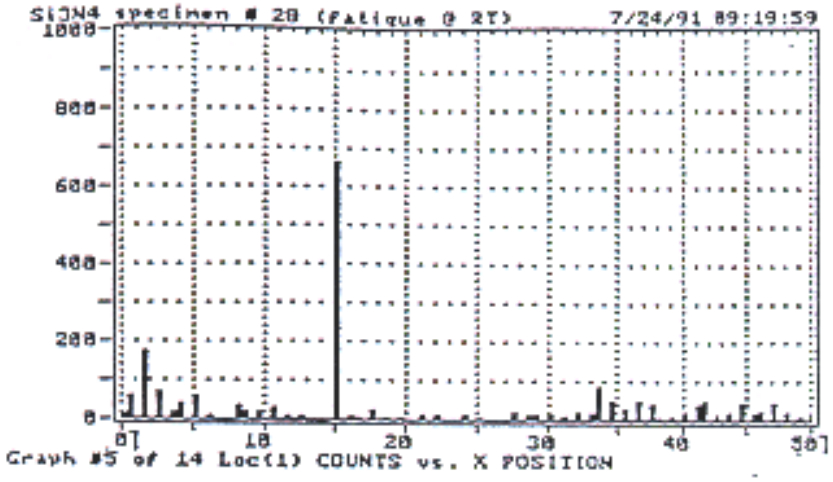

Figure 2.16 AE counts versus location for Si_3N_4 specimen under tensile fatigue (Jadaan et al. 1993)

However, these larger peaks of emission at the failure site only occurred very near to the end of the test. Earlier in the tests, the patterns of energy, counts, and events were randomly distributed throughout the specimen and did not concentrate at the failure site. Therefore, the source location techniques were quite successful in predicting the failure site, but that is not very helpful if all of the emission from the failure site is generated only shortly before failure.

2.4.4 A Successful Application

There is at least one application where acoustic emission is already being used as a routine nondestructive test method for a ceramic material that was found in the literature. This application involves the detection of ceramic substrate cracking during thermocompression bonding of an integrated circuit lead frame to

the substrate (Kahn and Miller 1979). If a crack in the substrate occurs, this may lead to failure later in the manufacturing process or after a complete circuit has been made. The acoustic emission test for this system was developed at the Engineering Research Center of Western Electric. A 650 kHz resonant sensor is attached to the thermode, which does the bonding. The signal from the sensor goes to a charge amplifier that applies a 40 dB gain and then it goes to a low noise amplifier that applies an additional 20 dB. After the amplification, the signal passes through a bandpass filter and then a buffer amplifier, before it reaches a peak detector. The bandpass filter is centered around the 650 kHz frequency. In a simple system, the peak signal amplitude is checked against a preset threshold amplitude. If the threshold is exceeded, an alarm goes off and then an automatic pen marks the defective circuit. This non-destructive test method has worked very well and has proven to be a way for identifying the ceramic substrates that have cracked.

2.4.5 Conclusions from the Literature Review

The literature review raises some concerns acoustic emission testing as a nondestructive test method for ceramics. From the research presented, it appears as though the detection of microcracking is an important concept for AE to be used effectively as a warning of failure. A number of tests show classic AE behavior with increasing emission to failure. In some cases, two changes in slope are present in the plots of cumulative emission versus time.

However, the research also shows evidence of little microcracking occurring when there is a large controlling flaw in the specimen. The tests that show this phenomenon used artificial flaws that were mostly on the surface of the specimen. These flaws, however, may not represent the actual ones found within the material.

It was shown that source location can be used in ceramics and can aid in AE testing by isolating the emission that comes from the controlling failure flaw. That emission can then be compared to the strength characteristics of the specimen.

The main concern from the literature review is whether a warning of failure can be detected or the emission only occurs right before final fracture. Which one of these processes occurs may be very test specific and could depend on the loading and stress distribution in the specimen, the size of the sample, and the orientation and size of the existing flaws.

Chapter 3: Preliminary Flexure Tests on Small Bar Samples

3.1 EXPERIMENT DESCRIPTION

In an attempt to obtain some preliminary information and before a more rigorous and standardized testing program was established, tests on some small bar samples were conducted. The main objectives of these tests were to see if existing equipment at the Ferguson Lab could be used effectively with these specimens, to try to establish a good method for loading these specimens with this equipment, and to obtain an idea of the type of acoustic emission data that would be generated from this material. Figure 3.1 shows a picture of one of the bar samples used for these tests.

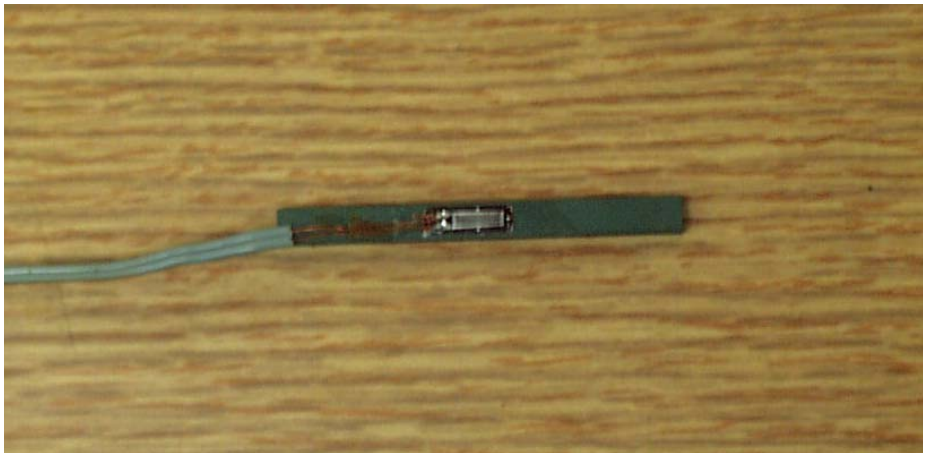

Figure 3.1 A typical bar sample with a strain gage attached

These specimens are the standard type for ceramics and are used in many different tests. They are defined in ASTM C1161-94, Flexural Strength of Advanced Ceramics at Ambient Temperature (ASTM 1994). There are three different sizes of specimens that can be used following this ASTM procedure. The samples that were made available for this testing program were dimensioned following the criteria for the middle-sized specimen (configuration B in the standard). These specimens have a length of at least 45 mm (most of them were approximately 47 mm) and have cross-sectional dimensions of 3.0 by 4.0 mm. ASTM C1161 provides specifications for testing these specimens in either three-point or four-point bending. Multiple configurations were attempted for this testing program in order to create the bending arrangements described in the standard. A more detailed description of the loading configurations is provided in Section 3.1.2.

3.1.1 Test Frame

A small test frame that was used for these preliminary tests is shown in Figure 3.2. The base of the frame consists of an inverted channel section that is welded to two angle sections that are approximately 18 inches long. The angles provide stability for the frame. The base channel supports two vertical channels that are welded to it. There is a horizontal channel section at the top of the frame that is bolted in place and can be adjusted to varying heights. A small Enerpac hydraulic ram is attached to the base channel and acts as the loading mechanism

Figure 3.2 The loading frame used for the flexural testing of the bar specimens

for this frame. The ram applies the load through the specimen by reacting it against the top horizontal channel. This channel has two bolts that are reacted against and act as supports. Their position on the channel is adjustable. Attached to the top of the hydraulic ram is a steel bar that can hold one or two rollers. The adjustable position of the rollers and the bolt supports allows for various configurations for different length specimens to be tested in both three-point or four-point bending. Figure 3.3 shows a close-up view of the reaction points. The load is measured with a load cell that is attached to the top of the hydraulic ram.

The load cell has a capacity of 500 lbs and is manufactured by Sensotec. It is also shown in Figure 3.3.

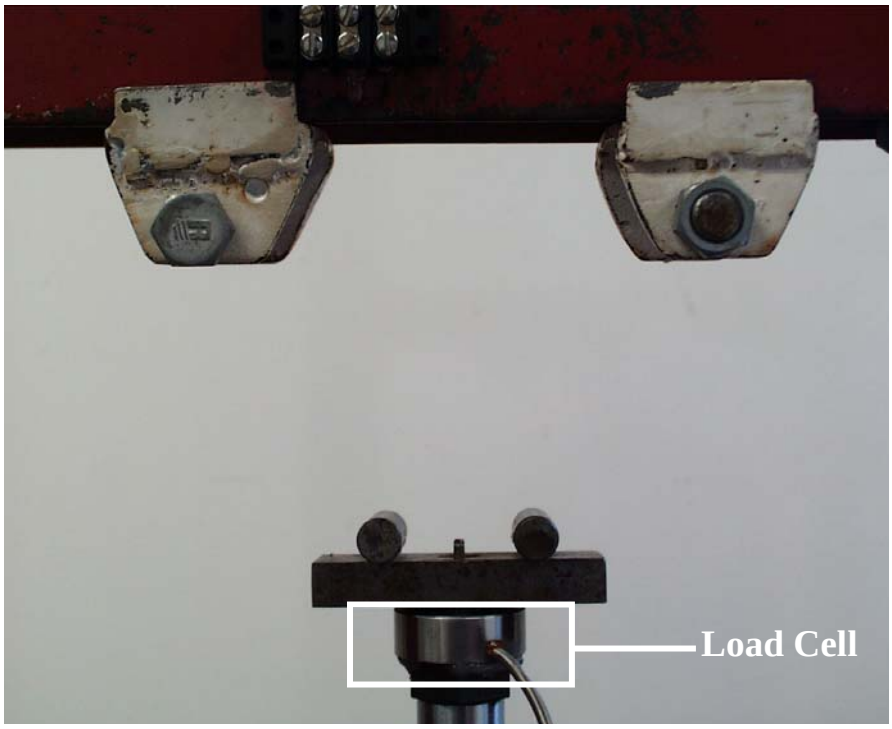

Figure 3.3 Support and loading components of the test frame

3.1.2 Loading

Because of the small size of the bar samples relative to the frame and supporting parts, various configurations to apply load to the bars were tried in order to see what would work best. Essentially, three different methods were used, three-point bending of the SiC bar by itself, four-point bending of the specimen attached to a steel bar, and four-point bending of the specimen attached

to an FRP bar. Attaching the SiC specimens to other materials was attempted to create a constant moment region in the sample (four-point bending) and because these bars of other materials fit better within this test frame and supports. The bonding agent that was tried during the first tests was a quick hardening, two-part epoxy. In the final attempt, a stronger two-part epoxy was employed that is used for strain gauging applications. In theory, the moment would be applied to the base material (steel or FRP) and then transferred to the SiC sample if sufficient bond could be achieved between the two. The steel or FRP should be under low enough stress in these tests so as to not create emission to affect the result. The sensor would be placed directly on the SiC sample in any case.

The load was applied to the specimen in increments with load holds of approximately two minutes in between the load increases. The amount of the load increments was basically dictated by the control of the hydraulic ram. The increments were made as small as possible. Unloads and then reloads were not used for this set of tests.

3.1.3 Instrumentation

The Transportation Instrument is a 24-channel acoustic emission data acquisition system manufactured by PAC. This instrument along with a Hewlett Packard (HP) 3497A data acquisition machine were used to record all of the data generated by these tests. The HP 3497A was used to acquire and record the load and strain data. A PAC Pico (S/N AA04) sensor was used with the Transportation Instrument to capture and process all of the acoustic emission data

during these tests. The Pico sensor is very small and is resonant at 500 kHz, a frequency that is higher than what is typically used. However, the small size of these specimens make this sensor satisfactory, as attenuation is not a concern. This sensor also utilizes an external amplifier, which helps to reduce its size. The external amplifier conditions the AE signal with a 100-1200 kHz bandpass filter and by applying a 40 dB gain to it. The location of the sensor on the sample varied with each test because of the three-point and four-point bending configurations. The value of the load and the strain were recorded at important times during each test. The strain gage was located at the center (lengthwise) of the specimen and would only fit on the larger dimension side (4 mm). The goal was to capture the maximum tensile strain imparted in the sample. Type FLA-5-3l-11 120-ohm resistance gages manufactured by the Tokyo Sokki Kenkyujo Corporation were used in this set of tests.

As mentioned previously, the load cell is made by Sensotec and has a capacity of 500 lbs. An external power supply was used for both the load cell and the strain gage. All amplification and conditioning of the load and strain signals was completed internally by the HP 3497A. The load and strain readings were recorded at the beginning and end of each load step increase.

3.2 TEST RESULTS AND ANALYSIS

A series of five tests were attempted during this preliminary test phase. A summary of how the five specimens were tested and how they failed is shown in Table 3.1.

Specimen	*Loading Method*	*Cause of Failure*
B1	4-point bending – attached to steel bar	Crushing at supports
B2	3-point bending – specimen by itself	Flexural failure
B3	4-point bending – attached to FRP bar	Insufficient bond
B4	4-point bending – attached to FRP bar	Insufficient bond
B5	3-point bending – specimen by itself	Flexural failure

Table 3.1 Summary of the preliminary bar sample tests

In test B1, the specimen was glued to a steel bar and tested in four-point bending. This specimen failed by crushing of the SiC at the supports caused by the higher loads required to induce bending strain into the steel and thus the SiC bar. Although crushing was the mode of failure, some good acoustic emission data was recorded from this test.

Specimen B2 was tested by itself in three-point bending. A large load increase resulted in failure of the specimen shortly after the test was begun and was caused by an inability to control how much travel (thus load) was given to the hydraulic ram. Therefore, this test yielded very little useful data.

In an attempt to replicate the first test and avoid the crushing of the SiC sample, the specimen was attached to an FRP sample and a little different loading configuration was used for B3 and B4. The FRP bar would not require as much load in order to induce the bending in the SiC sample. The loading configuration was changed so that the SiC specimen would not be bearing directly on the

supports and is shown in Figure 3.4. Two different adhesives were attempted for the two tests, but neither of them created sufficient bond for this method to be effective. In both tests, the SiC bar separated from the FRP specimen and thus there was no useful data obtained from the tests.

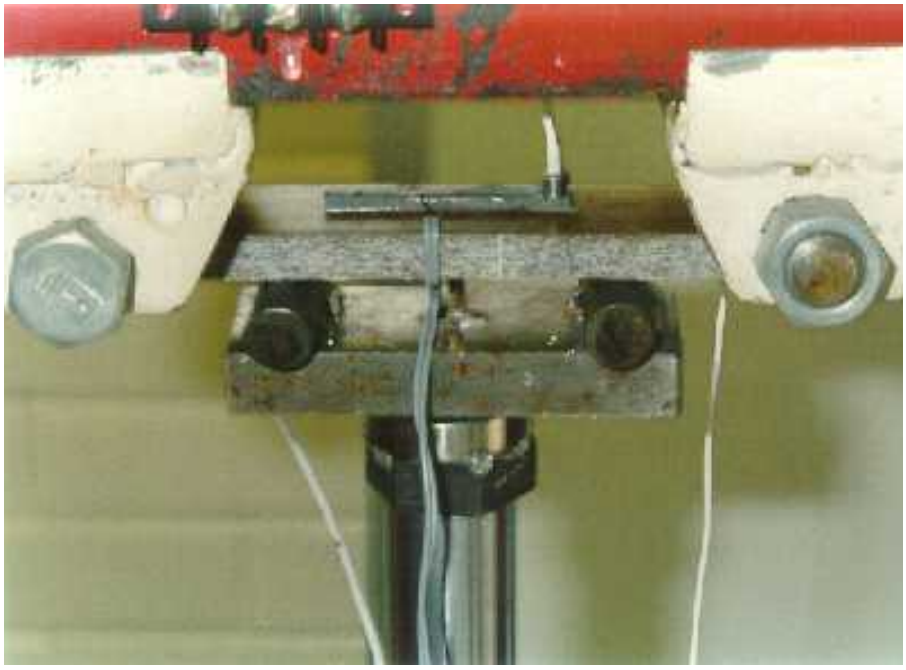

Figure 3.4 Loading configuration with SiC sample bonded to FRP bar with supports not bearing directly on sample

In the final trial, B5, the specimen was again loaded in three-point bending by itself, as it was for B2. This time much more care was taken to increment the load as slowly as possible. This final trial on B5 was more successful and some good results were obtained. Because of the situations described above, the more detailed results of these tests that are presented in the following paragraphs consist of only the first and last experiments, B1 and B5.

The duration versus amplitude plot for specimen B1 is shown in Figure 3.5. This plot shows that the emission from this test is genuine. There are no hits recorded within the block in the upper left corner of the graph, which are hits that are non-genuine emission that would be filtered out by a swansong filter. The hits lie in a good band, which is what is looked for in this plot.

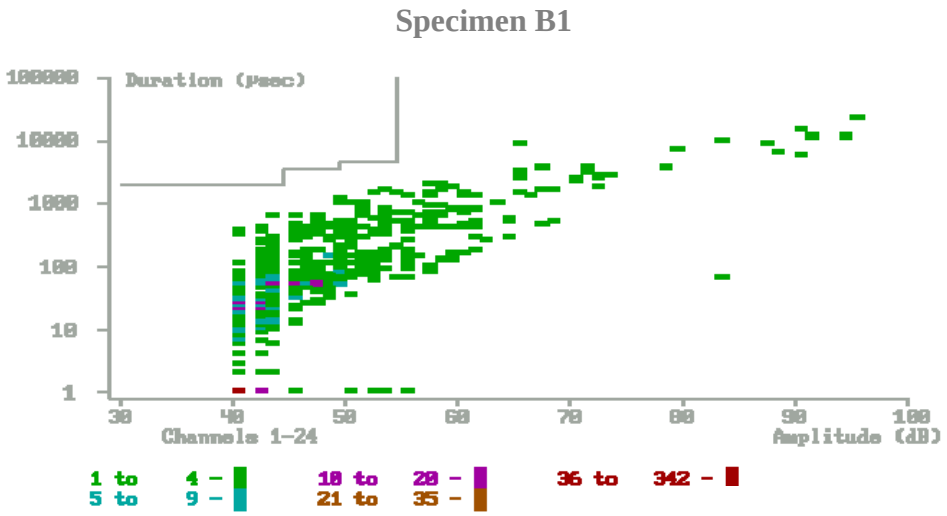

Figure 3.5 Log duration versus amplitude for specimen B1

Figure 3.6 is a plot of the amplitude of each hit versus time for B1. This plot shows that a great deal of emission was generated during the load increases at approximately 35 seconds and 187 seconds into the test. It can be observed that a significant amount of emission is also generated at about 220 seconds into the test, but the load is not increasing at this time. A load increase was attempted at this time, but this is when the SiC sample started to crush in compression at the supports. This data shows that silicon carbide does emit a significant amount of

emission and the hits after 220 seconds show the type of emission that results from a crushing failure.

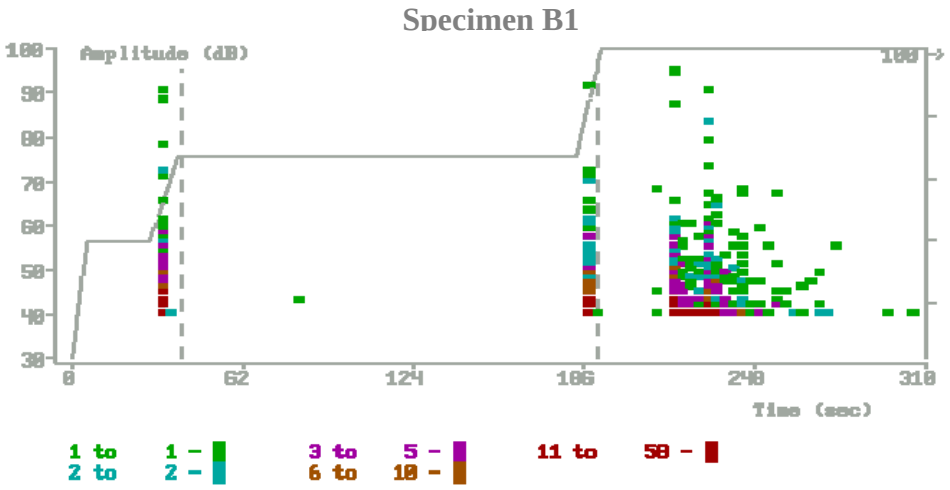

Figure 3.6 Amplitude versus time plot for specimen B1

The duration vs. amplitude plot for specimen B5 is shown in Figure 3.7. Once again the emission is well banded and appears to all be genuine.

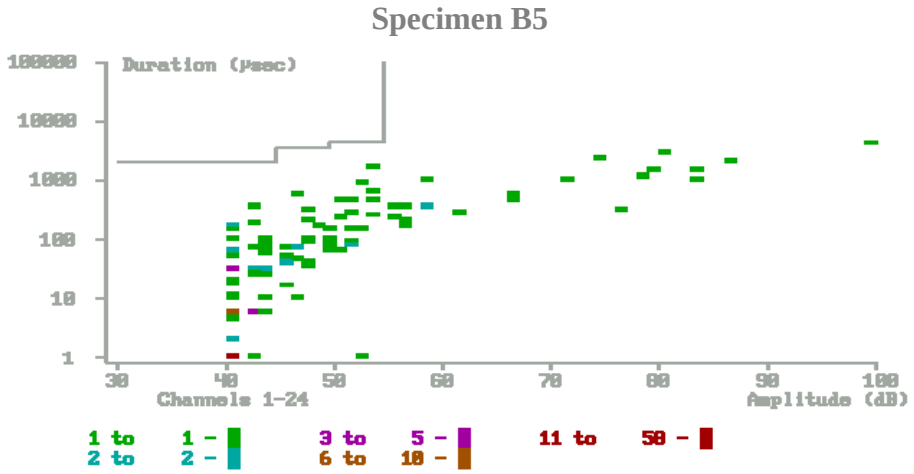

Figure 3.7 Log duration versus amplitude for specimen B5

The amplitude values for each hit as they occurred in time during this test are shown in Figure 3.8. This plot shows an increasing amount of emission with increasing amplitude hits as the specimen approaches failure. The increasing amplitudes and emission amount could serve as warnings of failure in a proof test situation for the full-sized SiC tubes.

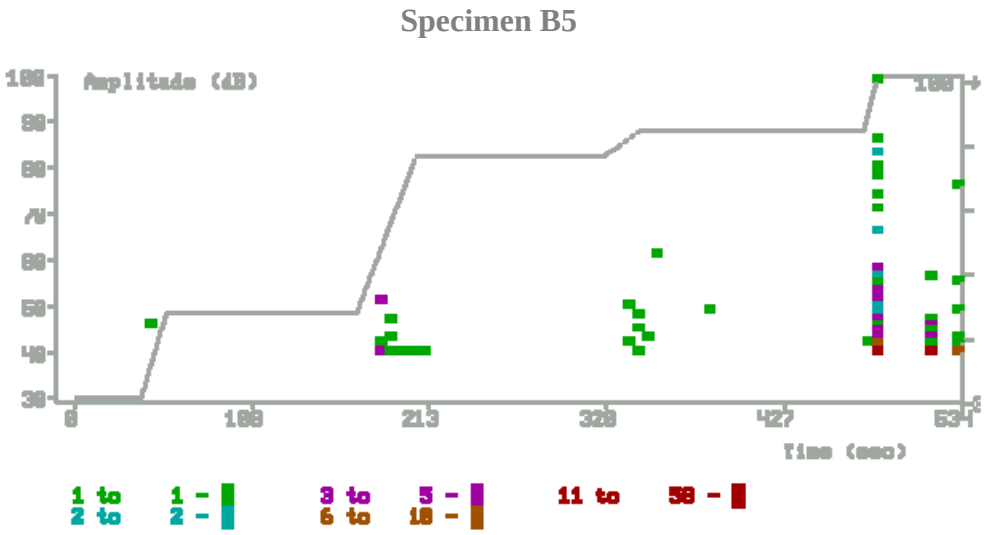

Figure 3.8 Amplitude versus time plot for specimen B5

3.3 SUMMARY AND CONCLUSIONS

The primary goals of this set of preliminary tests were to evaluate test methods for SiC and to try to obtain an idea of the type of acoustic emission that

would be detected from this material. These goals were achieved because it was learned very quickly that these small specimens would not be suitable for testing without special equipment. Although some very good data was obtained from specimens B1 and B5, these tests were not really satisfactory to obtain the quality of results desired.

The problems of the specimen size and not having fine control of the load could not be overcome. Although the three-point bending of the SiC beam by itself worked well for obtaining the acoustic emission data, the control of the load was difficult and the specimens fractured under a very small load. It was also impossible to use a conventional 150 kHz sensor on these small specimens. Use of the smaller 500 kHz sensor for these tests would not be practical in the field because of the greater attenuation in the larger specimens.

Bonding the SiC to another material was not successful because sufficient bond between the base material and the SiC bar could not be achieved. The effect that the base material has on the forces generated in the specimen and the possibility of the base material creating emission are additional problems with this approach. At a meeting on January 13, 1999 with the sponsors of the project, it was decided that a larger specimen type would be made available for testing and that a test frame would be created that would have the desired control and would be specifically designed for the new specimen type.

Chapter 4: Flexural Testing of C-ring Samples

4.1 EXPERIMENTAL PROCEDURE

After the completion of the flexural bar tests, it was realized that a different type of specimen was needed that would be more suitable for acoustic emission monitoring. The sponsors of this project had a number of C-ring specimens readily available. These specimens appeared to meet the requirements of size, load range, consistency and standardization that were required for the test program. A picture of one of these samples is shown in Figure 4.1 and it can be observed how this type of specimen gets its name.

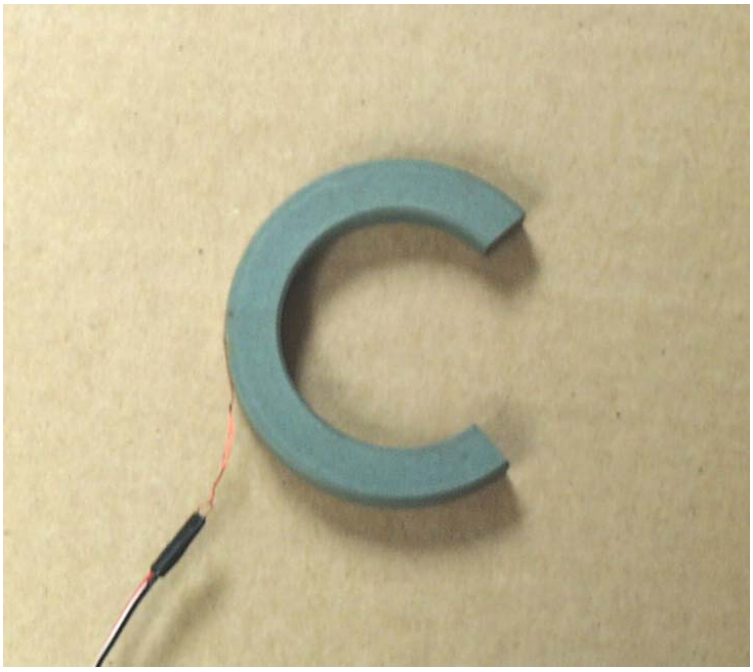

Figure 4.1 Example of a typical C-ring sample

The C-rings have been used in a test procedure developed by Ferber et al (1986) for determining the strength characteristics and statistical distribution of properties for ceramics used in tubular applications. These samples offer an alternative to the traditionally used flexural bar samples. As noted by Ferber et al, the small bar samples require complicated machining which can change the natural flaw population in the specimens. The C-rings can be sectioned and machined more easily into the required dimensions from the as-received tube, which is used commercially. In the test proposed by Ferber et al, the C-rings are stressed in a combined flexural and compressive manner by applying a compressive force to the top and bottom of the sample. The C-ring samples were incorporated into the experimental program of this project using a similar method for stressing the specimen.

4.1.1 Test Frame

A simple, but effective test frame was fabricated in order to load the C-ring by applying a compressive force to the top and bottom of the sample as described above. Figure 4.2 is a picture of the frame at the beginning of one of the tests. The main portion of the frame consists of a one inch thick base plate which supports two small steel channel sections aligned vertically and welded at their base. A horizontally aligned channel section is welded to the vertical channels on each side at the top of the frame. The horizontal channels support two 3/8 inch thick steel plates that house and support the loading mechanism. The frame also has an adjustable platform, which supports the test sample.

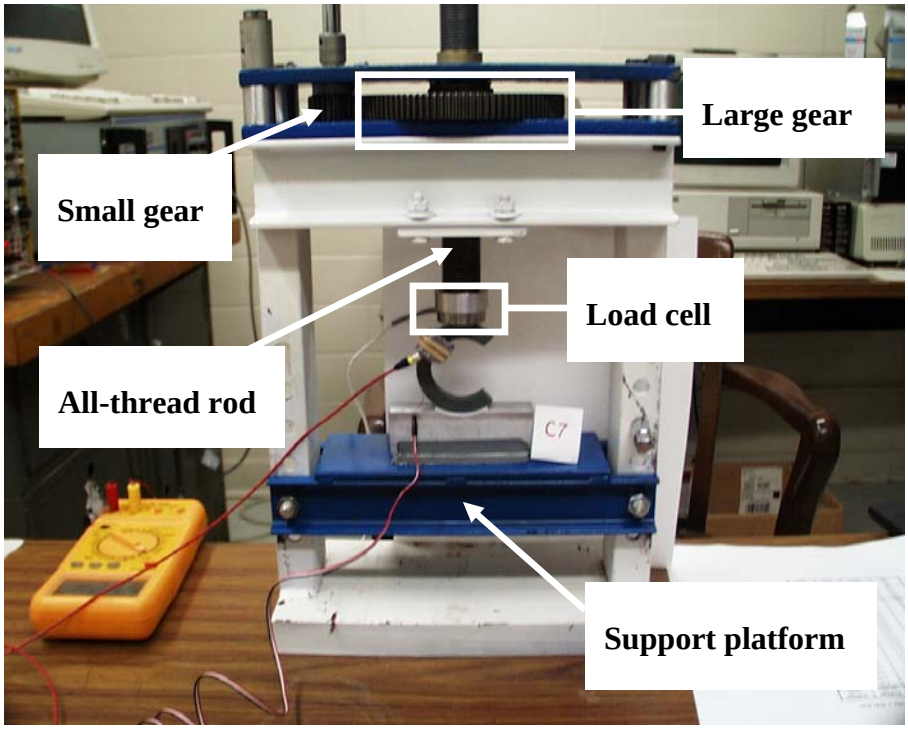

Figure 4.2 Test frame used for C-ring tests

The vertical channels have holes to allow for the support platform to be adjusted relative to the load head. This adjustable platform allows for different specimen geometries to be tested. The loading mechanism consists of an all-thread steel rod and two gears, one large and one small. The load is applied to the C-ring by lowering the all-thread rod. This is done by turning the smaller gear using a socket wrench. The small gear then turns the larger gear, which is connected to the all-thread rod. The approximate 4:1 ratio of the large gear to the small gear allows for very fine adjustment of the load with the turning of the wrench. A

friction clutch was also implemented into the test frame to stop the load from dropping off during a load hold.

4.1.2 Loading

A compressive force is applied to the top of the sample by lowering the load head. The load cell applies the force over a small circular area on the top of the C-ring. The specimen is supported on the platform by a piece of aluminum that has a cylindrical depression machined into it. The machined area is of slightly larger diameter than the outer diameter of the C-ring sample. Figure 4.3a shows how the aluminum piece supports the C-ring. This loading configuration applies compressive loads to the sample as shown in Figure 4.3b. The midplane of the C-ring undergoes the maximum stress.

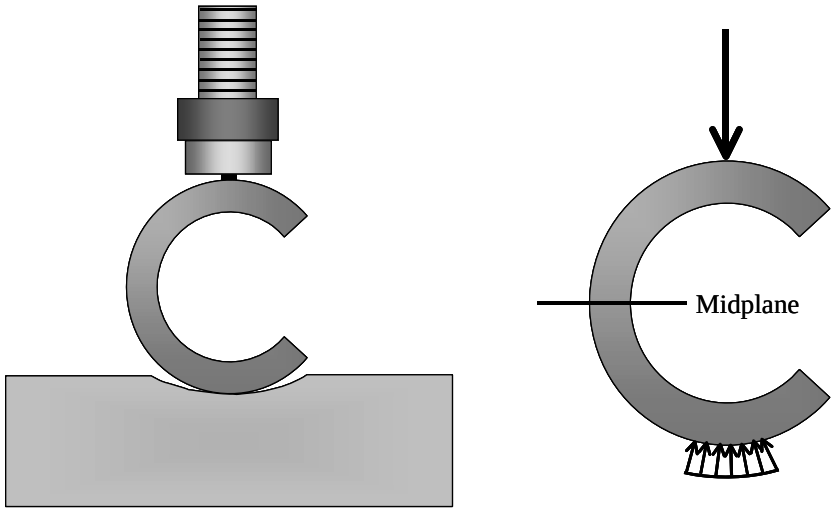

Figure 4.3 C-ring loading configuration

The load was applied in a series of steps with load holds and unloads. An initial load of 10% of the estimated maximum load was applied to the specimen. This was followed by a 5% unload. After that, the load was increased and decreased in 5% increments as shown in Figure 4.4. There are load holds of approximately 2 minutes after each load and unload. Actual loadings of the C-ring specimens varied from the idealized loading shown in Figure 4.4 and are shown later for each specimen tested through the load data or the strain data.

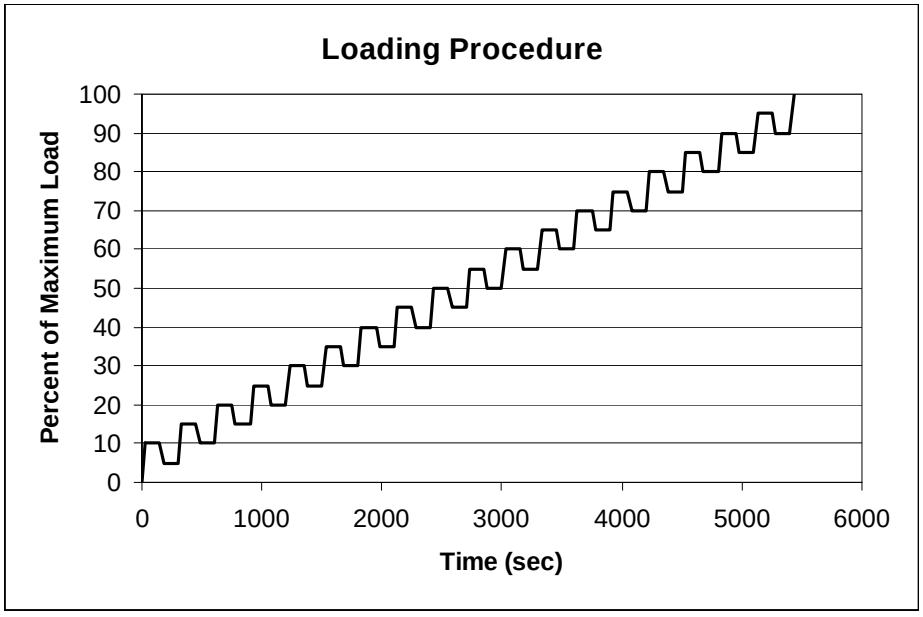

Figure 4.4 The step loading procedure used for the C-ring tests

The specimens were loaded in this manner in order to capture load hold and Felicity effect data. During the first few C-ring tests, there was difficulty in holding the load at a constant level. The load had a tendency to decrease significantly during an attempted load hold because of “back-up” in the gears.

Therefore, a backstop, holding mechanism was created. This proved successful and the improved load control can be observed in the data from the later C-ring tests as compared to the first.

4.1.3 Instrumentation

The LOCAN 320 acoustic emission instrument was the primary data acquisition machine used for the C-ring tests. This instrument not only collected all of the AE data, but also acquired load and strain data as parametrics. The LOCAN 320 is an analog instrument with an Intel 8 MHz CPU and is manufactured by PAC. The sensor used was a PAC R15 resonant sensor, which is resonant at 150 kHz. An external amplifier was used in conjunction with the sensor. Having the amplifier external to the sensor allowed for a smaller sensor to be used, which matched better with the specimen geometry and size. The external amplifier applied a 40 dB gain to the acoustic emission signal collected by the sensor and utilizes a 100-300 kHz bandpass filter. Figure 4.5 shows the location of the sensor on a C-ring sample. The side of the C-ring is really the only accessible location that has a flat surface to place the sensor. The sensor was typically placed above the midplane of the sample to avoid the coupling materials (vacuum grease, duct tape, rubber band, etc.) from interfering with the strain gage and also to attempt to avoid damage to the sensor that could result from having it located at the failure location of the specimen. Settings that were used in the LOCAN instrument for the collection of AE data are displayed in Table 4.1.

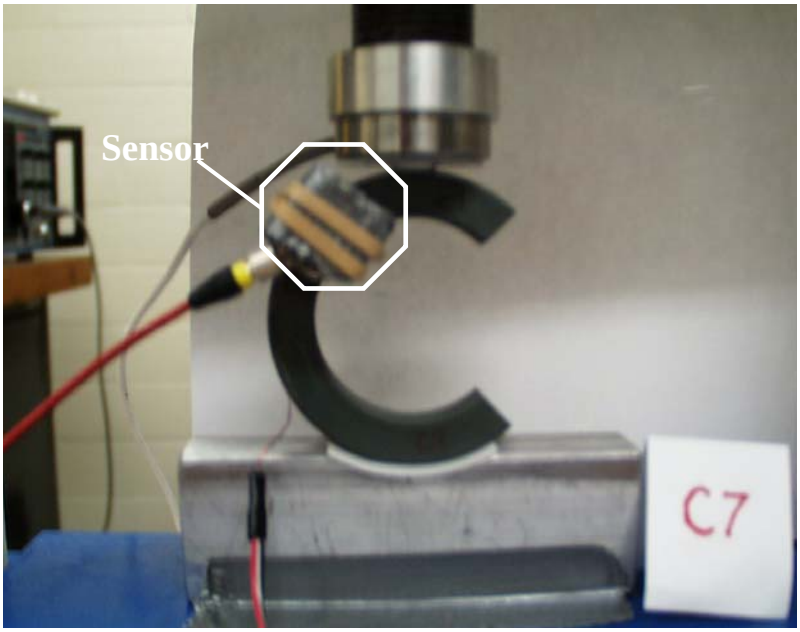

Figure 4.5 Location of the sensor during C-ring tests

Setting	*Value*	*Units*
Threshold	30	dB
Hit Definition Time	400	µsec
Rearm Time	200	µsec

Table 4.1 Settings used during the C-ring tests for the LOCAN 320

The load value and one strain measurement on the C-ring were also recorded during each test. The strain gage was placed at the center of the specimen on the outer diameter in an attempt to measure the maximum tensile strain induced in the sample. The location of the strain gage on the C-ring is shown in Figure 4.6. The strain gages are 120-ohm resistance gages manufactured by the Measurements Group, Inc. (type EA-06-125BT-120). The load cell is the same one used for the bar sample tests and has a capacity of 500 lbs. A set of amplifiers external to the LOCAN were used as a power supply and for signal amplification for both the load cell and the strain gage. The load cell signal was

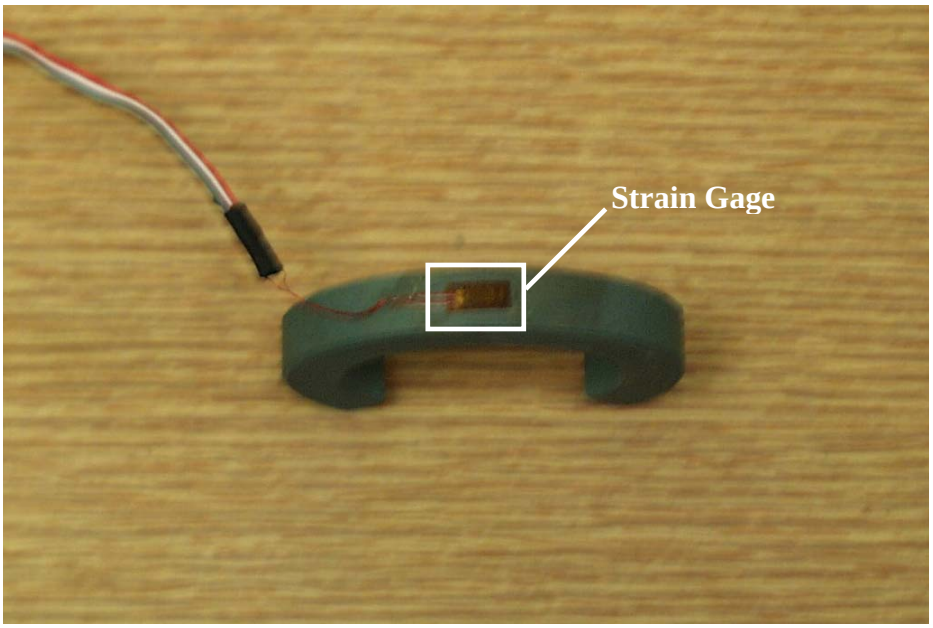

Figure 4.6 Location of the strain gage

amplified 500 times while the strain gage signal was amplified 5000 times. These amplifications were based on expected maximum readings from these instruments yielding approximately 10 volts based on their calibration and from 10 volts excitation for the load cell and 2 volts excitation for the strain gage. The load and strain readings were recorded once every second as parametric data by the LOCAN 320 data acquisition instrument.

4.2 PRELIMINARY STRESS ANALYSIS

Before the start of the C-ring tests, an approximate stress analysis was completed in order to gain a better understanding of the stresses that a C-ring would endure and to be able to establish an estimate for their failure load. The tangential stress (σ_t) can be approximated using simple bending theory for curved beams. A section can be cut at an angle θ from the midplane and then equilibrium is considered as shown in Figure 4.7.

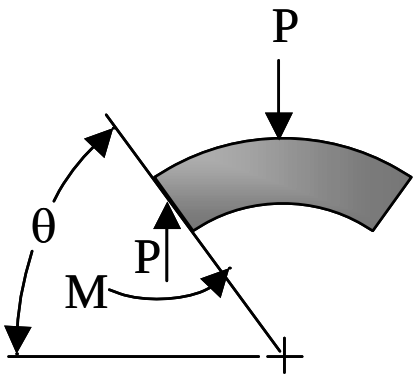

Figure 4.7 Equilibrium of a section cut at θ from the midplane

From this analysis the following equation is derived (Ferber et al. 1986).

$$\sigma_t = \frac{P \cdot R(r - r_a)}{A \cdot r(R - r_a)} \cdot \cos(\theta)$$

$$r_a = \frac{(r_o + r_i)}{2}$$

$$R = \frac{(r_o + r_i)}{\ln(r_o / r_i)}$$

r - radius of location where stress is to be determined

r_i - inner radius = 0.800 in.

r_o - outer radius = 1.175 in.

w - thickness = 0.375 in.

r_a - centroid

R - moment of interia

A - cross-sectional area

P- load = 200 lbs

As would be expected, tensile stresses are generated on the outer portion of the C-ring while compressive stresses are generated along the inner radius. Also, the maximum stresses occur at the midplane of the specimen where

$\theta = 0°$. Figure 4.8 shows how the tangential stress varies through the cross-section of a specimen for θ angles of 0°, 30°, and 45°. Timoshenko and Goodier (1970) report another set of equations that approximate this stress condition. These equations yield equal results to the equations presented above. Ferber et al report that the radial and shear stresses are very small for this geometry and therefore the tangential stress by itself can be used as an estimate for the maximum stress in the sample.

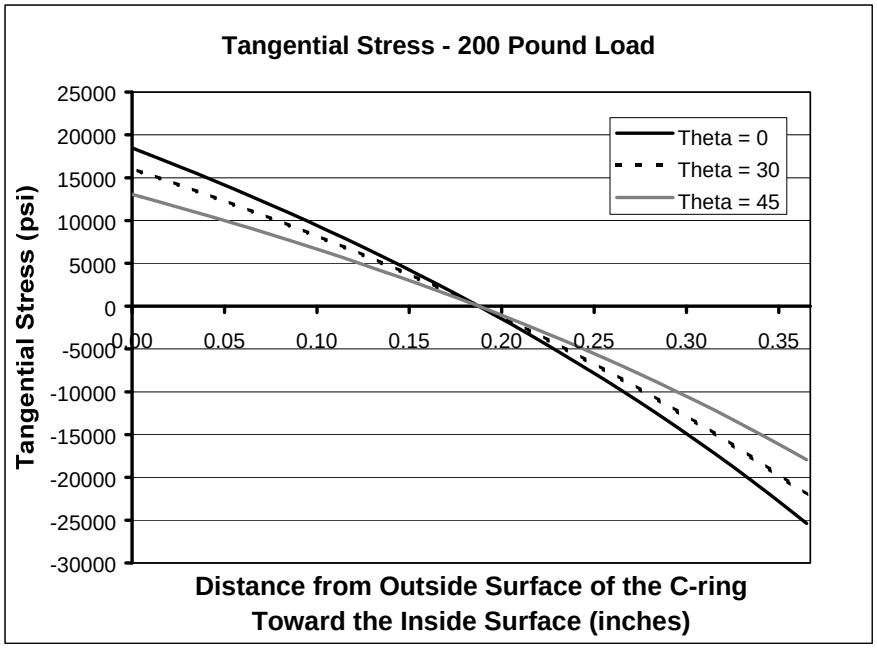

Figure 4.8 Tangential stresses through specimen cross-sections at various angles from the midplane

From test data provided by the sponsor, the maximum tensile stress of this material varies between 14,000 and 26,000 psi. The more recent material that is produced is closer to the higher end of that range and averages about 22,000 psi.

A tensile failure stress of 14,000 psi would be generated by a maximum load of 151.7 lbs on the C-ring while 281.7 lbs would be required to reach a tensile stress of 26,000 psi. Using the average failure stress of the more recent material, an estimate for the maximum load of 238.4 lbs is calculated. A slightly conservative estimate of 200 lbs was used as the value from which to calculate the percentages for the step loading procedure described in paragraph 4.1.2.

4.3 TEST RESULTS AND ANALYSIS

A total of nineteen C-ring tests were completed. The strain along the outside surface at the midplane, load, and the acoustic emission data were recorded for each test. The load and strain values were recorded automatically by the data acquisition system once every second. The acoustic emission was monitored continuously and recorded as it took place. Strain and load values were also stored with every acoustic emission hit that occurred. The results of are separated into stress and failure analysis, and acoustic emission data.

4.3.1 Stress and Failure Analysis

The values of maximum load, strain, tensile stress, and the number of failure locations for each specimen are displayed in Table 4.2. As can be observed, the failure loads of the C-ring sample varied between 181.5 lbs and 236.5 lbs, which correspond to approximate maximum tensile stresses of 16,750 and 21,830 psi respectively. These values correlate well with the value predicted by the preliminary stress analysis discussed in the previous section.

Specimen	Maximum Load (lbs)	Maximum Strain (μin./in.)	Tensile Failure Stress (x 10^3 psi)	Modulus of Elasticity (x 10^6 psi)	Fracture Locations
C1	209.5	533.3	19.3	36.3	1
C2	236.5	617.8	21.8	35.3	2
C3	215.1	617.8	19.9	32.1	3
C4	229.4	819.2	21.2	25.8	3
C5	234.5	562.1	21.6	38.5	2
C6	226.8	644.6	20.9	32.5	2
C7	225.8	571.7	20.8	36.5	2
C8	215.1	-	19.9	-	2
C9	211.5	-	19.5	-	1
C10	193.7	-	17.9	-	1
C11	201.3	537.2	18.6	34.6	2
C12	181.5	487.3	16.8	34.4	1
C13	233.4	610.1	21.5	35.3	2
C14	203.4	566.0	18.8	33.2	2
C15	230.9	612.0	21.3	34.8	2
C16	231.9	638.9	21.4	33.5	2
C17	217.1	577.5	20.0	34.7	2
C18	209.5	506.5	19.3	38.2	2
C19	205.9	560.2	19.0	33.9	1

Table 4.2 Stress, strain, and fracture location results from the C-ring tests

Data is missing in Table 4.2 for specimens C8 – C10. This is due to a computer malfunction and now that data is no longer available. In later discussion of the results, the acoustic emission data is often plotted with the measured strain in the specimens, so that they can be related. For tests C8 – C10, those plots will be shown with the load data instead of the strain. Some of the acoustic emission results for those tests are also not shown for the same reason.

Seventeen out of nineteen of the samples failed at loads between 200 and 236.5 lbs and the remaining two specimens' failure loads were not significantly

lower than the others. The average maximum load is 216.5 lbs, while the standard deviation was calculated to be 15.3 lbs. This is a fairly tight distribution of failure stresses for this material and would suggest that these samples were not significantly defective. In other words, a similar flaw size distribution existed in all of the specimens, at least within the region of maximum stress.

Also of significance and an interesting result in the tests is the number and position of the failure locations for each sample. As can also be observed in Table 4.2, the majority of the C-rings broke in two simultaneous locations while some others only had one failure location and two samples even fractured in three places. It is also interesting to note that not all the specimens fractured at or near the midplane section of the C-ring (location of the maximum theoretical stress). Figure 4.9 shows examples of the types of failures that were observed in the tests.

Figure 4.9 Pictures of the failed specimens

In fact, some samples even have failures that are located at θ angles of 70^o away from the midplane. This phenomenon can be explained by the fact that the areas away from the midplane are still under significant stress as shown previously in Figure 4.8 and that there may have been some flaws of slightly larger size (but still not large in general terms) in those areas. The multiple failure locations were caused by secondary effects of the specimen still being under load, while one area was already fracturing. This failure sequence appeared instantaneous to the naked eye. The multiple failure locations in many samples would also strongly suggest that there was not a single large controlling flaw in those samples, but a distribution of small flaws of similar size throughout the specimen.

4.3.2 Acoustic Emission Results

The acoustic emission data acquired from the C-ring tests provided very promising results. There were some definite general trends in the acoustic emission patterns as the specimen progressed towards failure. These trends were prevalent in most of the tests and were especially so after the first few tests. During the first few tests, a number of details in the test procedures needed to be worked out. In the initial two tests, it was suspected that noise from the support under the C-ring and from the load cell rubbing on the top of the specimen was creating acoustic emission. The AE data from specimens C1 and C2 will not be considered. In the following tests, Teflon pads were placed between the specimen and the support and also between the load cell and the specimen. The Teflon pads did an excellent job of eliminating the noise. The general trends in the acoustic

emission behavior will be presented and the results from a few of the tests that did not follow these trends will be discussed.

4.3.2.1 General Trends in the Acoustic Emission Behavior

The key general trend that was observed in the acoustic emission data from the C-ring tests is an increase in the cumulative signal strength that began at approximately 70% - 85% of the final failure load. This increase or change in slope of the cumulative signal strength is referred to as the "knee" in the curve, as was discussed in Chapter 2. Figures 4.10a and 4.10b are typical results and show this increase in emission.

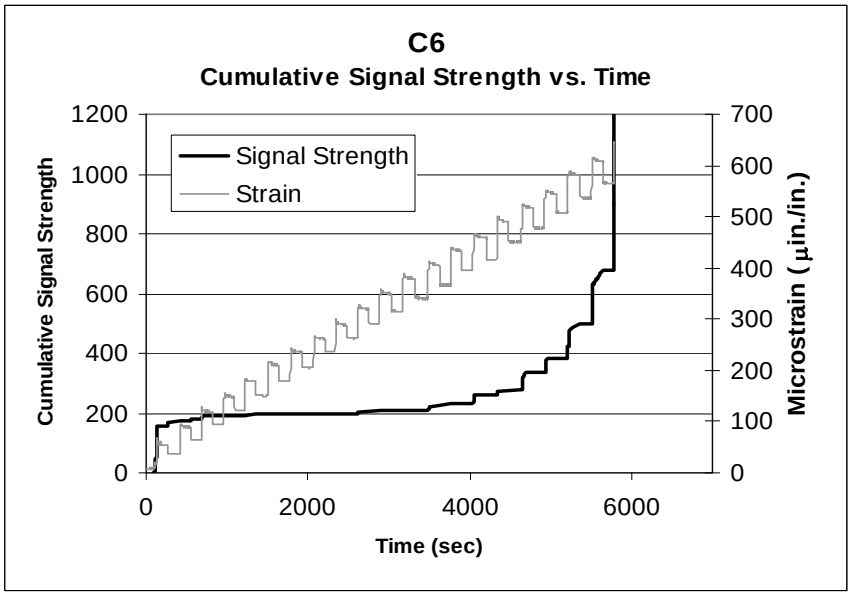

(a)

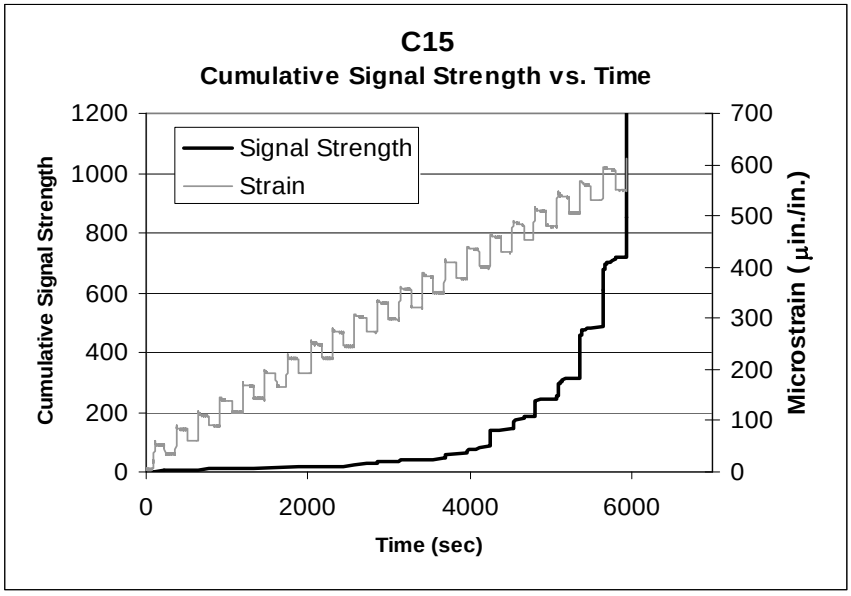

(b)

Figure 4.10 Cumulative signal strength vs. time for (a)C6 and (b)C15

In both plots, the knee occurs at approximately 420 – 450 μin./in. This increase in signal strength at a load significantly below the failure load is important because it is an indication that the specimen is on its way to failure. In conjunction with the increasing signal strength is the historic index. The historic index graph helps to locate when the "knee" in cumulative signal strength curve occurs by comparing the most recent hits to that of all the previous hits. An increase in the historic index correlates well with the change in slope of the cumulative signal strength plot. Figures 4.11a and 4.11b are the corresponding historic index graphs for tests C6 and C15. It can be observed that the increase in historic index corresponds well to the time of the increase in the cumulative signal

strength that was shown earlier. The historic index for C6 (shown in 4.11a) is distorted slightly because of some early emission. However, the historic index starts to increase steadily at approximately 4000 seconds, which corresponds well to the "knee" shown in Figure 4.10a. For C15, the cumulative signal strength begins to increase sharply at about 4200 seconds and a relatively large increase in the historic index of C15 occurs at that same time. Therefore, the historic index can also provide a warning of failure and could be used as a criterion for investigating this material.

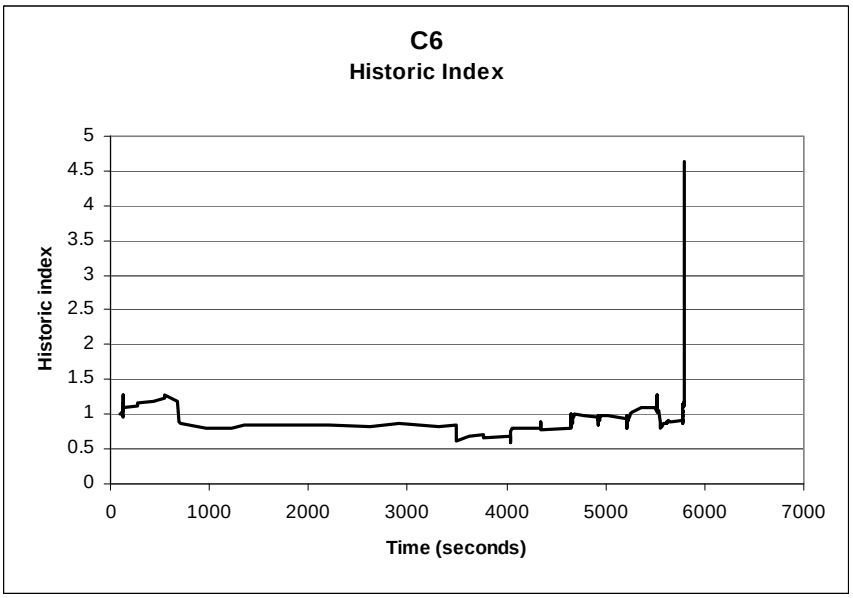

(a)

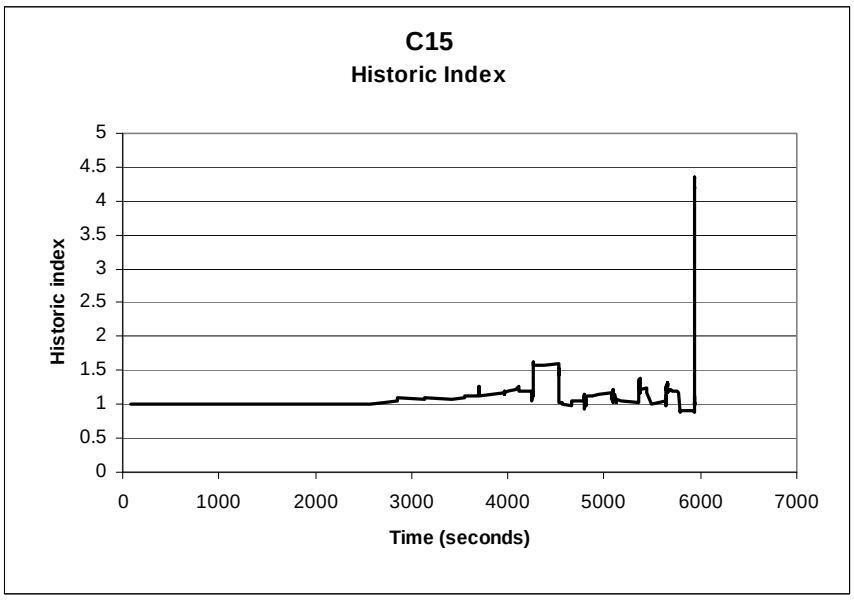

(b)

Figure 4.11 Historic index vs. time for (a) C6 and (b) C15

Having hits with increasing amplitudes and signal strengths as the specimen approached failure was another general trend witnessed in the acoustic emission behavior of these C-rings. Figures 4.12a and 4.12b show this trend with the amplitude values for the individual hits for specimen C6 and C15. Figures 4.13a and 4.13b provide examples of the increasing signal strength hits as failure is approaching, again from those same specimens.

The data for the remaining specimens that exhibited the typical behavior are shown for reference at the end of this section as Figure 4.14 through Figure 4.23. The (a) figure is cumulative signal strength versus time and the (b) figure is amplitude versus time for the individual hits for these specimens

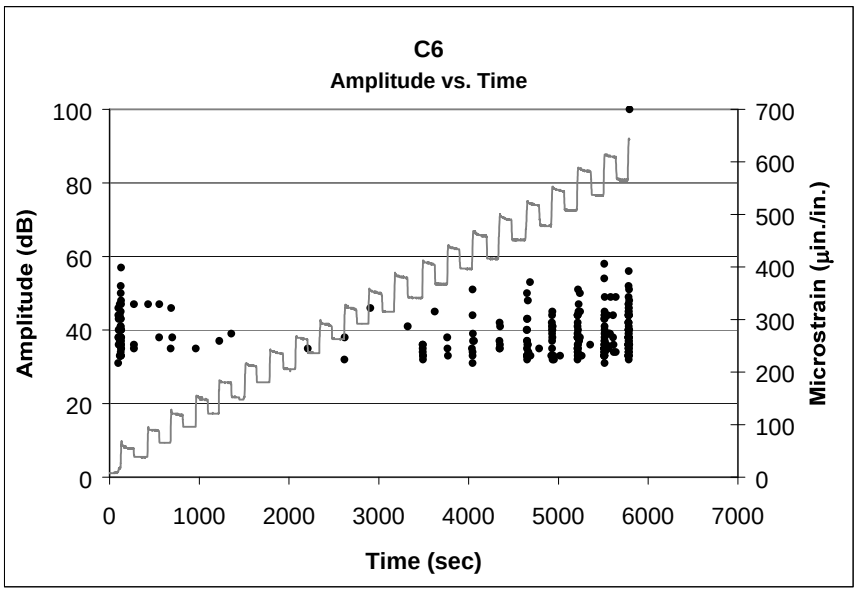

(a)

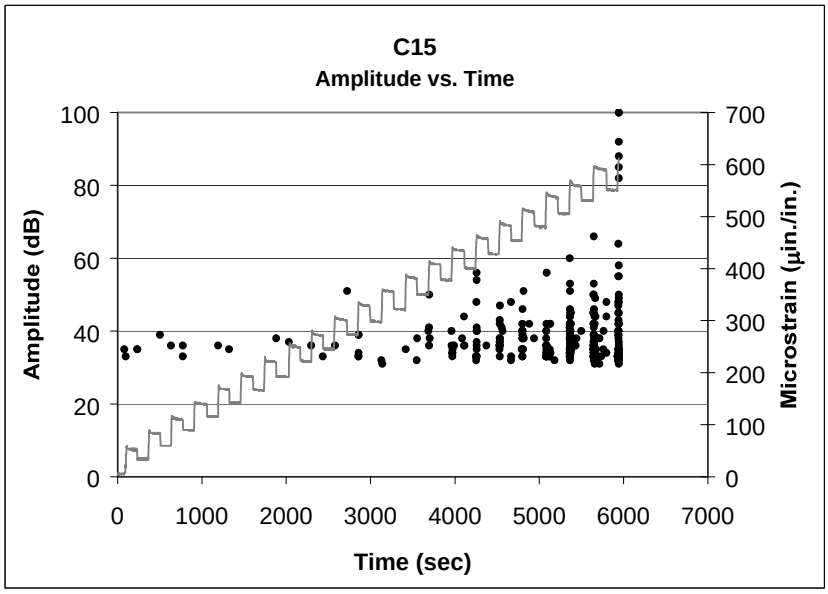

(b)

Figure 4.12 Amplitude versus time with the strain data overlapped for (a) C6 and (b) C15

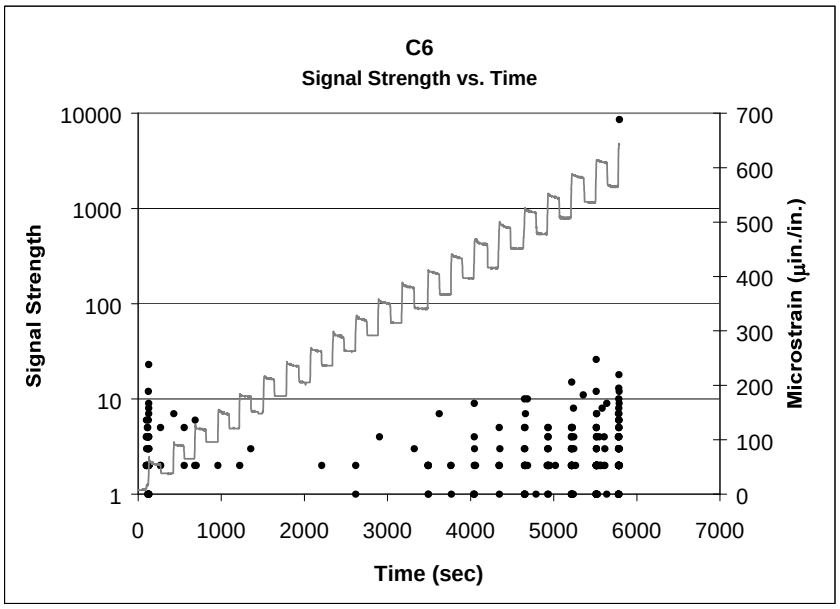

(a)

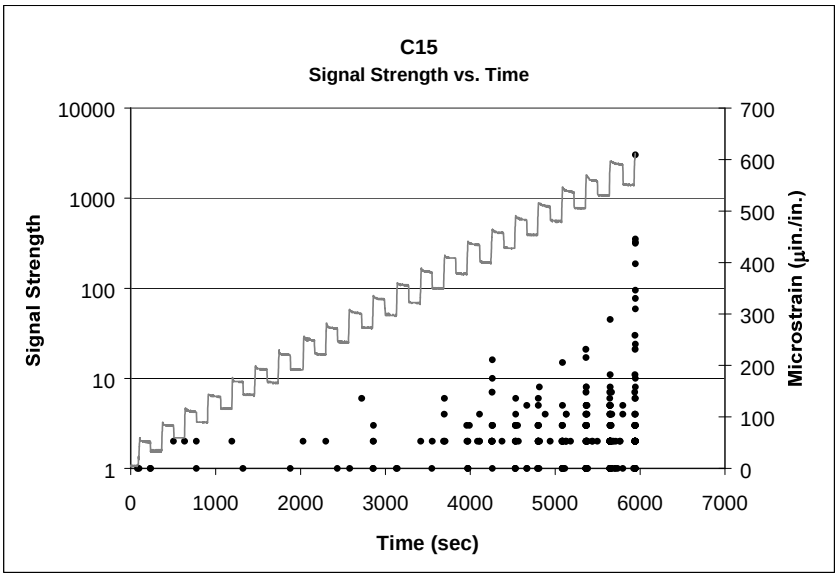

(b)

Figure 4.13 Signal strength versus time with the strain data overlapped for (a) C6 and (b) C15

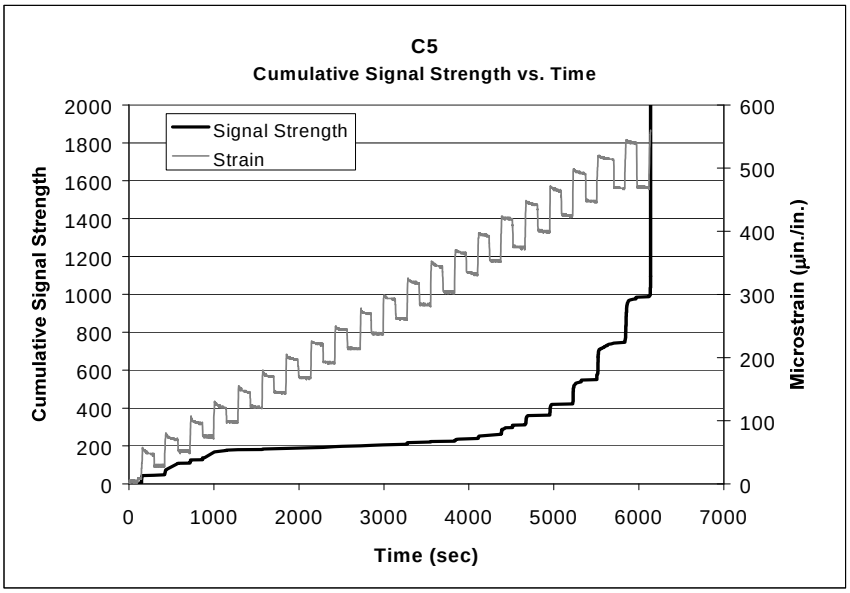

(a)

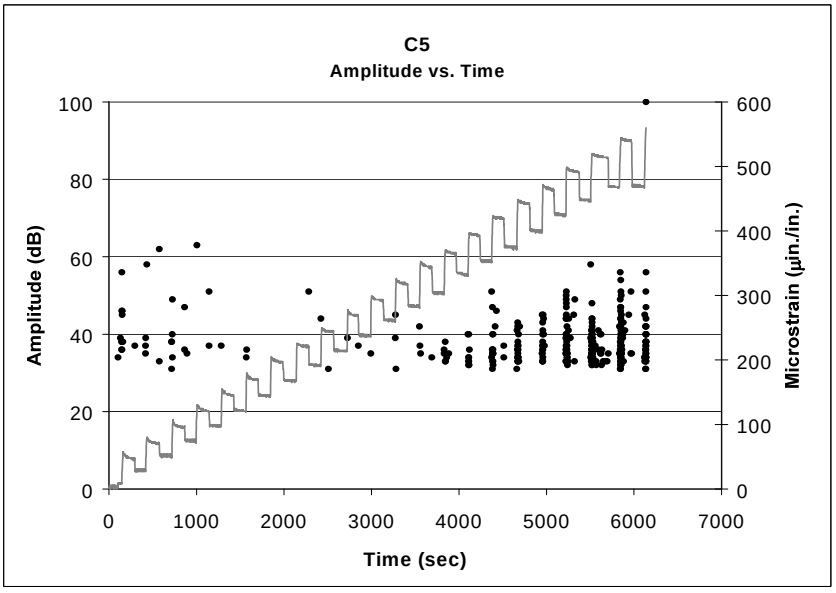

(b)

Figure 4.14 Acoustic emission data for C5, (a) cumulative signal strength versus time (b) amplitude versus time, with the strain data

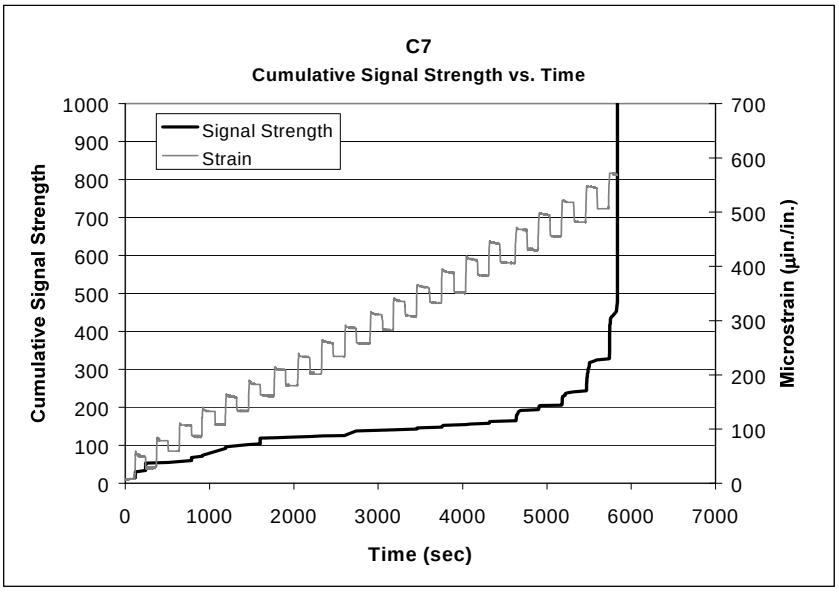

(a)

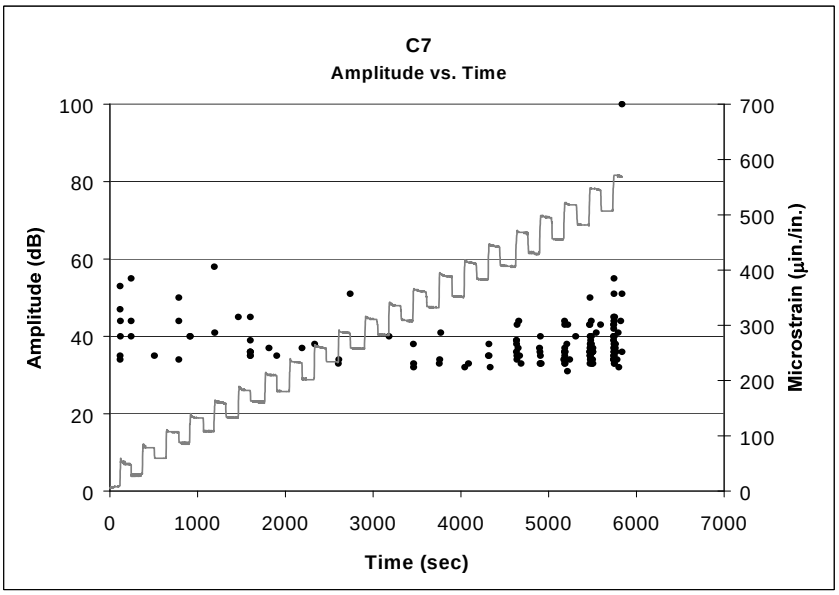

(b)

Figure 4.15 Acoustic emission data for C7, (a) cumulative signal strength versus time (b) amplitude versus time, with the strain data

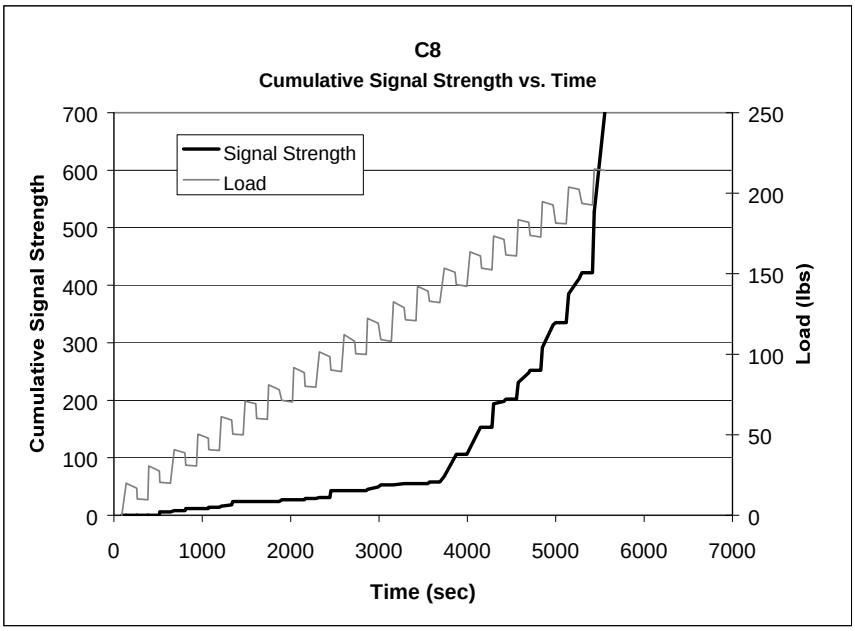

(a)

Data Not Available

(b)

Figure 4.16 Acoustic emission data for C8, (a) cumulative signal strength versus time (b) No data available for amplitude versus time

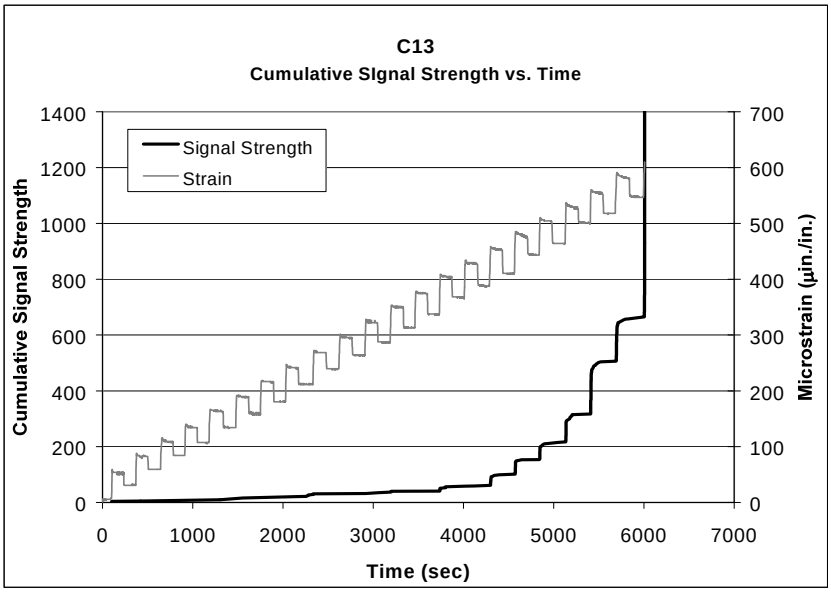

(a)

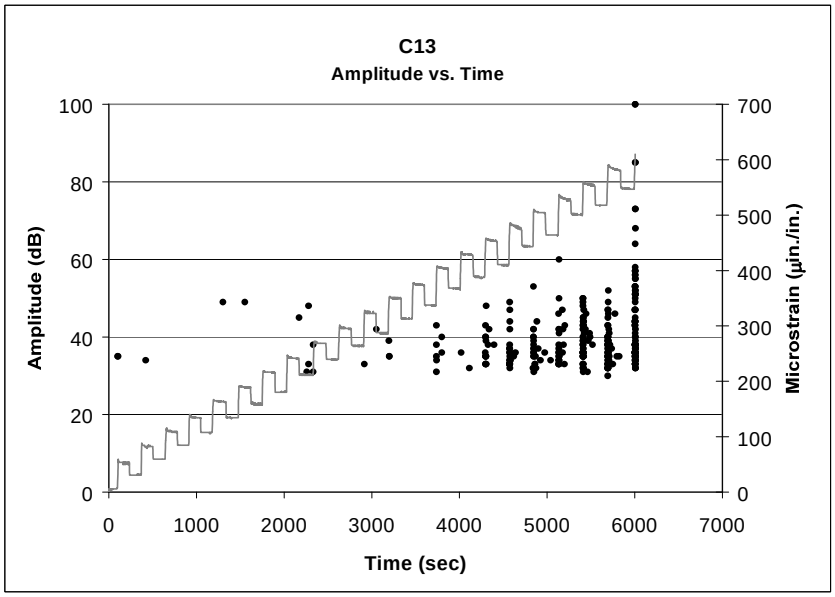

(b)

Figure 4.17 Acoustic emission data for C13, (a) cumulative signal strength versus time (b) amplitude versus time, with the strain data

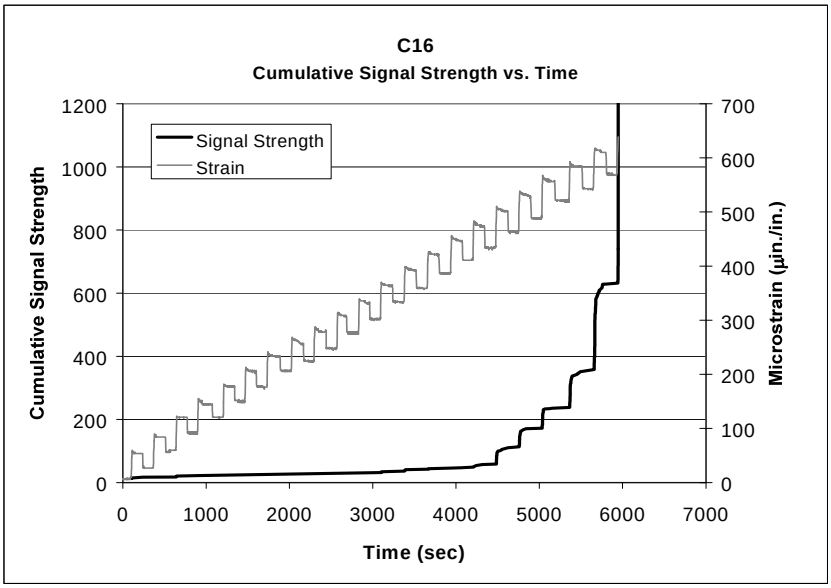

(a)

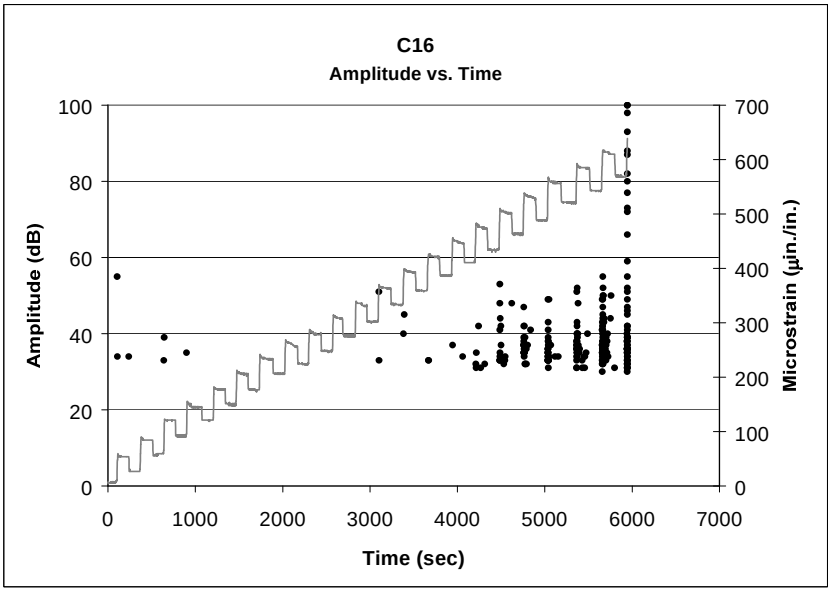

(b)

Figure 4.18 Acoustic emission data for C16, (a) cumulative signal strength versus time (b) amplitude versus time, with the strain data

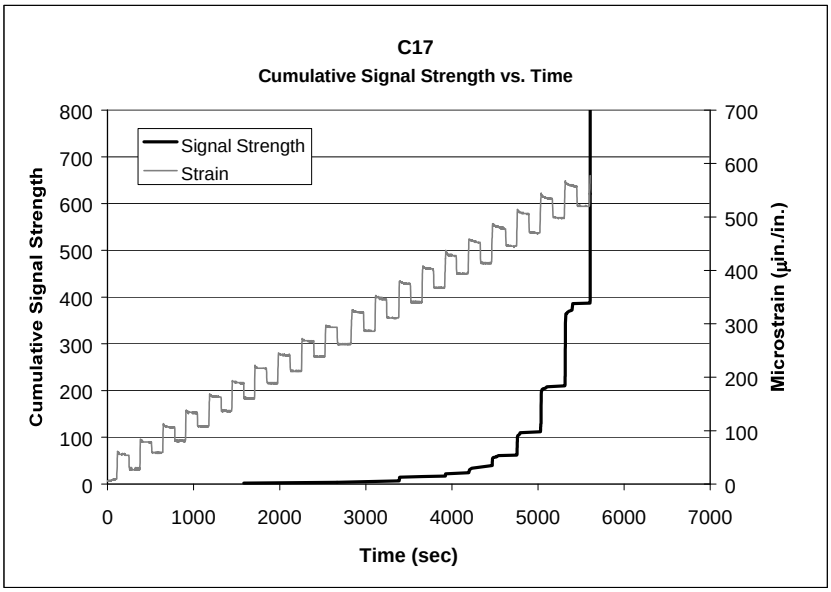

(a)

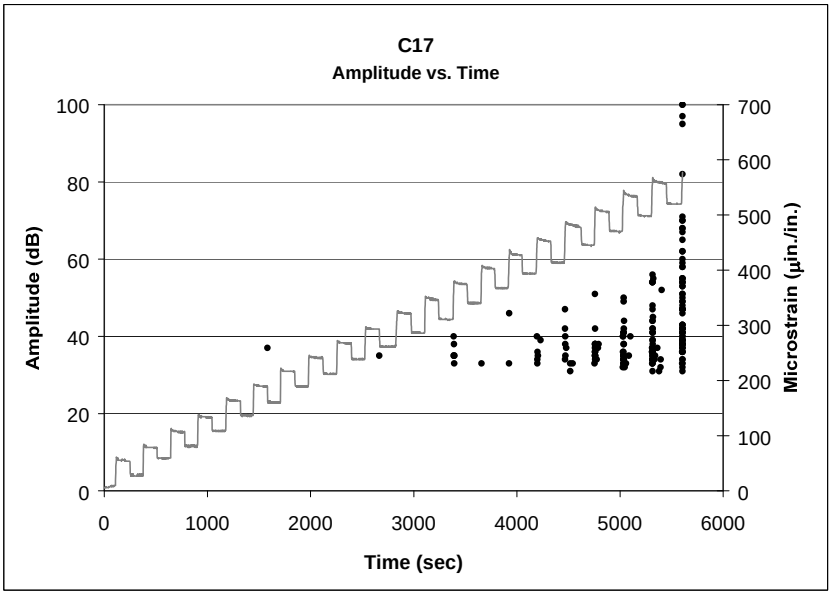

(b)

Figure 4.19 Acoustic emission data for C17, (a) cumulative signal strength versus time (b) amplitude versus time, with the strain data

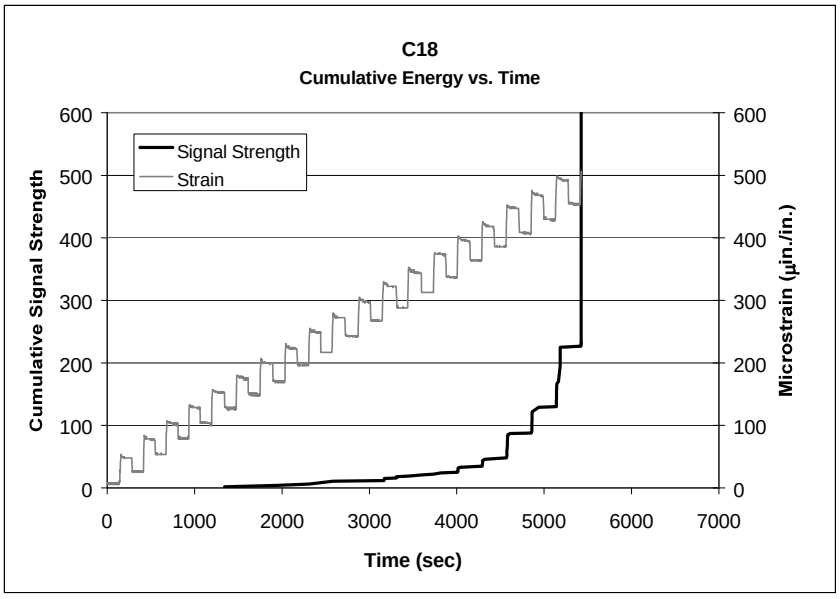

(a)

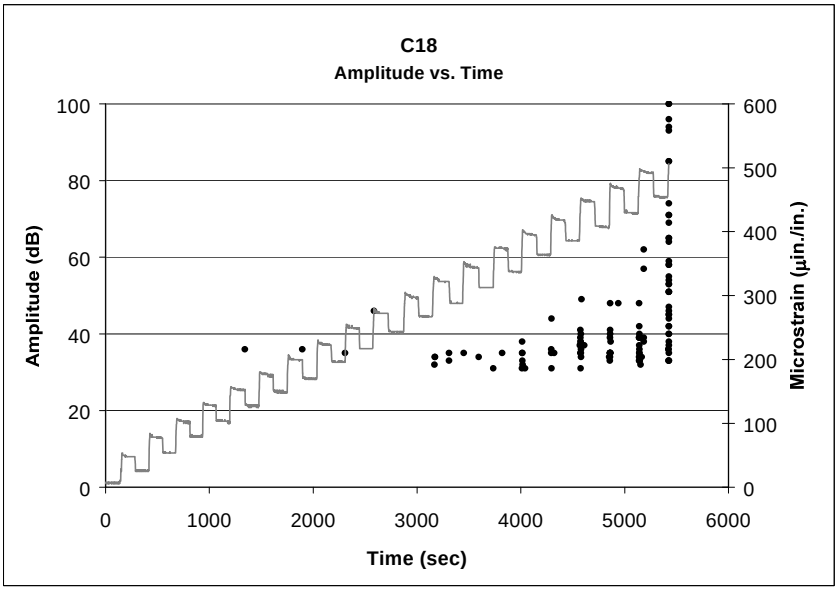

(b)

Figure 4.20 Acoustic emission data for C18, (a) cumulative signal strength versus time (b) amplitude versus time, with the strain data

4.3.2.2 Special Cases of the C-Ring Tests

Test specimens C3, C4, and C14 behaved differently than the rest of samples. The cumulative signal strength versus time plots for these tests are shown as Figures 4.21a, 4.21b and 4.21c, which exhibit fairly continuous emission with some bursts and then a large increase at failure. These specimens exhibited a greater amount of emission than a majority of the other tests, but did not show the "knee" in the cumulative signal strength curve. Thus, the acoustic emission data did not provide a warning of failure for them, at least not in the same since as it did for the specimens that displayed the typical behavior.

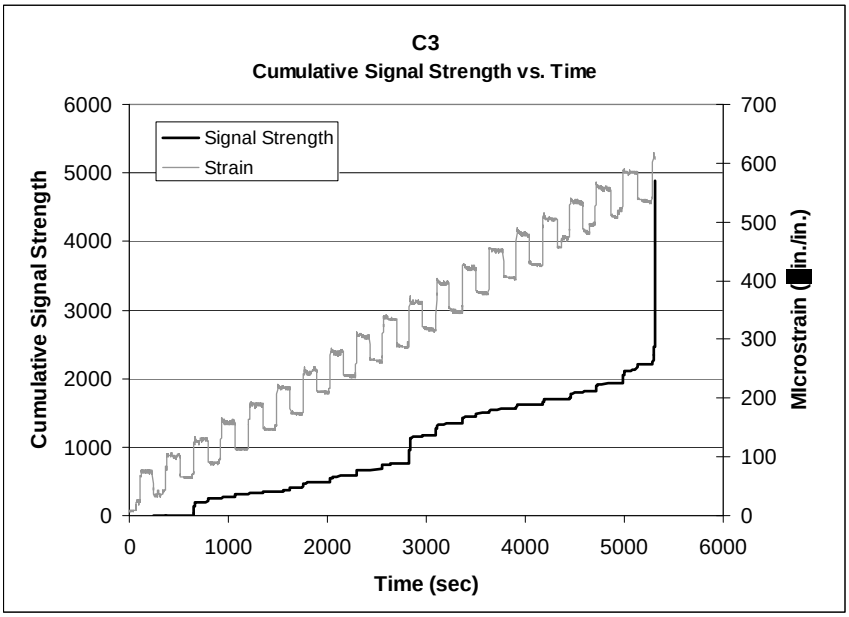

(a)

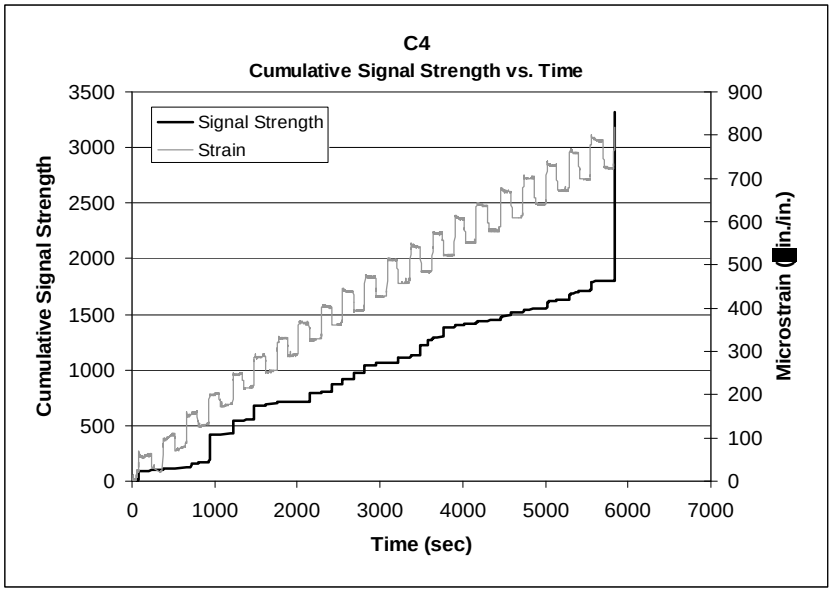

(b)

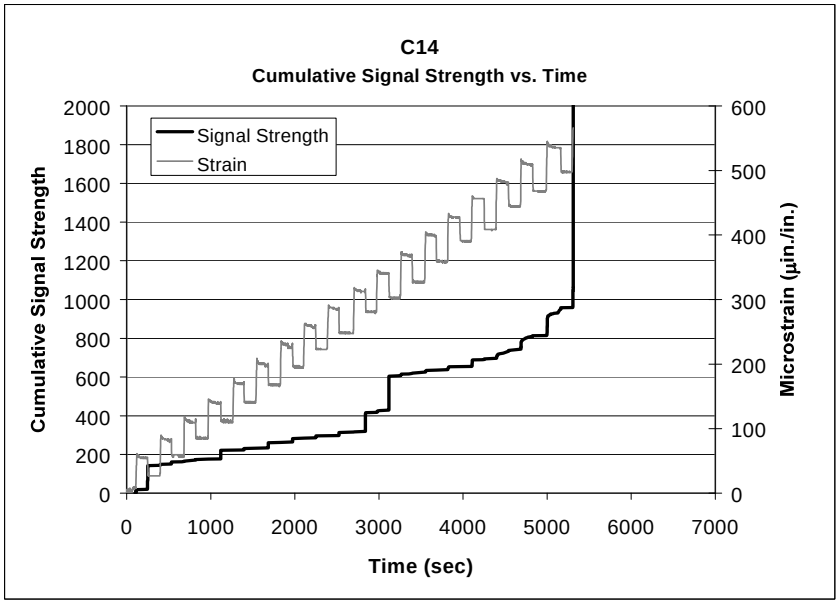

(c)

Figure 4.21 Cumulative signal strength versus time with the strain data for (a) C3, (b) C4, and (c) C14

The amplitude versus time plots for the individual hits from these specimens are shown as Figures 4.22a, 4.22b, and 4.22c. High amplitude hits coincide with the emission bursts. These large amplitude hits are likely from substantial microcracking or from the coalescing of microcracks. However, these events were not a precursor to an early failure by these specimens as their strengths were scattered and within the range of the rest of the tests. The failure loads for C3, C4, and C14 were 215.1 lbs, 229.4 lbs, and 203.4 lbs respectively.

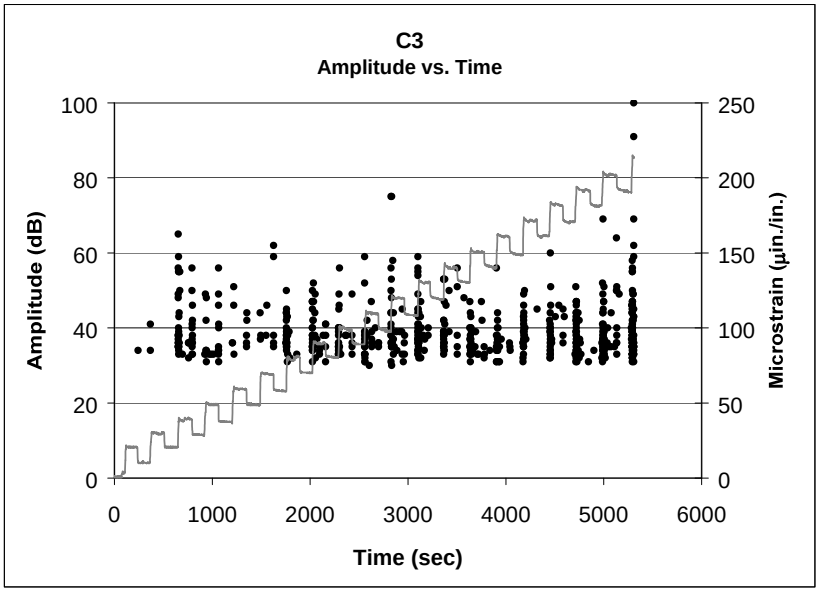

(a)

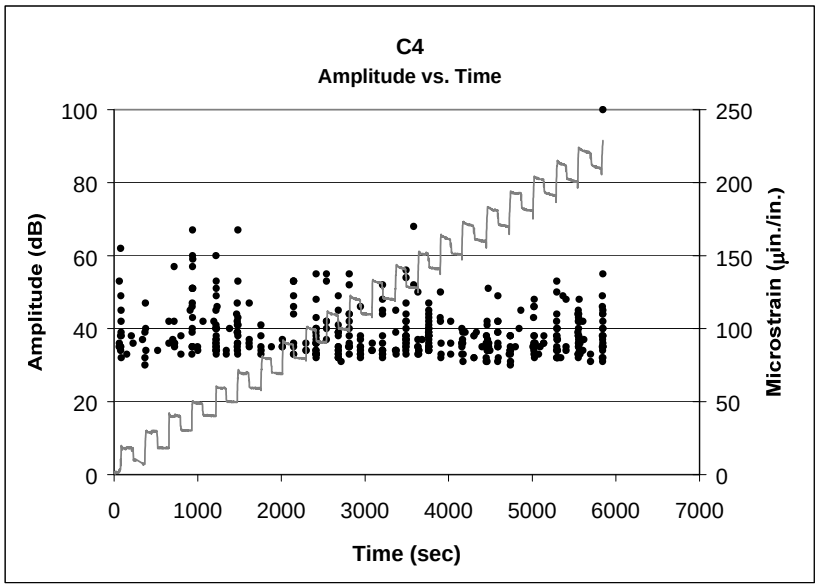

(b)

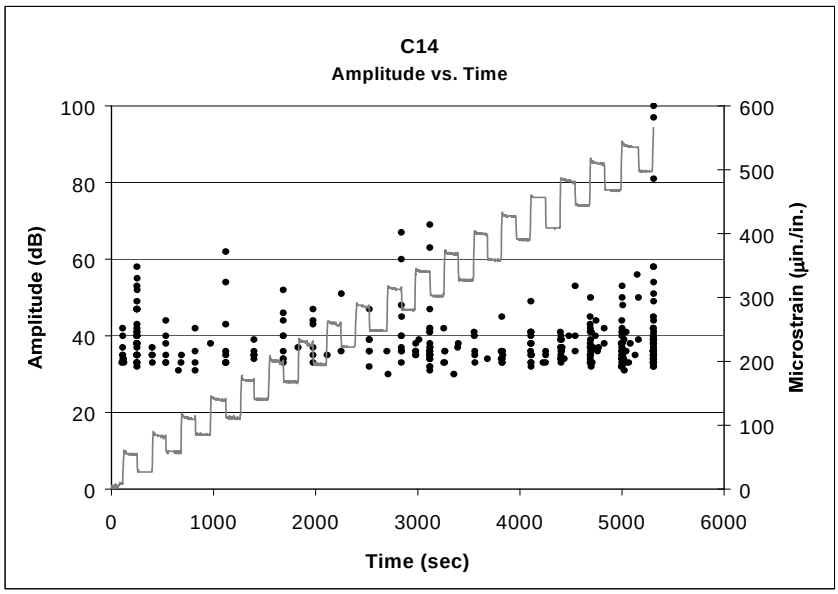

(c)

Figure 4.22 Amplitude versus time with the strain data overlapped for (a) C3, (b) C4, and (c) C14

Specimens C3, C4, and C14 are showing a significantly greater amount of microcracking than the majority of the other specimens, especially early on in the tests. The logical conclusion is that these specimens had considerable flaws in regions away from the maximum stress. There were significant events occurring that may have been caused by initial flaws, but they did not have an effect on the failure load. It is interesting to note that C3 and C4 are the only two specimens that fractured in three locations.

The next two C-ring tests are related in that they both fractured in one location and that their acoustic emission behavior did not follow the general trend found in most of the other tests. These were samples C10 and C12, which had the two lowest failure loads of all the tests. C12 failed at a load of 181.5 lbs, while C10 fractured at 193.7 lbs. The fact that these specimens only had a single failure location and also had low failure load may indicate that they contained a single flaw or multiple flaws of slightly larger size than the other specimens. The study of these samples is important because they may provide insight as to what to expect from the acoustic emission from silicon carbide tubes that are flawed. Figures 4.23a and 4.23b display the cumulative signal strength versus time charts for C10 and C12.

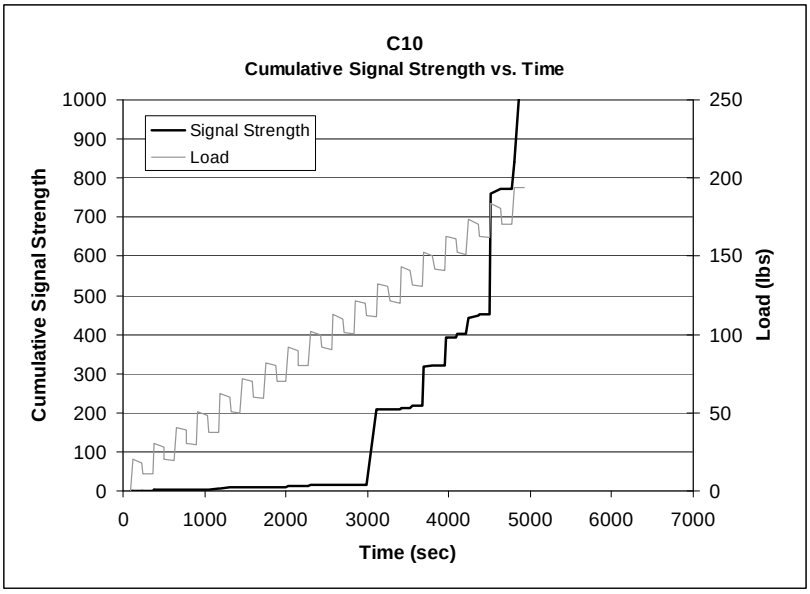

(a)

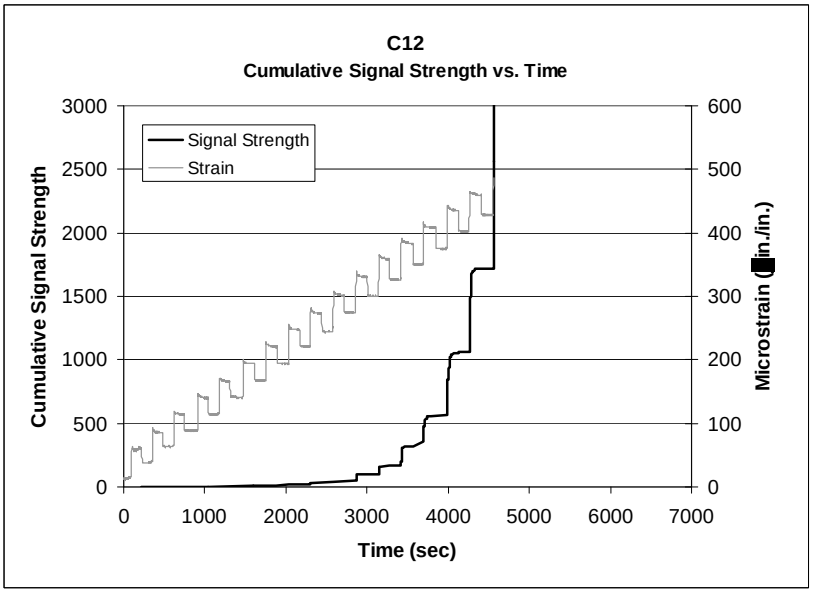

(b)

Figure 4.23 Cumulative signal strength versus time with the strain or load data for (a) C10 and (b) C12

The knees in the cumulative signal strength plots occur at a much lower strain or load level in these tests compared to the typical tests. The knee is observed at approximately 340 μin./in. for C12, while for C10 it occurs at a load of approximately 120lbs. Based on the data from the other tests, 120 lbs would correlate to a strain of approximately 320 μin./in. These strains at which the knee occurs are significantly lower than those for the typical tests (C6 and C15), which were 420 – 450 μin./in. Both of these specimens produced hits with amplitudes greater than 60 dB and with signal strength values greater than 50 much earlier in the test than other specimens did, except for C3 and C4. These larger hits occurred multiple cycles before fracture while the majority of the other specimens did not yield hits with values that high until they were on the load cycle in which they failed.

The historic index versus time for specimen C12 is shown in Figure 4.24. The historic index confirms the early knee that was discussed above, as a change is observed at approximately 2900 seconds. This time for the increase in emission correlates well with the initial knee that was observed. A larger change in the historic index occurs at approximately 3400 seconds, which is the time that the emission starts to increase rapidly.

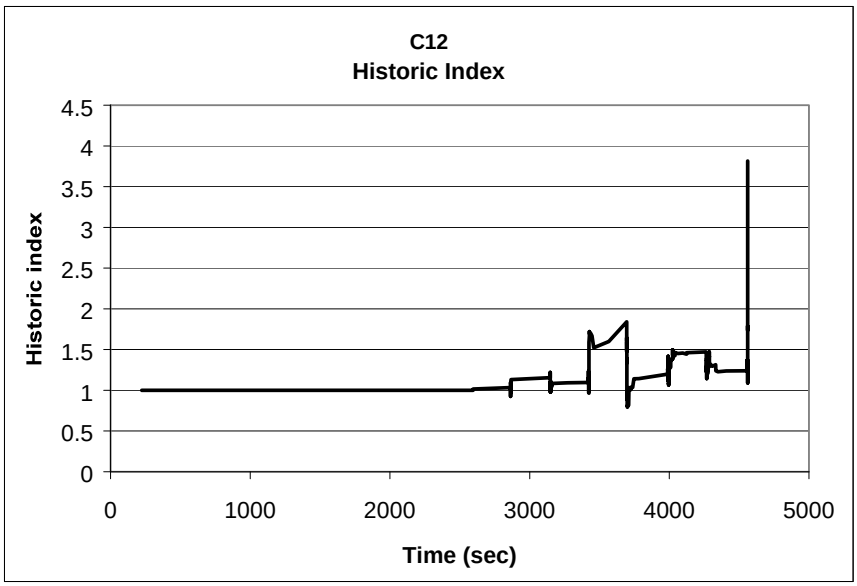

Figure 4.24 Historic index vs. time for C12

The failure location of C12 was about 10° from the midplane of the specimen. However, the failure location of C10 seemed to propagate from the edge of a visible surface abrasion near the top of the specimen. This was the only specimen that only had one fracture location, which was not near the midplane of the specimen. The others that failed at one location all fractured very close to the midplane cross-section.

Samples C10 and C12 suggest that early high energy and amplitude hits are an indication that the specimen may be significantly flawed or damaged. The fact that the fracture of C10 propagated from a visible abrasion at its outside surface and that these two specimens had the two lowest failure strengths adds credit to that theory.

The final three specimens that displayed a slightly different pattern in their emission are C9, C11, and C19. The behaviors of these specimens were very similar to each another and their failure loads were also about the same. C9 had a maximum load of 211.5 lbs, C11 failed at 201.3 lbs, while C19 reached 205.9 lbs. The cumulative signal strength versus time plots for these three specimens are shown in Figures 4.25a, 4.25b 4.25c.

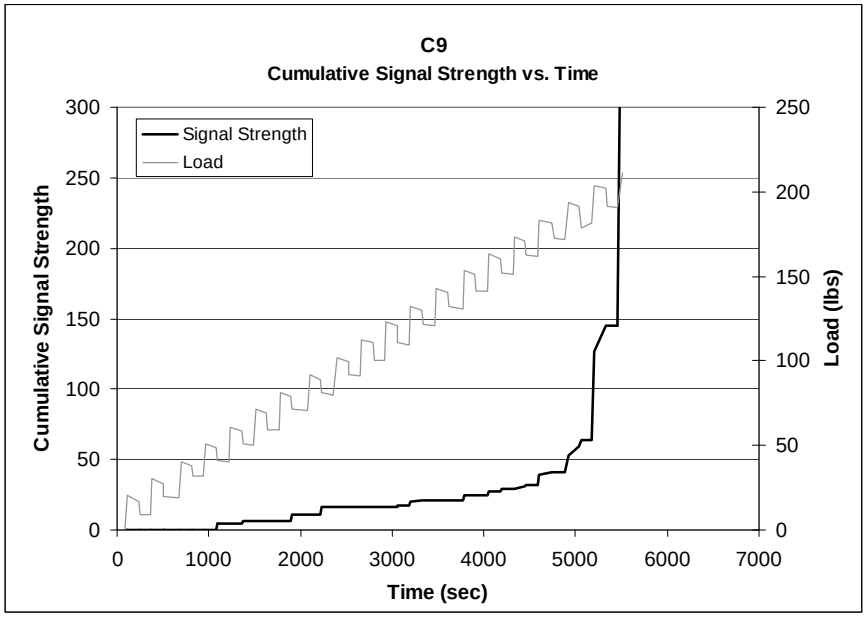

(a)

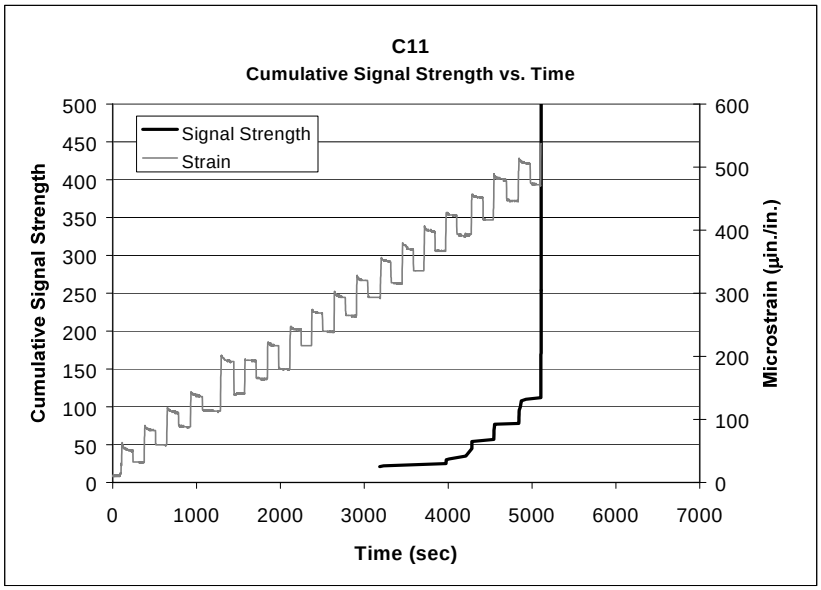

(b)

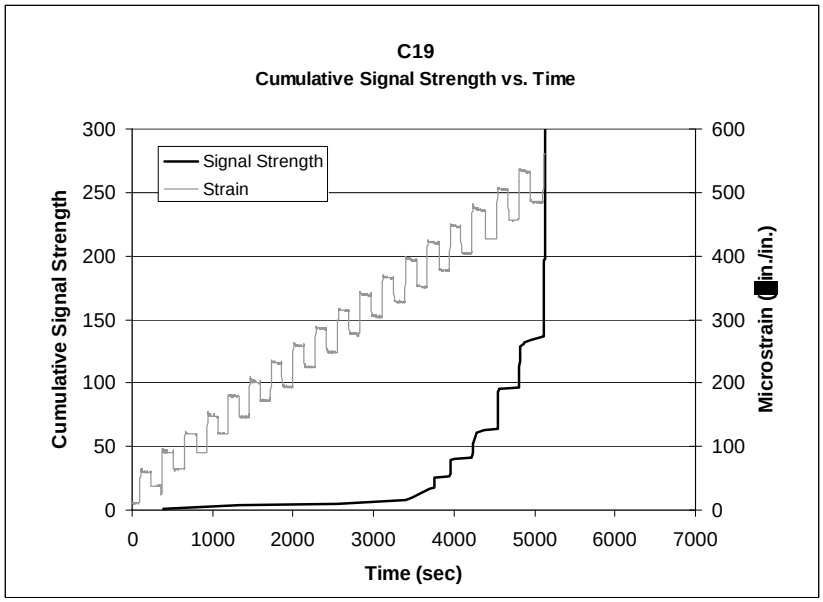

(c)

Figure 4.25 Cumulative signal strength versus time with the strain or load data for (a) C9, (b) C11, and (c) C19

These specimens behaved somewhat like the typical tests discussed previously, but they exhibited low amounts of total emission and that emission did not provide as much warning of failure as the typical samples. The lack of warning is especially true for C9 and C11. The knees in the cumulative signal strength plots occur somewhat later in these tests, similar to the typical results, but unlike C10 and C12. The knee is detected at approximately 400 μin./in. for C19 and 425 μin./in. for C11 . It occurs at a load of approximately 175 lbs for C9, which correlates to a strain of approximately 470 μin./in and is only a few cycles before failure.

Figure 4.26 is a plot of the historic index versus time for C19. The overall lack of emission and an absence of a warning of failure for this specimen can be observed in this plot.

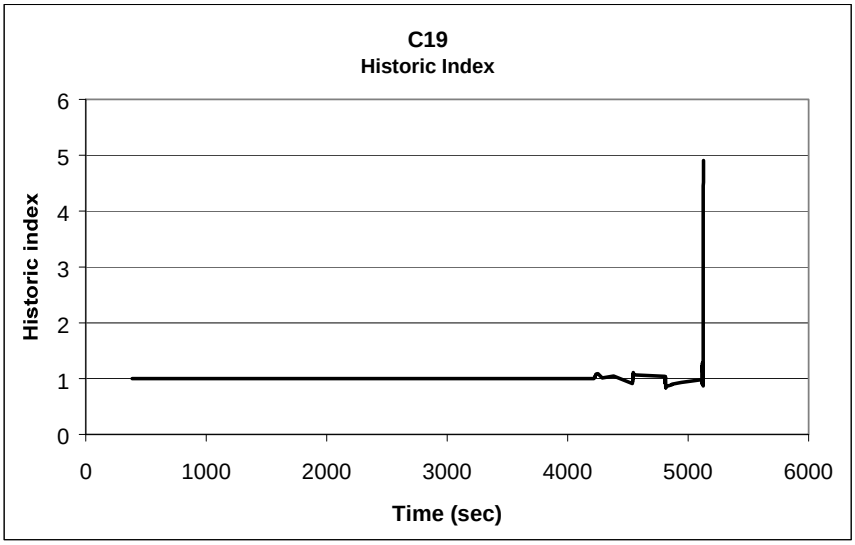

Figure 4.26 Historic index vs. time for C19

Specimens C9, C11, and C19 did not behave in the same manner as the typical tests and also did not follow one of the other patterns that were presented. The low amount of total emission in these specimens indicates that very little microcracking took place in these C-rings before failure. It is not understood what may have caused the absence of microcracking in these specimens. It should also be noted that C9 and C19 failed in one location, while C11 failed in two locations similarly to the typical tests. The failure location of C9 was directly at the midplane of the sample and C19's fracture occurred at only a small angle away from the midplane.

4.4 SUMMARY AND CONCLUSIONS FROM C-RING TESTS

The C-ring testing program yielded a tremendous amount of valuable data and information. These tests provided an excellent acoustic emission characterization for silicon carbide under flexural stresses. The repeated trends of hits with increasing amplitude and signal strength along with being able to locate the "knee" in the cumulative signal strength plot as a warning of failure were prevalent in the majority of the tests. The number and location of the fractures in the specimens provided some insight into how the specimens were behaving and how they related to the acoustic emission results that were collected.

However, the important aspect to this research is being able to detect those samples that are defected while only applying a stress that is well below a stress level that would cause damage in a good specimen. The overall C-ring results did

not necessarily yield the information necessary to achieve this goal. The results from samples C10 and C12 suggest that early high energy and amplitude hit may be an indication of a defective sample. However, the rest of the samples, which were all with in the range of 200 lbs to 236.5 lbs did not necessarily follow that trend. Some of the samples with lower maximum loads had less emission and some that had high failure loads had a great deal of emission. The fact that there was not a large range of failure loads is also problematic. Even the two weakest specimens were only 15%-20% lower than the average of the others. In a sense, it is like all the specimens that were tested were in "good" condition or in other words had relatively small flaws. This is a problem because the specimens would have be stressed to a fairly high level in order to detect any differences in the acoustic emission data and thus get an indication of the failure load. After these results, the decision was made to attempt to test some even larger specimens that would have more, larger defects. Also, in order to make any flaw significant, a more uniform stress (tensile) would be beneficial.

Chapter 5: Internal Pressurization Tests of SiC Cylinders

5.1 Experimental Procedure

The C-ring tests reported in the previous chapter provided an understanding of the acoustic emission behavior of silicon carbide. One limitation of the C-ring tests was the relatively small volume of the sample under high tensile stress, which is the cause of failure. Accordingly, it was decided to test a series of cylinders under internal pressure. With this type of specimen, all of the material in the test sample is under hoop tension, and a significant defect anywhere in the specimen could be the originating point of failure.

An acoustic emission test procedure is empirical and application specific. Knowing this, it was recognized that it would be beneficial to move the experimental program to testing samples closer to the actual tubes for which the proof test is being developed. The use of sections of the actual cylinders used in the manufacturing process moved the testing in the direction it needed and provided larger specimens with the advantage that more material would be under tensile stress.

The high cost of the full sized cylinders made it desirable to cut them into a number of shorter test sections of approximately 2 inches long. These were tested first. After experiments on eleven specimens of the shorter length, two tests were completed on much larger tubes (approximately 13 inches) that are

closer to the length of the actual part. Figure 5.1 is a picture of one of the shorter length tubes that is ready for testing.

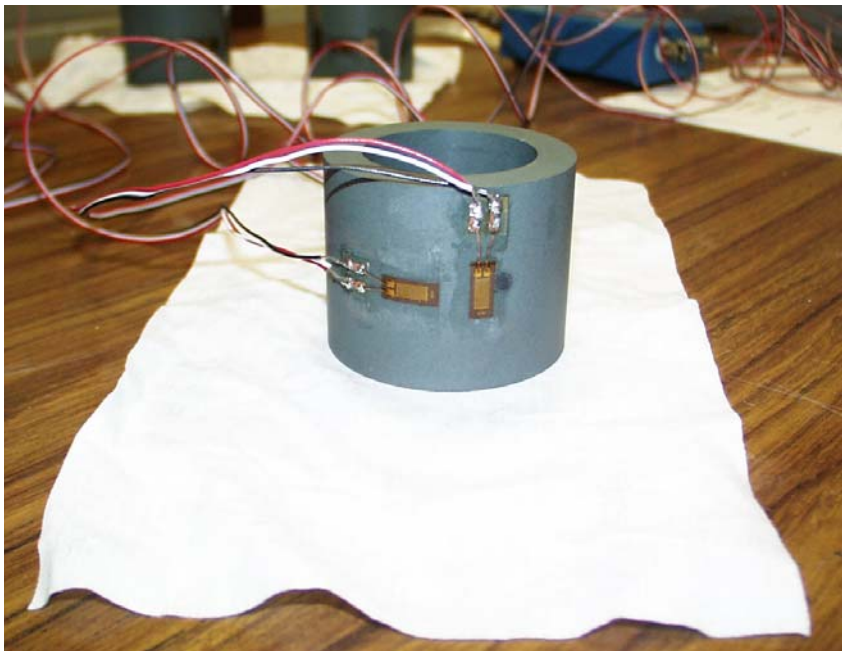

Figure 5.1 Example of a typical SiC cylinder used for these experiments

5.1.1 Test Frame and Equipment

Because of the very high value of internal pressure that would have to be achieved in order to fracture one of these specimens, a fairly complex test frame was fabricated. An internal pressure value of over 6,000 psi was estimated as the maximum pressure that may be required for these tests (a more detailed description of the estimated failure pressure is provided in Section 5.2) and it was also desired that little or no axial stress be imparted. The test frame shown below in Figure 5.2 was created to fulfill the design requirements.

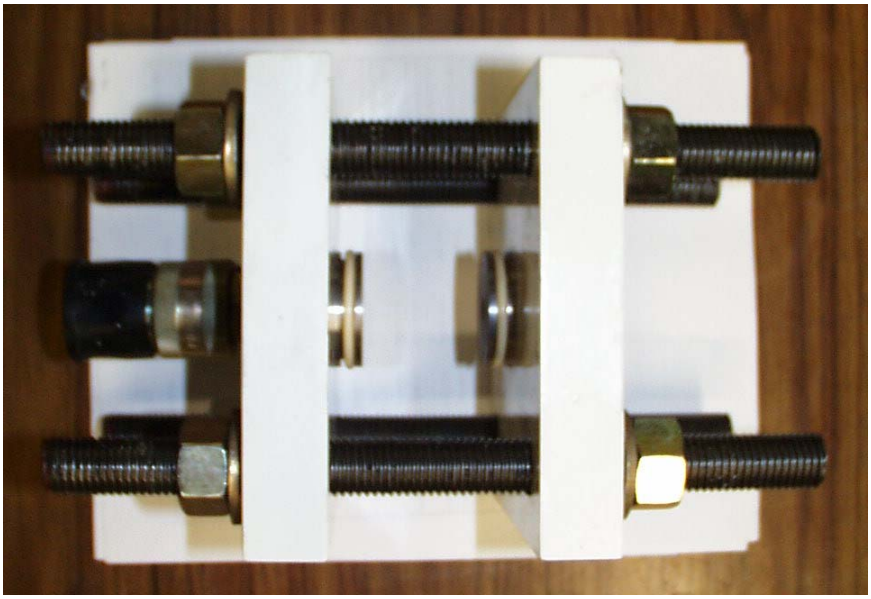

Figure 5.2 Test frame used for the cylinder tests

The basic components of the frame are two steel plates and four 3/4-inch B7 alloy steel all-thread rods. A circular plug that fits just inside the cylinder diameter is machined out of each plate. Each plug contains a groove, which is machined to tight tolerances and is where an O-ring is positioned. The O-rings are type 43005682-220 manufactured by Parker Seals and they seal the system and allow for the pressure to build up inside the cylinder. The nuts on the four rods are reacted against and they hold the steel plates in place as the pressure is increased. Because the O-ring seals fit so tightly within the samples, the nuts on the rods are also used to get the plugs all the way inside the specimen before a test begins. Each steel plate and plug has a hole in it. One of the plates has the proper fitting to attach a hose to the outside of the plate. Hydraulic fluid is pumped into the sample through the hose attachment and through the hole in the plug to

provide the pressure. A 10,000 psi capacity Power Team hand pump was used to supply the hydraulic fluid into the system. The hole in the second plate was used to try to remove all air from within the tube. Before each test, the specimen was filled with hydraulic fluid while the frame was positioned in a vertical position. This forced all the air out of the hole in the top steel plate. That hole would then be sealed tightly with a small threaded cap. For safety considerations, the frame was then placed in a containment box made out of steel. Figure 5.3 below shows the frame and test specimen inside of the containment box. A 3/8-inch thick sheet of clear plexiglass was used for the top of the containment unit. This permitted the specimen and the frame to be observed during an experiment. The same equipment was employed for the longer cylinder tests, only longer threaded rods were substituted to accommodate those specimens.

Figure 5.3 Containment box used for safety during the internal pressure tests

5.1.2 Loading

As the internal pressure within the cylinder is increased, a hoop tensile stress is imparted on the entire specimen. The circular plugs carried the axial pressure to the test frame, with the result that the axial forces in the cylinder were low and limited to that imparted by friction of the O-ring seals. The same step loading procedure that was used for the C-ring tests was used for the pressure tests on the short tubes. This loading diagram was shown in Figure 4.4. A slight variation to this procedure was used for the longer tubes. Actually, the same step pattern was used, but when the pressure reached 2700 psi, the specimen was unloaded back to zero pressure. The specimens would be cycled to 2700 psi three times in this manner, then on the fourth cycle taken to failure. The reason for using 2700 psi will be discussed later in Section 5.4.

The workings of the test system had an effect on the loading procedure. A drop in pressure (usually between 300-700 psi) would take place following a load hold after an unload. This was caused by the pressure within the pump dropping below the pressure in the rest of the system while the valve was closed during the hold. When the valve is opened in order to increase the pressure again, equilibrium in the system would have to be regained causing a quick loss in pressure within the specimen. During two of the tests, there was a problem holding the pressure at a constant level when desired. This was due to a less than perfect seal between the O-ring and the specimen. The specimens not being machined to the exact dimensions required was most likely the main reason for the improper seal, but a damaged O-ring could have also caused a problem.

5.1.3 Instrumentation

Much of the same equipment and instrumentation that was utilized for the C-ring tests was also used for the internal pressure tests. The LOCAN 320 was again used as the primary data acquisition instrument during these tests. The same R15 sensor type and external pre-amplifier were also used. Because of some violent failures during the pressure tests, a few sensors were damaged requiring new ones of the same type to be used. Since the flat ends of the tubes were not accessible, the placement of the sensor for these tests was difficult. The easiest location for attaching the sensor was just on the top of the specimen as it sits within the test frame, as shown in Figure 5.4. No matter where the sensor was placed it was always on a curved surface. Care was taken to ensure that the line contact between the cylinder and sensor passed through the center of the faceplate of the sensor. The settings for Threshold, HDT, and Rearm Time used in the LOCAN were the same for these tests as displayed in Table 4.1 for the C-ring tests.

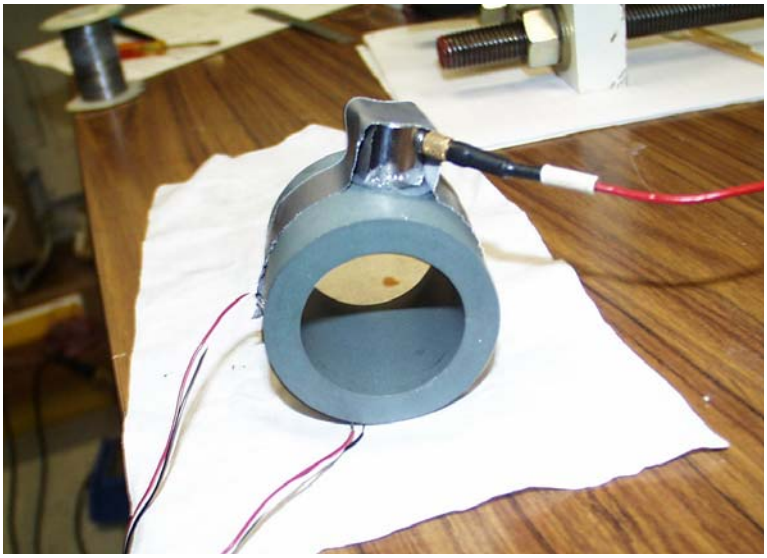

Figure 5.4 Sensor location for cylinder tests

Two strain measurements and the pressure value were recorded for each of the internal pressure tests. One strain gage was used to capture the hoop strain on the outside surface of the specimen and the other gage measured the axial strain. Figure 5.5 shows the orientation and location for these strain gages. For the first internal pressure tests, two gages of type EA-06-125BT-120 that were used for the C-ring tests were placed on the specimen separately in their proper locations. In latter tests, type EA-03-250TM-120 strain gages manufactured by the Measurements Group were used. This type of gage has the capability of measuring the two perpendicular strains on one combined gage, which made their installation easier. A 10,000 psi capacity Sensotec pressure transducer was placed at the front of the hand pump to measure the pressure value. The same external amplifiers used for the C-ring tests were also employed in these tests for the power supply and to amplify the signal for the strain gages and the pressure

transducer. The strain gage signal was again amplified 5000 times while the pressure transducer signal was amplified 300 times. Once again, the LOCAN recorded the pressure and strain once every second as parametric data.

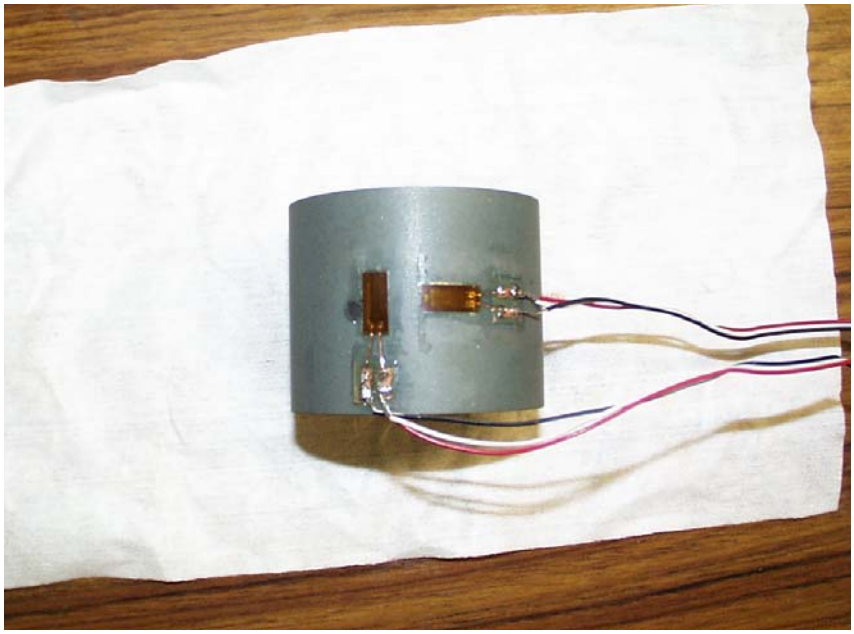

Figure 5.5 Hoop and axial strain gages on a cylinder sample

5.1.4 Sample Preparation

Due to the high pressures that were required to test these specimens, very tight tolerances were required for the dimensions of the inside diameters of the cylinders, the steel plugs, and the O-rings. The machined dimensions for the cylinder diameter and the steel plugs were based on the specifications of the available O-rings relative to the original diameter of the specimens. The inside diameter of the cylinders was machined to 1.625 (+0.002/-0.000) inches, while

the outside diameter for the steel plugs was 1.622 (+0.000/-0.001) inches. The dimensions for the O-ring groove in the steel plugs were also specified by the O-ring manufacturer.

A thin film of epoxy was applied to the inside surface of the specimens before they were installed into the test frame. The epoxy was required because the silicon carbide is a somewhat porous material. Without the coating, the hydraulic fluid would get forced out through the wall of the cylinders as the pressure is increased. A flexible epoxy was chosen so that it would not contribute to the strength of the SiC specimen or create emission at the low failure strains of these cylinders

5.2 PRELIMINARY STRESS ANALYSIS

As was done for the C-ring tests, a preliminary stress analysis was carried out. Timoshenko (1930) provides stress equations for a circular cylinder of constant wall thickness that is subjected to uniform internal pressure. The basic equations, known as the Lamé equations, are shown below and approximate the stress condition for these tests very well.

$$\sigma_t = \frac{P \cdot r_i^{\,2}}{r_o^{\,2} - r_i^{\,2}} \cdot \left(1 + \frac{r_o^{\,2}}{r^2}\right)$$

$$\sigma_r = \frac{P \cdot r_i^{\,2}}{r_o^{\,2} - r_i^{\,2}} \cdot \left(1 - \frac{r_o^{\,2}}{r^2}\right)$$

σ_t = tangential stress (psi)

σ_r = radial stress (psi)

P - applied internal pressure (psi)

r - radius at which stress is to be calculated

r_i - inner radius = 0.800 in.

r_o - outer radius = 1.175 in.

The radial stress is always compressive under this type of loading while the tangential stress is always tensile. The variation in the tangential stress through the thickness of the material is negligible for thin-walled cylinders, but is important for thick-walled specimens like these. Figure 5.6 shows the variation of the radial and tangential stresses through the cross-section when 6000 psi internal pressure is applied. The tangential stress is maximum at the inner surface of the cylinder and decreases to a stress of about 2/3 of that value at the outer surface. The ratio of the inner to outer tangential stresses can be determined by the following formula:

$$\frac{(\sigma_t)_{max}}{(\sigma_t)_{min}} = \frac{r_i^2 + r_o^2}{2r_i^2}$$

For this geometry, the maximum stress at the inner surface is 1.59 times the maximum stress at the outer surface.

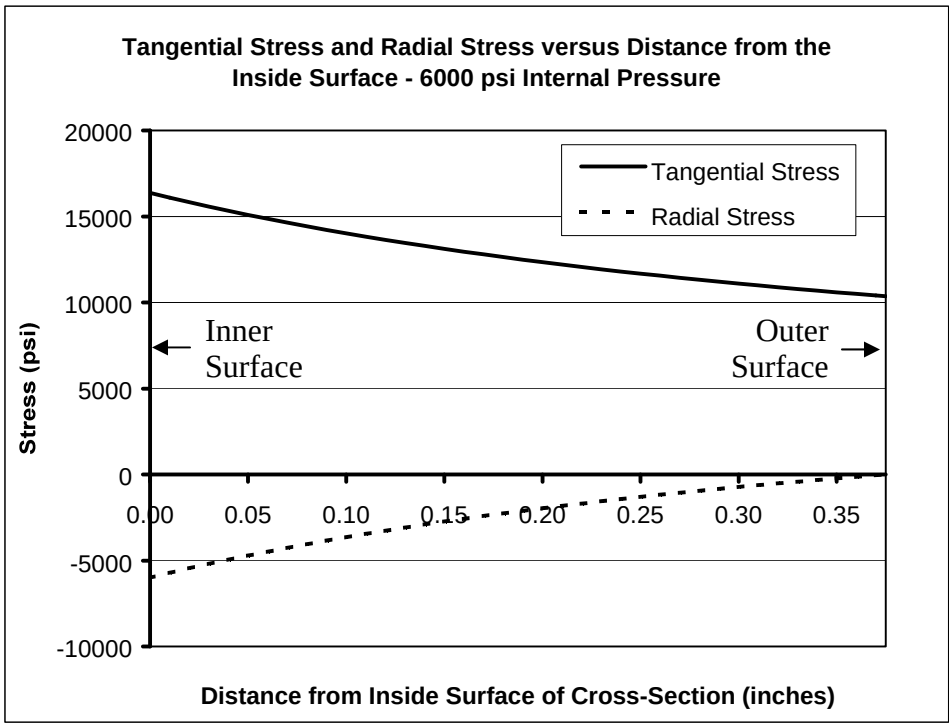

Figure 5.6 Tangential and radial stresses through the cross-section for 6000 psi internal pressure

The average stress to cause failure in the C-ring test was approximately 20,000 psi. By applying a factor of 0.85 to account for the size effects and the purely tensile stress in the specimen, a failure stress of 17,000 psi is estimated for these specimens (assuming that they are not significantly defected). Using the above formulas, an internal pressure of 6,300 psi would cause the estimated failure stress to be reached at the inner surface of the cylinder. A slightly conservative value of 6000 psi was used as the estimated maximum pressure from which the percentages for the step loading procedure were calculated.

5.3 SHORT CYLINDER TEST RESULTS

Three different variations of the silicon carbide material were used in the eleven short cylinder tests. The various material types were used to aid in trying to understand the variation in behavior that would occur between a SiC specimens in good condition compared to one in poor condition. The first six specimens (ST1-ST6) came from the same batch of uncoated, machined material. This material was similar to that used for the C-ring tests, which had an average failure stress of approximately 20,000 psi. The sponsors provided test data from bar specimen tests for this material that had average failure stresses of about 22,000 psi. The other five cylinders came from broken pieces of three different tubes that had already been used in service. One of the broken tubes was an older form of this material whose properties were not as good. The average failure stress of this type of SiC was about 13,000 psi according to previous test data. Two short cylinder samples (ST8 and ST11) were salvaged from this piece of broken tube. The other pieces of tube were a much more advanced and recent form of this material, which had previous failure stresses of approximately 26,000 psi. Three short cylinders (ST7, ST9, and ST10) were machined out of this part and were implemented into the testing program.

5.3.1 Strength and Fracture Results

A summary of the maximum pressures reached to cause fracture of the cylinders is shown in Figure 5.7.

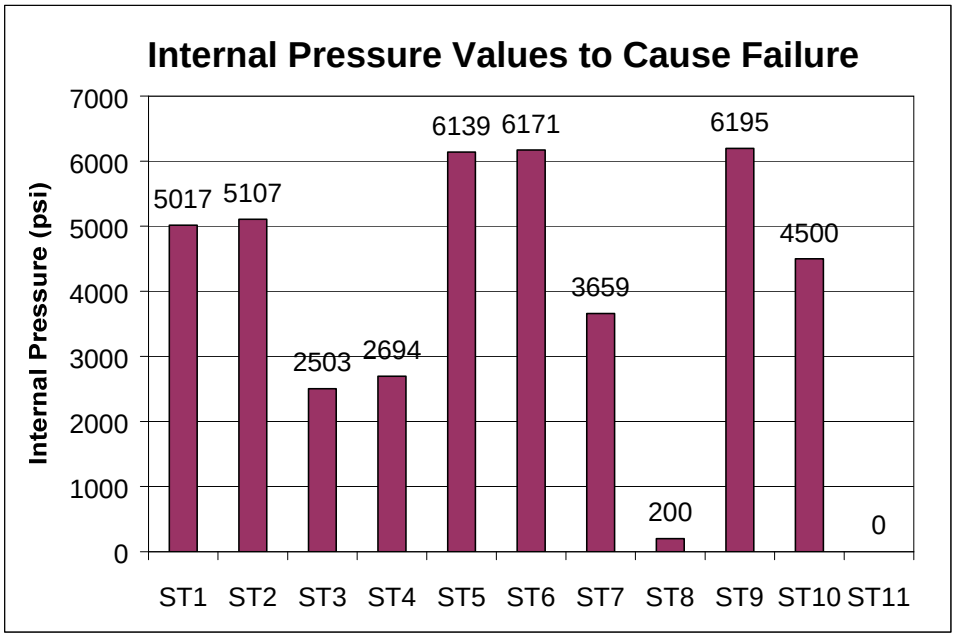

Figure 5.7 Failure pressures for short cylinders tests

The failure pressure of ST8 and ST11 immediately stand out as being extremely low. These specimens were the two that came from the weaker, older tube that had been used in service. This material was not strong enough to withstand the stresses caused by machining the inside diameter as ST8 had visible cracks on its inside surface before the test began. Although not visible, it appears that ST11 had similar defects. ST8 fractured during the very first load increase and reached a pressure of approximately 200 psi while ST11 fractured before the test even began during the tightening of the nuts that forces the steel plugs and O-rings into the tubes. Very little valuable information was obtained from these tests.

The maximum pressures for the remainder of the tests were between 2503 and 6171 psi, so the greater variation in failure stresses was achieved as desired.

The average failure pressure in these specimens, not including ST8 and ST11, was 4665 psi while the standard deviation was 1445 psi. Specimens ST5, ST6, and ST9 all reached and exceeded the values of 6000 psi, which was the estimated failure pressure calculated in the stress analysis of Section 5.2. The remainder of the specimens failed at pressures much lower than that, which suggest that they either contained larger flaws or flaws that were located and orientated in such a way as to significantly reduce the strength of the specimen.

Table 5.1 provides additional information on the strength and fracture results from the short cylinder tests. The elastic modulus is calculated by dividing the estimated maximum stress at the internal surface by the estimated maximum hoop strain at the internal surface.

Specimen	Failure Pressure (psi)	Est. Maximum Stress (psi)	Max. Measured Hoop Strains (μin./in.)	Est. Max. Hoop Strain at internal surface (μin./in.)	Mod. of Elasticity X 10^6 psi	Number of Failure Locations*
ST1	5017	13551	260.2	413.7	32.75	> 10 (7)
ST2	5107	13794	277.7	441.5	31.24	>10 (7)
ST3	2503	6761	116.5	185.2	36.50	4 (4)
ST4	2694	7276	147.6	234.7	31.01	5 (5)
ST5	6139	16581	289.3	460.0	36.05	>10 (8)
ST6	6171	16668	297.1	472.4	35.28	>10 (8)
ST7	3659	9883	147.6	234.7	42.11	6 (6)
ST8	200	540	-	-	-	2 (2)
ST9	6195	16733	242.7	385.9	43.36	>10 (9)
ST10	4500	12155	192.2	305.6	39.77	>10 (8)
ST11	0	0	-	-	-	3 (3)

* The first value in this column is the number of substantially large failure sections from the test, while the number in parenthesis is the number of longitudinal strips created (some of the longitudinal strips may have been broken into more than one section).

Table 5.1 Strength and fracture results from the short cylinders tests

The average maximum hoop (tangential) strain measured on the outside surface at failure for the tests was 219 μin./in. The axial strains that were recorded were extremely low as was desired for these tests and this will be discussed further later. The average hoop strain of 219 μin./in. is much lower than the average maximum strains calculated for the C-ring tests, which was 591.4 μin./in. However, it must be kept in mind that the strain gages were placed on the outside surface of the cylinder. It was shown in Section 5.2 that the maximum stress/strain occurs at the inside surface of the cylinder. The difference in stress/strain, assuming a constant elastic modulus throughout the cylinder, for the inside surface versus the outside surface is a factor of 1.59 for this geometry. By applying the 1.59 factor, the average maximum hoop strain on the inside surface is calculated to be 348 μin./in, which is still well below the average calculated for the C-ring. This result is to be expected because of the poor performance of some of the cylinders and it also appears as though the material used for test ST7, ST9, and ST10 (sections of a broken tube of high quality material used in service) had a higher modulus of elasticity than the material used for the first six short cylinder tests and the C-ring tests. There is also the effect of some negative radial stress on the inside surface of the tubes. If the average of the two cylinders that did reach the 6000 psi pressure from the first six short tube tests is taken with the 1.59 factor applied, the average maximum hoop strain on the inside surface of these specimens is 466 μin./in. This value is approximately 80% of the average maximum strain measured in the C-ring tests. That result correlates well considering the estimated failure stress in the cylinders was taken

as 17,000 psi, based on an 85% factor for size effects. This factor was used to reduce the measured average stress of 20,000 psi from the C-ring results.

Figure 5.8 shows typical axial strain data that was observed during each test of the short tube tests. Since there is no directly applied axial force on the specimen and because of the tensile hoop strain induced on the specimen, the axial strain should be compressive due to Poisson's Effect.

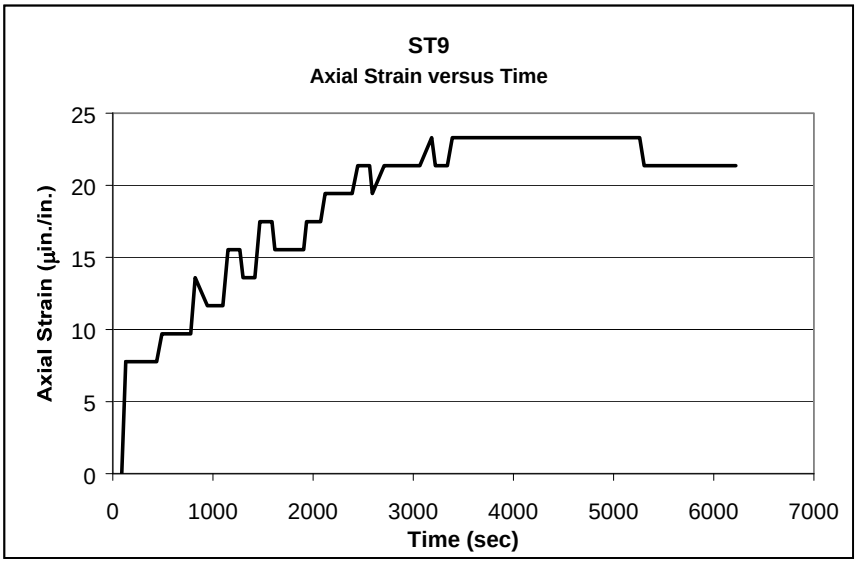

Figure 5.8 Axial strain versus time for ST9

However, the measured axial strain was tensile (although a very small value) at the beginning of the tests and then stayed fairly constant for the remainder of the tests. The tensile axial strains may have been caused by a bending effect on the short cylinder. This occurs because there is no internal pressure on the ends of the cylinder beyond the O-rings and the middle of the cylinder is expanded more than the ends. This seems to be confirmed by the long cylinder tests (Section 5.4.1),

which show negative axial strain when away from the ends. The bending effect causes a tensile axial strain on the outer surface and a compressive axial strain at the inner surface near the longitudinal center of the specimen. Another possible reason for the tensile strains is the pressure pushing the steel plugs apart. The friction from the O-rings could cause the cylinder to be pulled with the plugs. This effect would be a better explanation for the tensile axial strains leveling off later in the tests, as the pressure overcomes the friction coefficient.

As in the C-ring tests, the way in which the specimens fractured provides additional insight as to their behavior. Referring back to Table 5.1, the samples that attained an internal pressure of at least 2500 psi shattered in many pieces of primarily longitudinal strips. There was also a general trend that the higher the pressure that the specimen sustained, the more fracture locations there were. Figure 5.9, which is a plot of the number of longitudinal failure strips versus the failure pressure, shows that trend. The two weaker specimens that also contained significantly larger defects before the test only fractured into two or three longitudinal pieces. Figure 5.10 shows examples of failed specimens. Figure 5.10 (a) is the fracture pieces retained from specimen ST5, which reached an internal pressure of 6139 psi. A picture of the sections from ST8, which failed during the first loading increment (approximately 200 psi), is shown in Figure 5.10 (b).

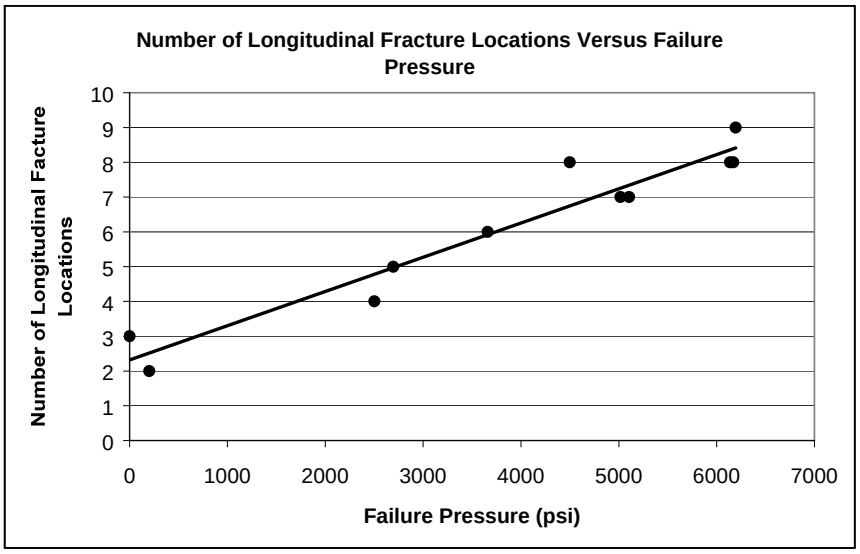

Figure 5.9 The number of longitudinal fracture sections versus failure pressure

(a)

(b)

Figure 5.10 Examples of the fractured sections from the short cylinder tests (a) ST5 (b) ST8

These fracture results can also be explained by the theory presented in Chapter 4 for the fracture of the C-rings. For a specimen that reached a high internal pressure, the entire specimen would be at a very high stress level. As the specimen would begin to fracture in one location, the stresses would get transferred to other locations causing many failure locations that appeared to occur simultaneously. For a specimen that did not reach as high of an internal pressure, the same phenomena would take place, but less fracture sites would be created. The majority of the volume of the specimen, in this case, would not be under as high a stress. Thus, when one location began to fracture and the stresses were redistributed, only a limited number of other locations would reach a critical

stress. For specimens ST8 and ST11, the stress was so concentrated around some severe initial defect, that fracture only occurred in enough sites (two or three) to drop the load.

The effect on these results of initial stresses and defects imparted on these specimens from the machining of the inside diameter and also from the force of pushing the steel plugs with the O-rings into the specimens should be considered. The strains were monitored during the installment of the plugs in the specimens and very low strains were typically recorded. They gradually decreased before the test as the O-ring deformed with time. However, the strain gages were placed at the center of the specimen and it is possible that locally high stresses were induced at the ends of the cylinders during the installment of the plugs into the specimens.

5.3.2 Acoustic Emission Results

The acoustic emission data from the tests on the short cylinders were not as promising as that from the C-rings. There were no general trends found within a majority of the tests. Therefore, a more in depth analysis of the data was conducted to see if more insight could be gained. The emission data were separated into hits that occurred during new loading, reloading, and load holds. A reload is considered a load increase at a time when the load is still lower than its previous maximum. A new load is a load increase at loads that the specimen has not been up to previously. Figure 5.11 shows the load hold, reload, and new loading times during a typical loading cycle. These data could then be analyzed

independently. Although there was not a single repeating general trend in these tests, there were groups of specimen whose AE patterns were quite similar.

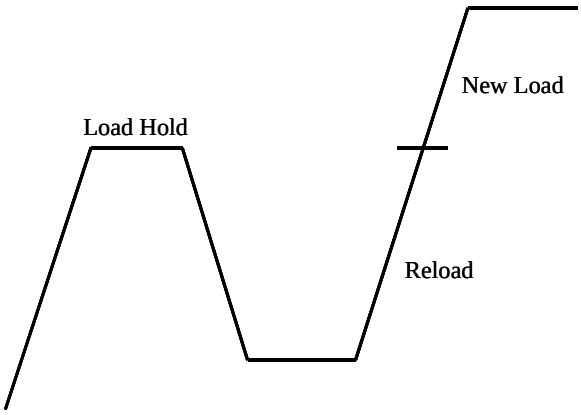

Figure 5.11 A typical loading cycle showing the load hold, reload, and new load times

5.3.2.1 Specimens Showing a Warning of Failure

Two cylinders, ST1 and ST3, displayed a warning of failure in their acoustic emission data. ST1 was very successful considering it was the first attempt at this new type of experiment. There was a slight problem holding the load once a high pressure was reached that was due to a faulty hose. The hose was replaced for the tests that followed. Figure 5.12 shows the cumulative signal strength versus time plot for ST1. Although not much can be discerned from this plot other than a jump in emission at approximately 3800 seconds due to an accidental pressure drop, further analysis of the data displays a warning of failure.

The emission data that occurs during the pressure drop may be at least partially due to background noise.

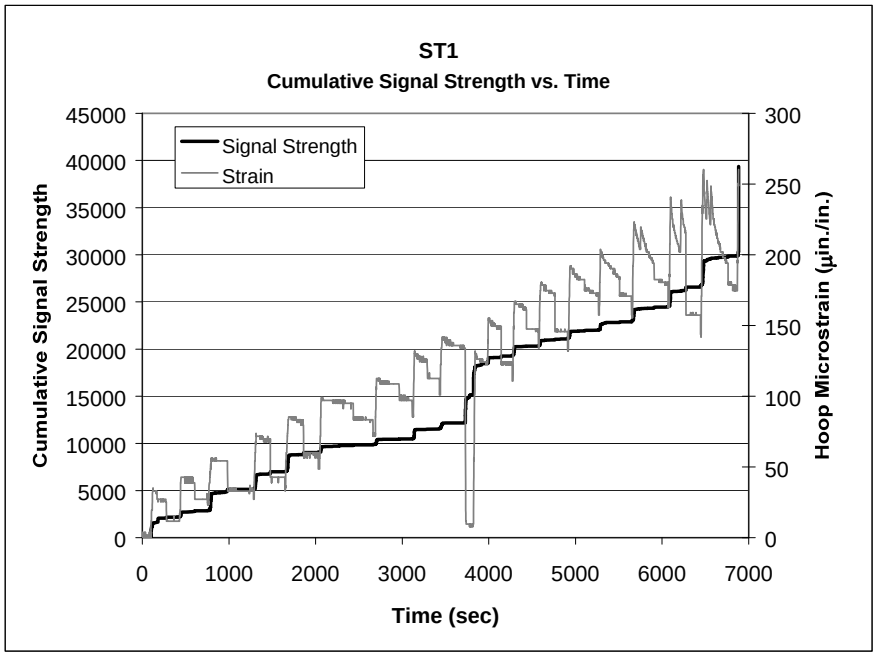

Figure 5.12 Cumulative signal strength versus time for ST1

Separating the data into the new load and reload data and also the load hold data shows that a warning of failure was exhibited by the AE from this test. Figure 5.13 (a) shows the cumulative signal strength for each pressure step for only the new load and reload data. The pressure steps are plotted on the horizontal axis in terms of the percent of the estimated maximum pressure. The estimated maximum pressure was calculated as 6000 psi during the stress analysis discussed in Section 5.2, which was based on the Lamé equations. This provides a common base for all tests for those types of plots. Other than some early emission during the first few load steps and the jump that occurred during the

pressure drop, the emission levels are relatively constant until about 85% of the maximum pressure is reached and then the emission increases at each load step until failure. Figure 5.13 (b) shows the amplitude values versus time for each individual hit for the new load and reload data. Again after the accidental load drop, a trend of increasing amplitude hits can be observed with the increasing pressure levels.

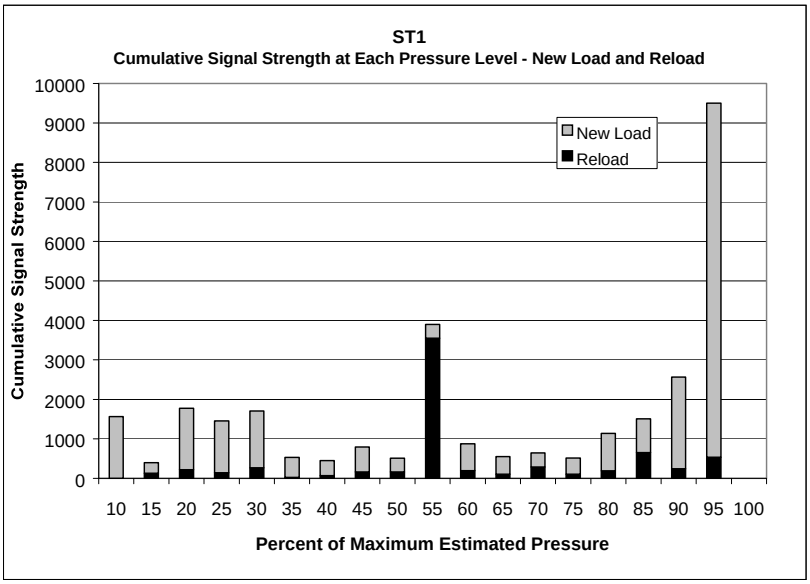

(a)

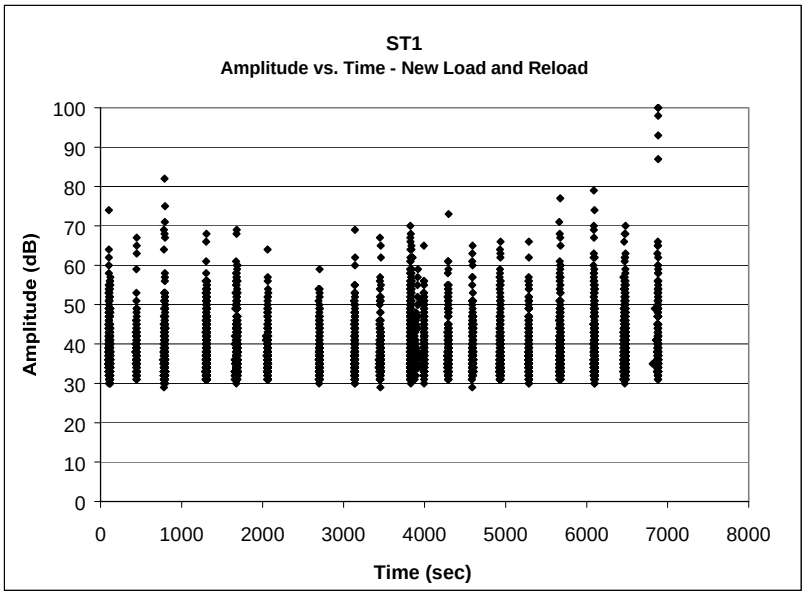

(b)

Figure 5.13 New load and reload data from ST1 (a) cumulative signal strength at each pressure step (b) amplitude versus time

The load hold data confirms this trend as well. Figure 5.14 shows the cumulative signal strength at each load level during the load holds. After about 65% of the maximum load is reached, the cumulative signal strength at each pressure level shows a generally increasing trend with increasing pressure.

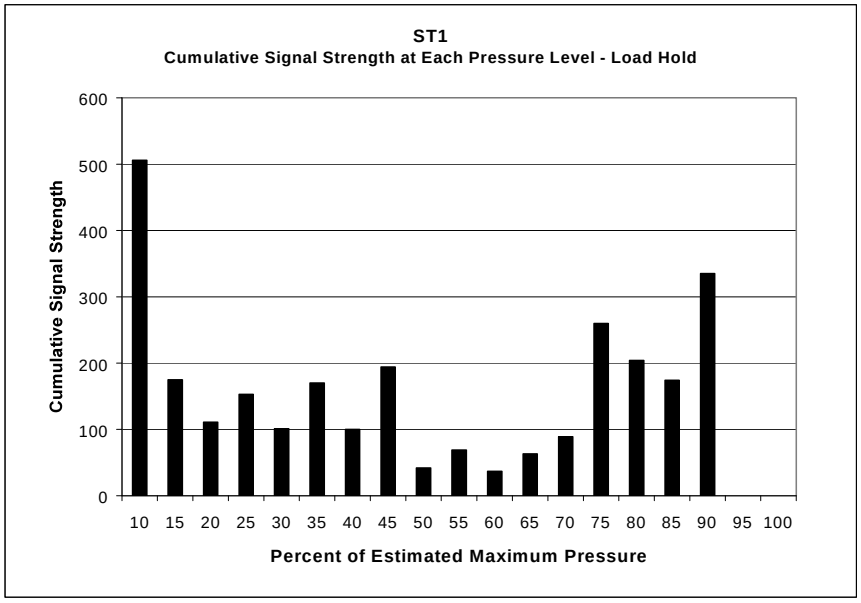

Figure 5.14 Cumulative signal strength at each pressure level during the load holds for ST1

The Felicity Effect was examined as a possible evaluation criterion for these tests as well. The Felicity Ratio is the ratio of the load or strain at which a significant amount of emission occurs to the previous maximum load or strain that the specimen has endured when cyclic loading is used. Significant emission is defined as 30 total hits, a cumulative signal strength of 70, or a single hit with a amplitude of 60 dB or greater. These values were based on previous experience and by trying different values to see which estimated an important occurrence the best. One value of the Felicity Ratio can be calculated for each 5% pressure increase in the step loading procedure for the short tube tests.

Figure 5.15 shows the value of the Felicity Ratio for ST1 plotted against the estimated maximum pressure. The plot shows a conventional pattern from the

Felicity Ratio data. The fairly high value (close to 1.0) that is consistent throughout most of the test is an indication that the specimen is not appreciably damaged at those times. The Felicity Ratio then decreases near the end of the test, which is a warning that condition of the specimen is worsening and that it is approaching its failure pressure.

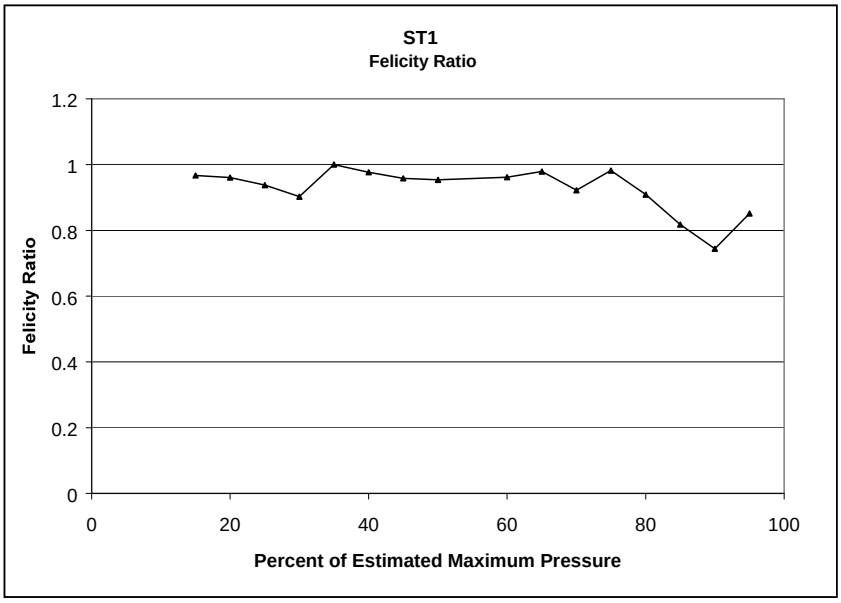

Figure 5.15 Felicity Ratio versus the percent of estimated maximum pressure for ST1

Specimen ST3 displayed a similar behavior to ST1. It should be noted that ST3 only reached a maximum internal pressure of 2503 psi while ST1 reached 5017 psi. Also, the total amount of emission for ST3 at a given strain level is much less than ST1, but it also displayed warnings of failure, Figure 5.16 is the cumulative signal strength versus time plot for ST3 and it shows and ever increasing slope for the emission as the pressure is increased.

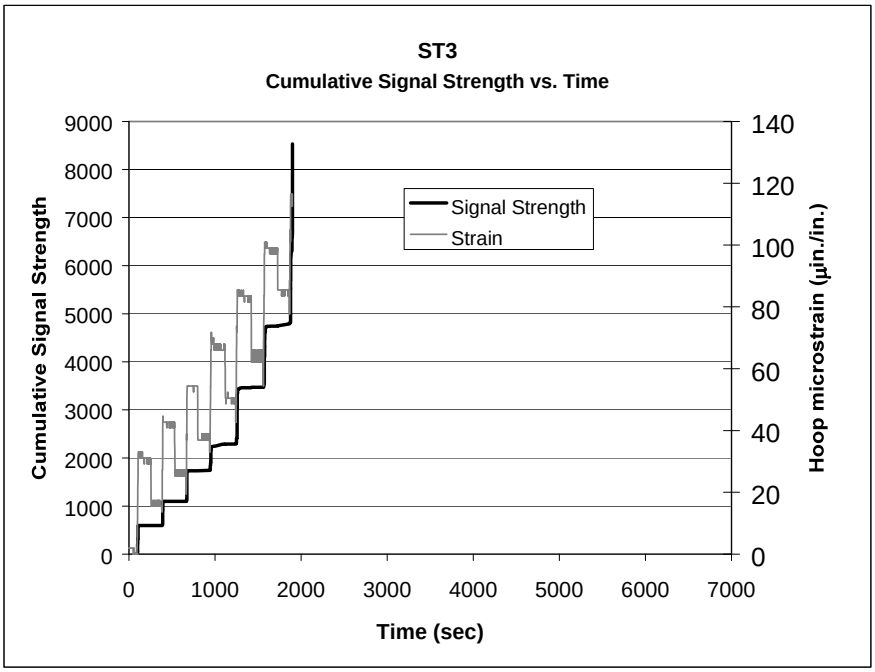

Figure 5.16 Cumulative signal strength versus time for ST3

The new load and reload data and also the load hold data also display increasing emission with increasing pressure as a warning. Figure 5.17 is a chart of the cumulative signal strength that occurred at each pressure level for the new load and reload data from ST3. Increasing signal strength at each pressure level during the load holds is shown in Figure 5.18.

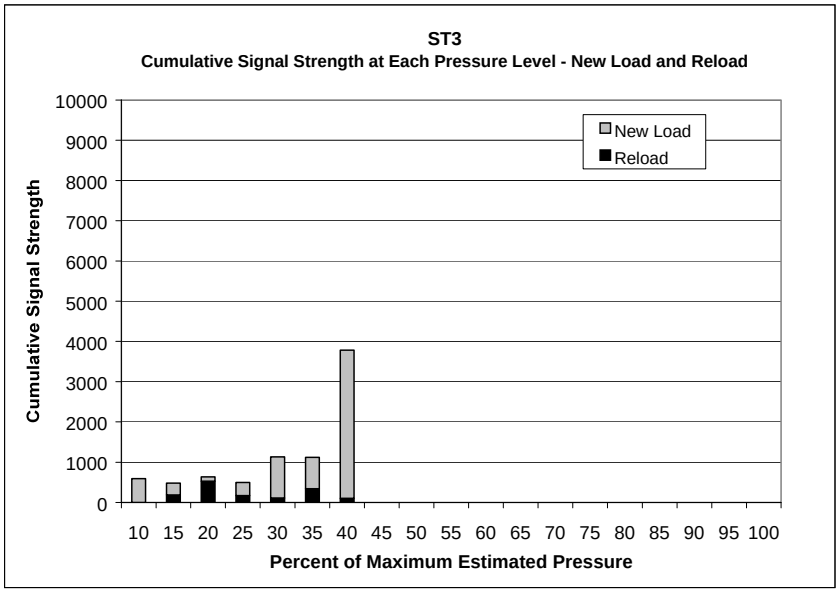

Figure 5.17 Cumulative signal strength for each pressure level for the new load and reload data from ST3

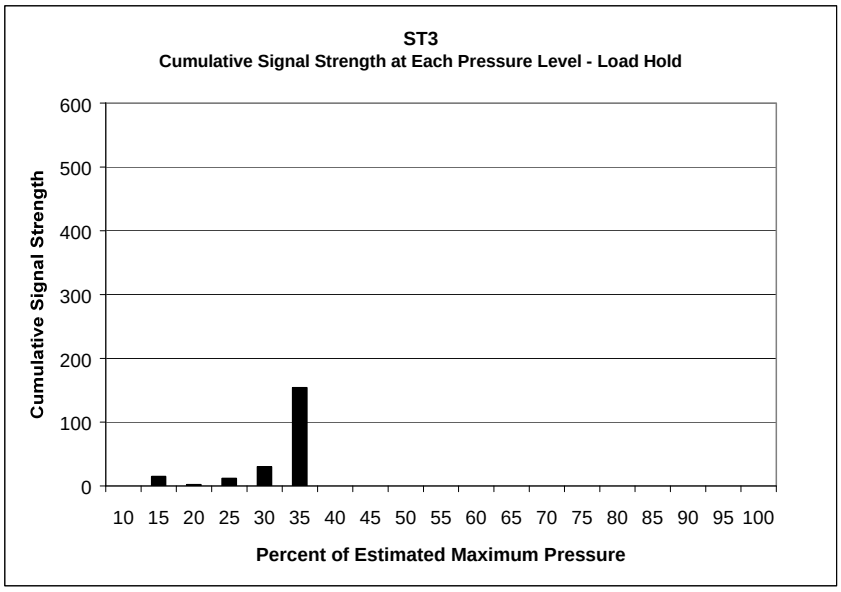

Figure 5.18 Cumulative signal strength for each pressure level for the load hold data from ST3

The Felicity Ratio data for ST3 is shown in Figure 5.19. The value is quite low throughout the entire test. This pattern for the Felicity Ratio is different than ST1 and may help to distinguish those specimens who are damaged will not sustain a high pressure.

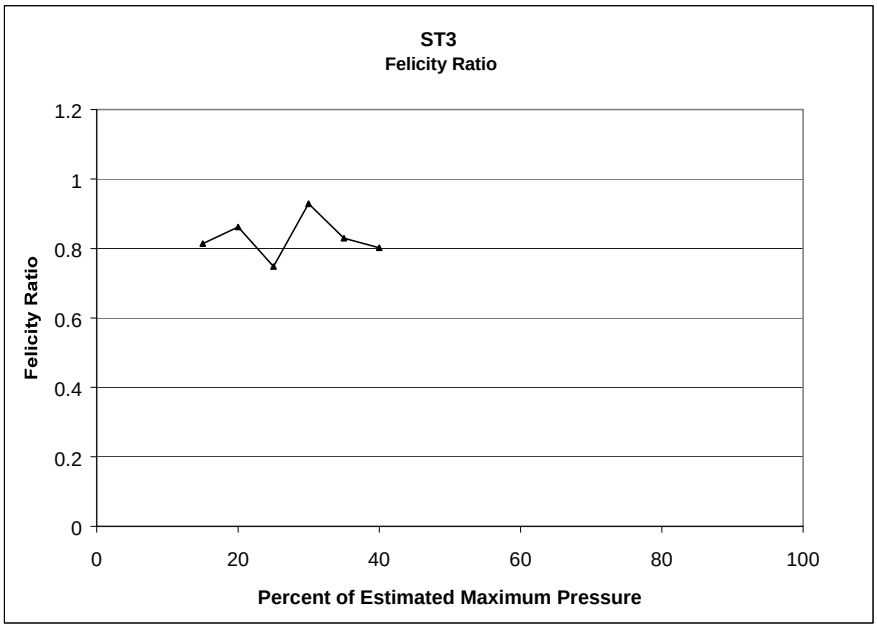

Figure 5.19 Felicity Ratio versus the percent of estimated maximum pressure for ST3

5.3.2.2 Specimens With Early Emission Then Going Quiet Before Failure

Cylinders ST2, ST4, and ST9 all show a similar pattern of having a great amount of emission early on in the tests before going quiet. The specimens remained quiet throughout the remainder of the tests until the final pressure increase is reached when a large amount of emission occurs again. The AE data from these specimens, in essence, provides no warning of failure. This pattern is similar to some of the cases that were discussed in the literature review in Chapter 2. Figures 5.20, 5.21, and 5.22 display the AE data that show this trend for specimens ST2, ST4, and ST9 respectively. The (a) figure is the cumulative signal strength versus time plot throughout the entire test and the (b) figure is the cumulative signal strength at each pressure level for the new load and reload data only.

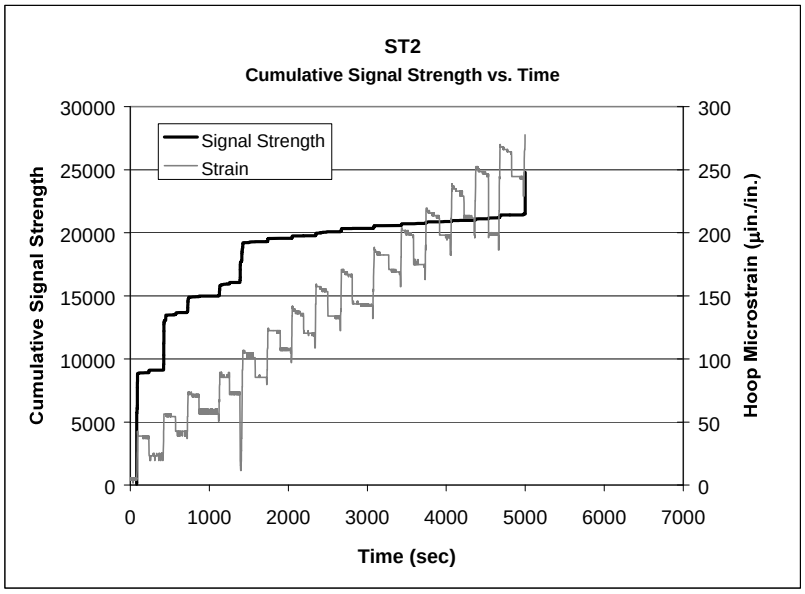

(a)

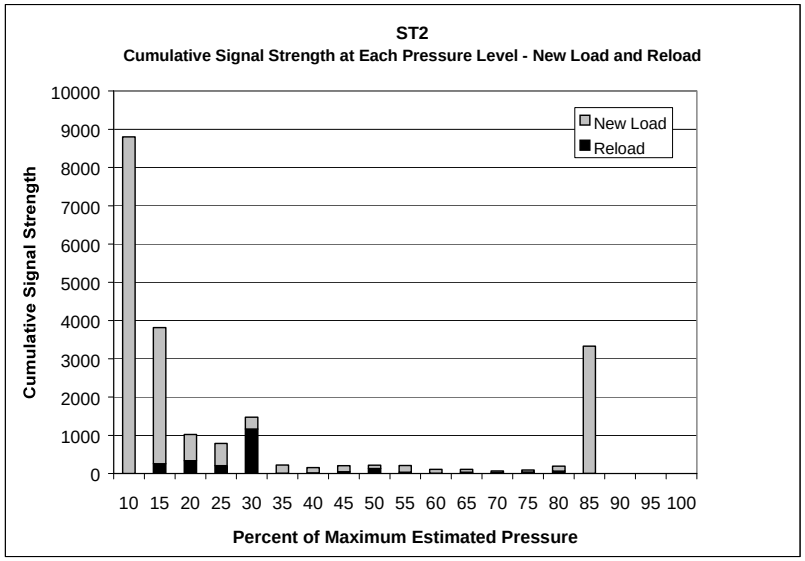

(b)

Figure 5.20 Cumulative signal strength data for ST2 (a) versus time (b) at each pressure level for only the new load and reload data

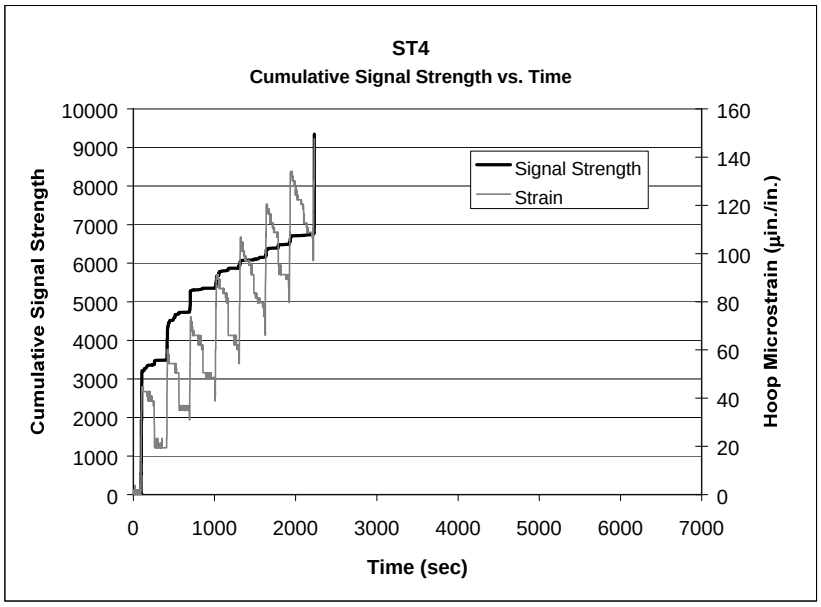

(a)

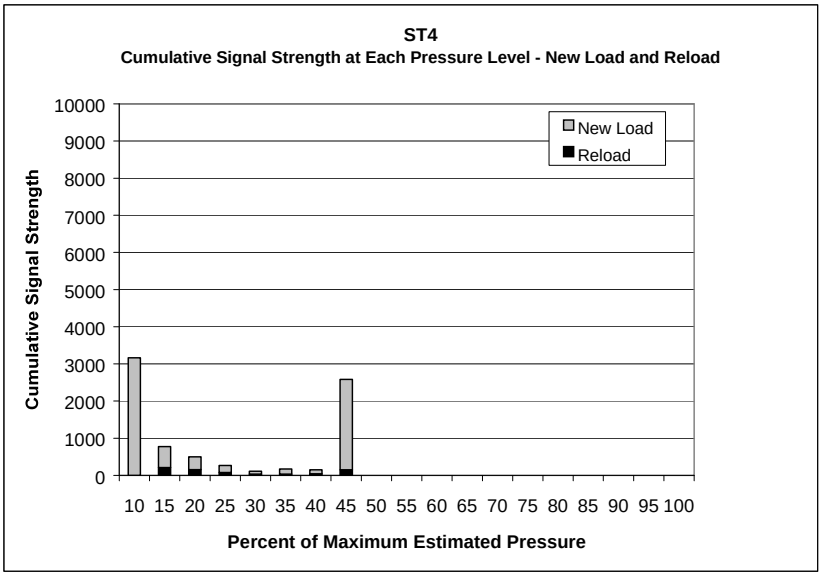

(b)

Figure 5.21 Cumulative signal strength data for ST4 (a) versus time (b) at each pressure level for only the new load and reload data

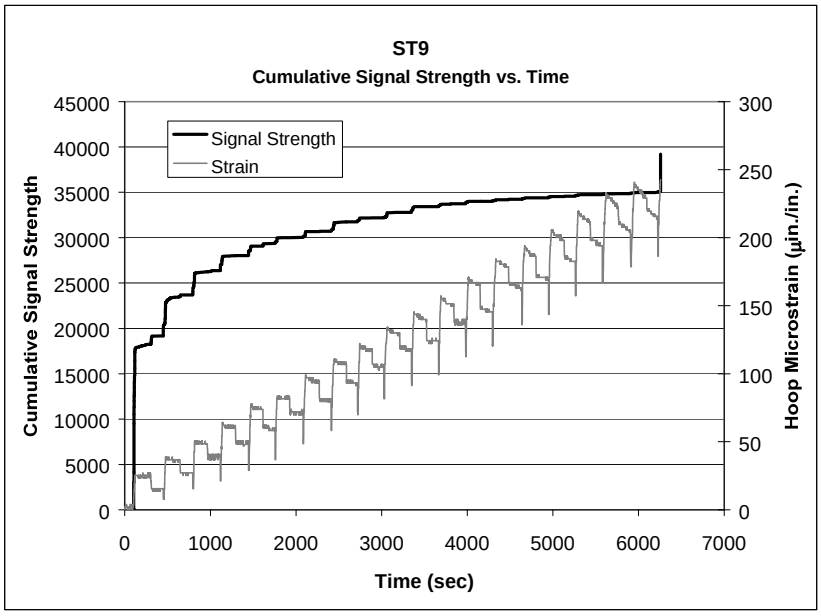

(a)

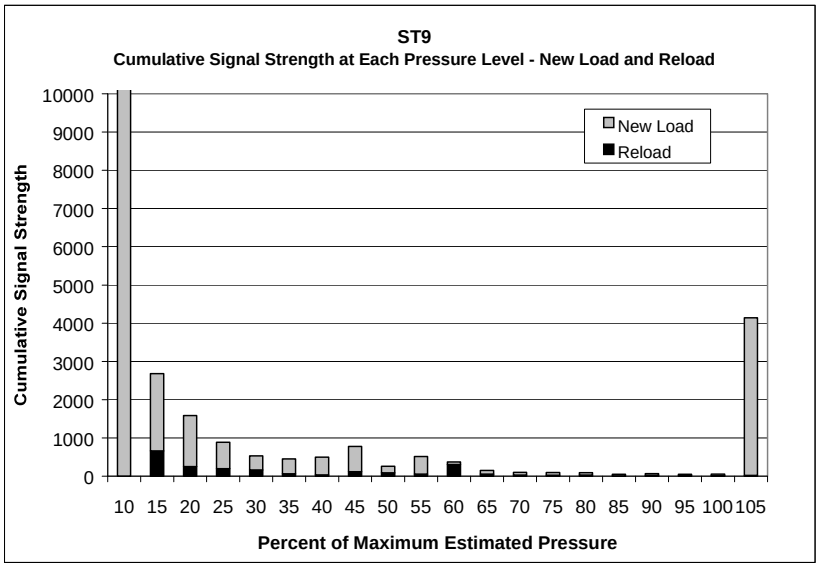

(b)

Figure 5.22 Cumulative signal strength data for ST9 (a) versus time (b) at each pressure level for only the new load and reload data

This early emission with little warning of failure trend is also observed in the load hold data. Figure 5.23 shows the cumulative signal strength at each pressure level for specimen ST2 as an example. The remainder of the plots from these tests also show the large amounts of early emission without warning of failure.

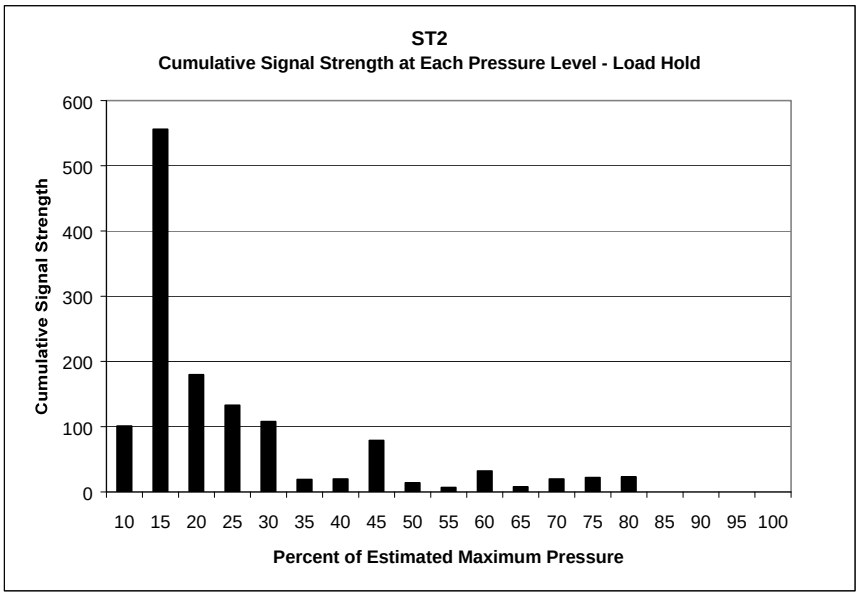

Figure 5.23 Cumulative signal strength at each pressure level during the load holds for ST2

Figure 5.24 shows the Felicity Ratio versus the estimated maximum pressure for specimen ST2. After fairly low values for the first few pressure steps, the Felicity Ratio varies between 0.99 and 1.07 for the remainder of the test. The Felicity Ratios close to or above one would indicate that is this specimen is not damaged and should be able to sustain a high pressure, which it does.

However, the ratio should begin to decrease near the end of the test as failure is approached.

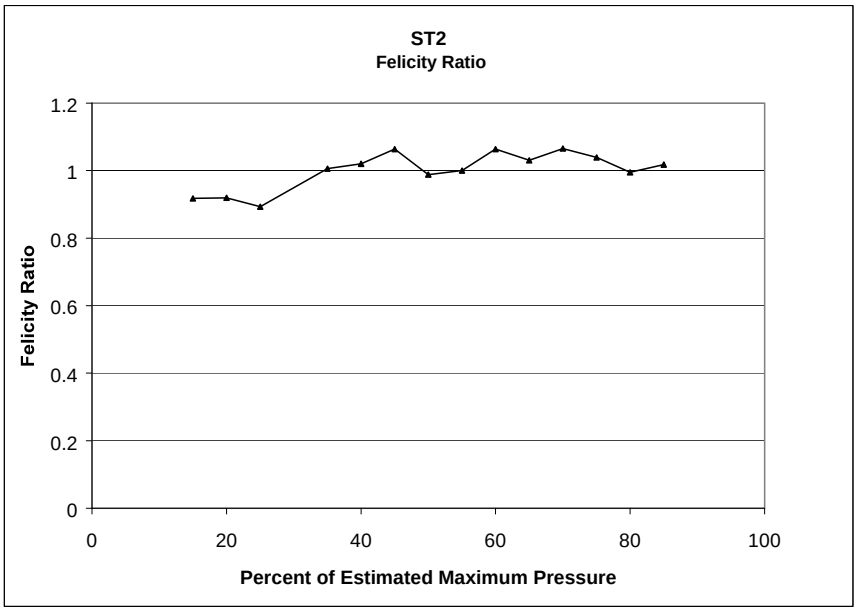

Figure 5.24 Felicity Ratio versus the percent of estimated maximum pressure for ST2

The Felicity Ratio data for ST4 is shown as Figure 5.25. For this test the Felicity Ratio starts out very low and then increases to a value of one or higher. This pattern is contrary to conventional data, which shows that the Felicity Ratio decreases as failure is approached. Also, the fact that the pattern for the Felicity Ratio for ST4 begins somewhat similarly to ST2, but that it failed at a much lower pressure is discouraging. It appears as though the Felicity Ratio data is coinciding with the rest of the acoustic emission data for these tests. The Felicity Ratio shows a warning of failure when the other AE data does, but does not provide a warning of failure when the remainder of the AE data does not.

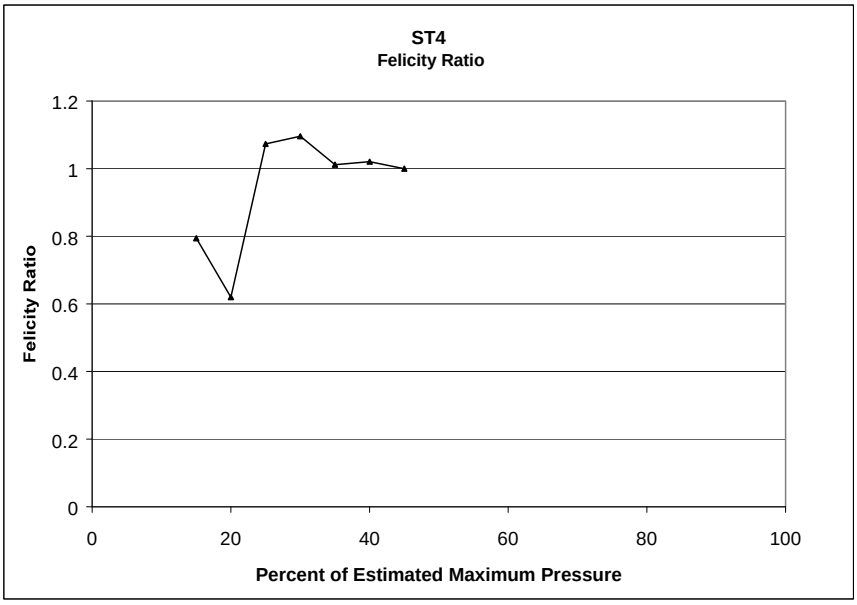

Figure 5.25 Felicity Ratio versus the percent of estimated maximum pressure for ST4

ST2 and ST9 both had relatively high amounts of total emission and achieved fairly high maximum pressure values of 5107 psi and 6195 psi respectively. However, for a given level of strain, ST4 had much less total emission than ST2 and ST9 and had a failure pressure of 2694 psi. Although the patterns in the emission were very different, this is the same trend as was observed between ST1 and ST3.

5.3.2.3 A Specimen With Constant Emission Throughout the Test

After a large jump in emission during the second load increase, the emission for specimen ST7 continued at a relatively constant rate throughout the

remainder of that test. The cumulative signal strength versus time plot for this specimen is shown in Figure 5.26.

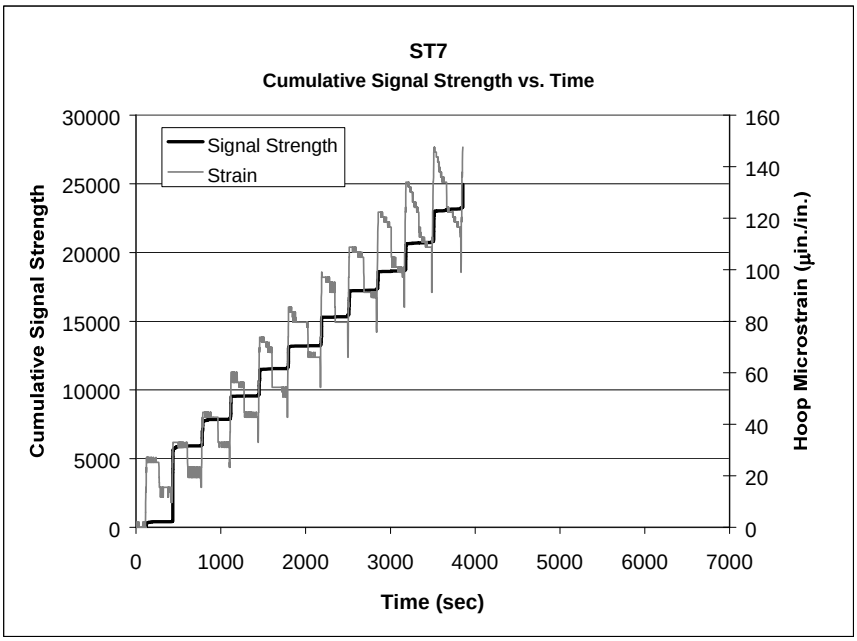

Figure 5.26 Cumulative signal strength versus time for ST7

A relatively high amount of total emission was recorded for this specimen. However, the emission increases at almost a constant rate except for the large increase during the second pressure step. Again for this specimen, no real warning of failure could be observed. The new load and reload data from ST7 also show the relatively constant amount of emission that occurred. Figure 5.27 (a) is the cumulative signal strength at each pressure level for the new load and reload data from specimen ST7. The amplitude versus time plot for the individual hits from the new load and reload data from this specimen is displayed as Figure 5.27 (b).

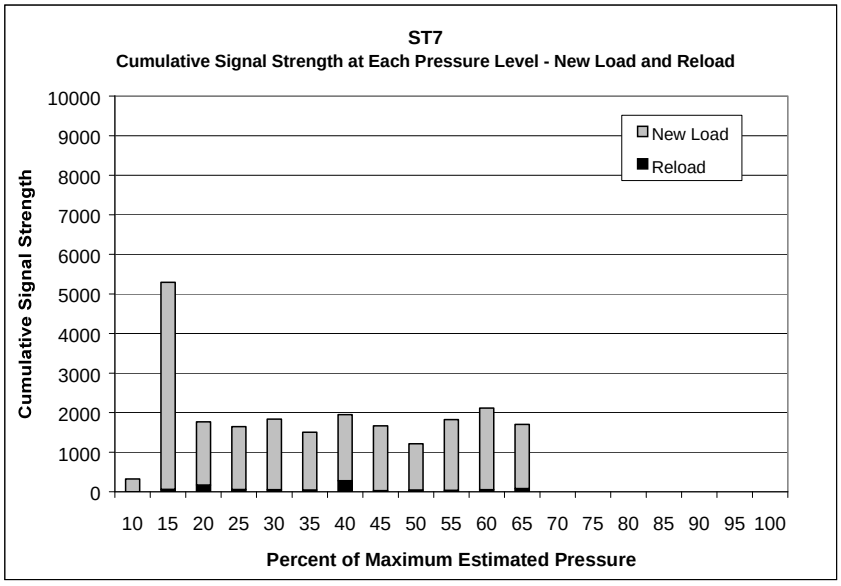

(a)

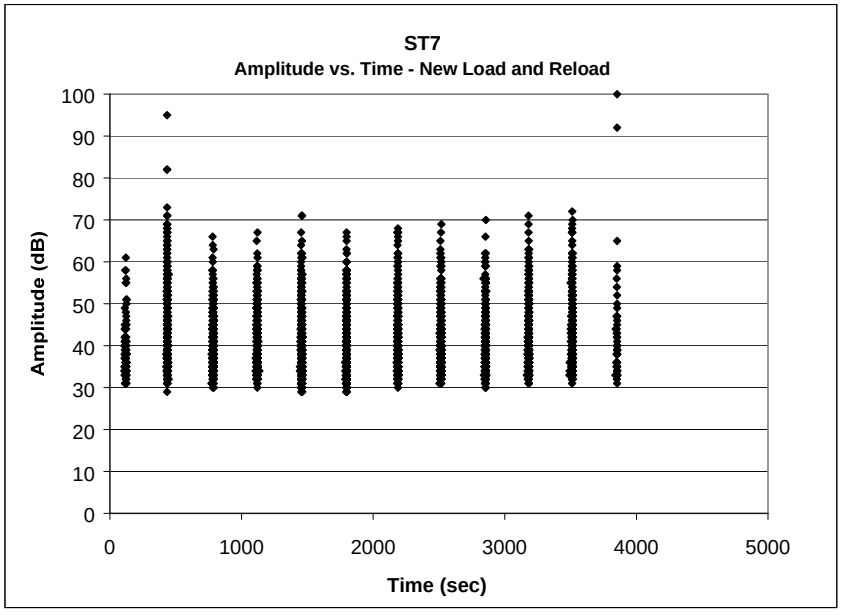

(b)

Figure 5.27 New load and reload data from ST7 (a) cumulative signal strength at each pressure step (b) amplitude versus time

The cumulative signal strength at each pressure level during the load holds for ST7 is shown as Figure 5.28. Some indication that the specimen is progressing towards failure can be observed from the load hold data, unlike the rest of the emission. The signal strengths at each pressure level are generally increasing after the first few pressure steps, but the data is not conclusive.

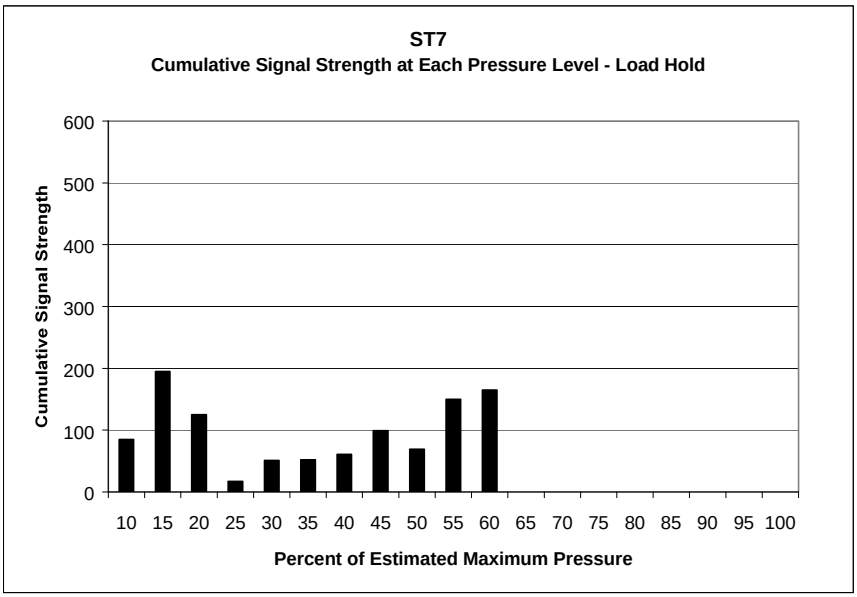

Figure 5.28 Cumulative signal strength at each pressure level during the load holds for ST7

5.3.2.4 Specimens Showing No Discernable Trends in Their AE Results

The remainder of the short cylinder specimens ST5, ST6, and ST10 showed no real pattern to the AE results. The cumulative signal strength versus time plots for specimens ST6 and ST10 are shown as Figures 5.29 and 5.30 respectively. At first glance, these specimens appear to have relatively constant emission similar to ST7. ST6 does have a large emission increase near the end of

the test, but this was due to an accidental drop in the internal pressure as shown by the strain data in Figure 5.29. Again, much of the emission that occurs during the pressure drop may be caused by background noise.

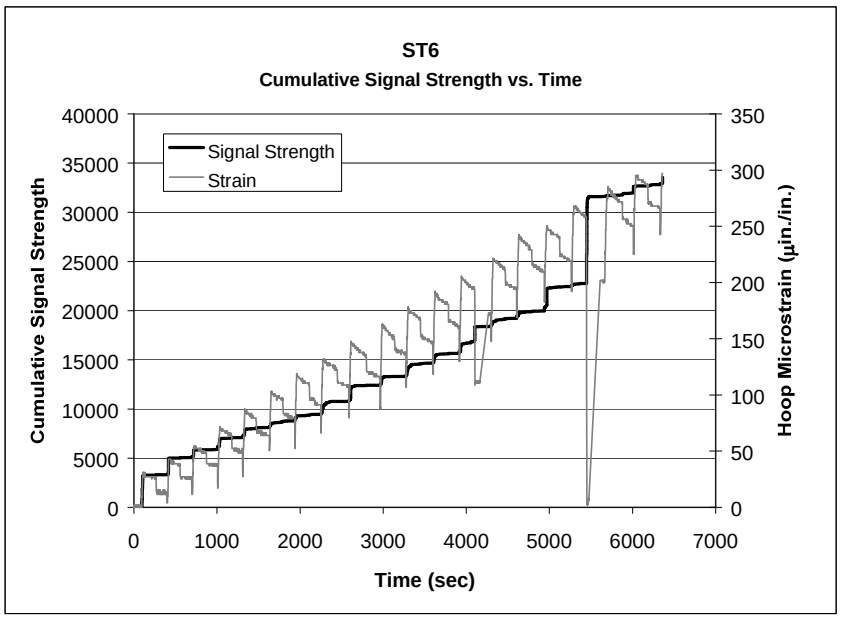

Figure 5.29 Cumulative signal strength versus time for ST6

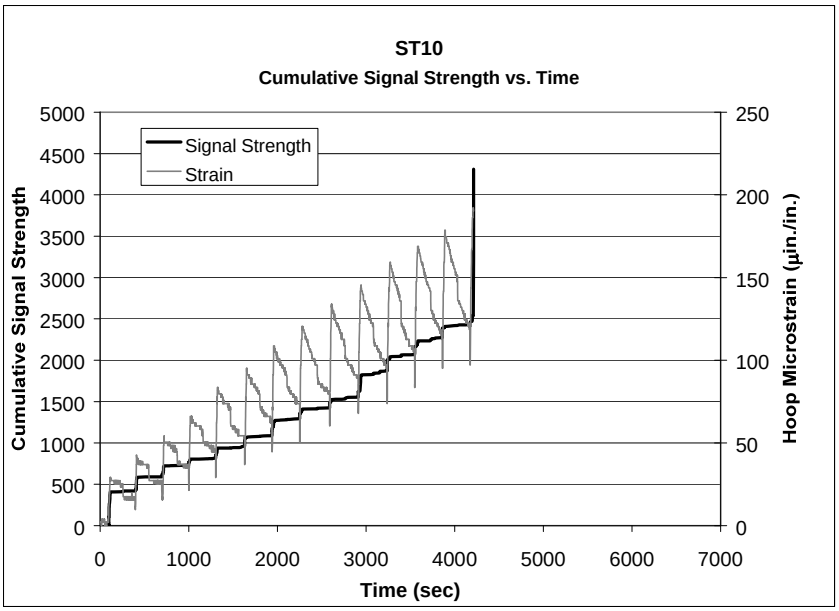

Figure 5.30 Cumulative signal strength versus time for ST10

However, a closer look at the data from these tests show that the amount of emission at each load step varies a great deal with no pattern to it for the load hold data and also for the new load and reload data.

Specimen ST6 produced a great deal of emission during the test while ST10 had a very low amount of total emission for a given strain level. The strain data from ST10 shows that there was difficulty in holding the pressure at a constant level during this test. This inability to control the pressure was due to this specimen's inside diameter not being machined to the specified tolerances, thus causing a poor seal. Not being able to hold the pressure properly most likely altered the results of this test.

The AE behavior of the specimen that is the most difficult to explain is ST5. The cumulative signal strength versus time plot for ST5 is shown as Figure 5.31.

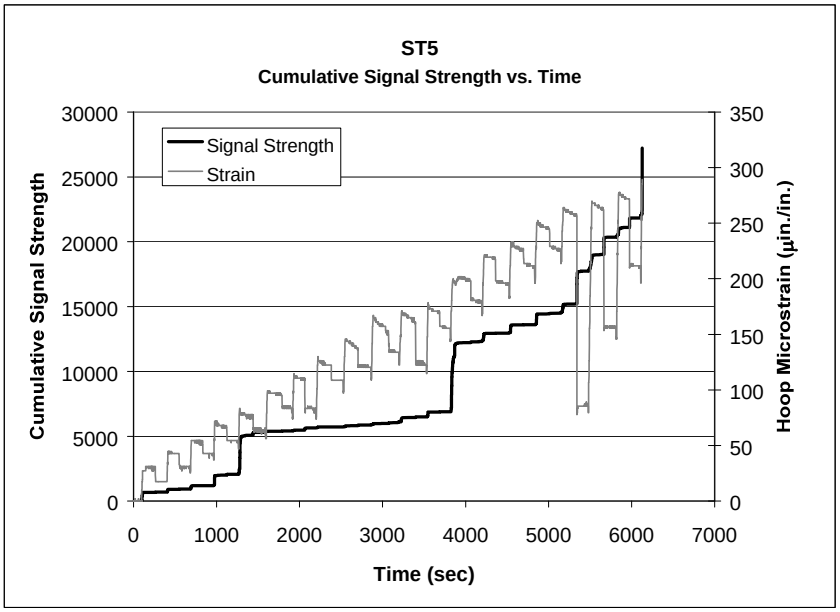

Figure 5.31 Cumulative signal strength versus time for ST5

This specimen has two large increases in the AE that was generated. One occurs at about 30% of the estimated maximum failure pressure and the other occurs at 70% of that value. There was even a tremendous amount of load hold emission at those intervals. Figure 5.32 (a) is the cumulative signal strength at each pressure level and Figure 5.32 (b) is the amplitude of each individual hit versus time for the load hold data from ST5.

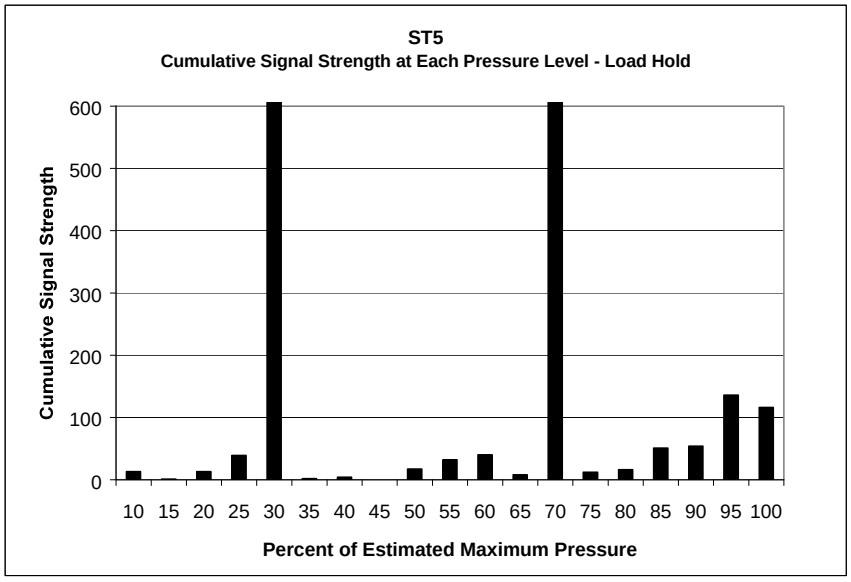

(a)

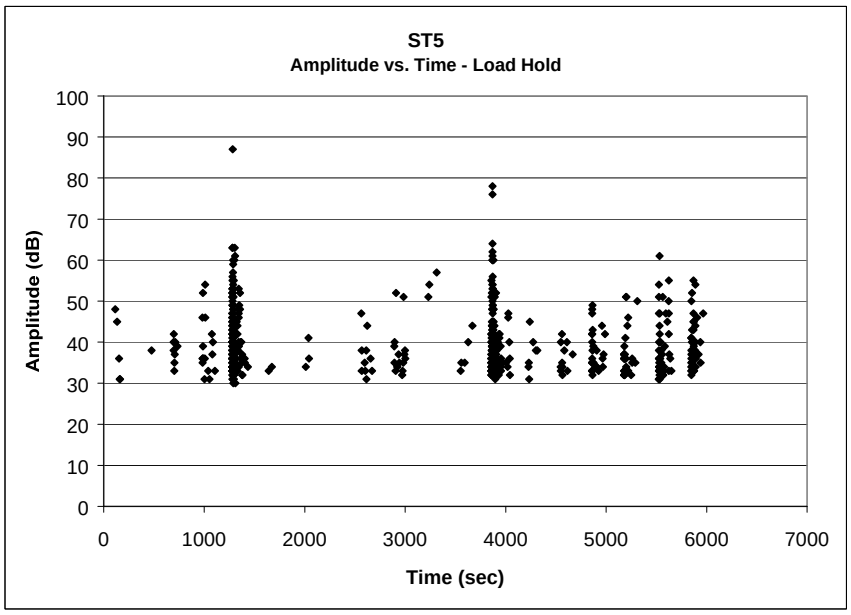

(b)

Figure 5.32 Load hold data from ST5 (a) cumulative signal strength at each pressure (b) amplitude versus time

These plots show the large amounts of emission occurring at those times, including very high amplitude hits. It appears as though significant cracking occurred at the times that the emission jumped. There is some evidence of increasing emission amounts leading up to those events in the new and reload data from this specimen. After these events, the emission goes relatively quiet again. It is not known why the specimen did not fail during or shortly after these events and how it was able to attain such a high maximum pressure.

Table 5.2 summarizes the information provide in the preceding sections.

Specimen	*Failure Pressure (psi)*	*Type of Acoustic Emission*	*Total AE#*
ST1	5017	Warning of failure	High
ST2	5107	Early emission with no warning	High
ST3	2503	Warning of failure	Low
ST4	2694	Early emission with no warning	Low
ST5	6139	No pattern with large jumps	High
ST6	6171	No pattern / almost continuous	High
ST7	3659	Continuous emission	High
ST8	* Failure during first load increment *		
ST9	6195	Early emission with no warning	High
ST10	4500	No pattern / almost continuous	Low
ST11	* Failure during installation into the test frame *		

# The Total AE refers to the cumulative signal strength right before final fracture
Low = below 10,000 Medium = 10,000 – 20,000 High = more than 20,000

Table 5.2 Summary of the AE results from the short cylinder tests

The peculiar results from the short cylinder tests may be able to be explained by considering the location and orientation of a significant flaw on a specimen. If a flaw is orientated longitudinally (perpendicular to the applied stress), then this flaw may not generate much emission until it suddenly extends to complete fracture when a critical stress level is reached. There was evidence of this behavior discussed in the Literature Review in Chapter 2. A flaw that is orientated parallel to the applied stress or at least some fairly large angle from perpendicular may show much more microcracking and coalescence at the crack tip as it curves to be perpendicular in the direction of the stress. The location of the flaw may be extremely important as well. Although the entire specimen is in tension, there is a gradient of tensile stress through the cross-section as was shown in Section 5.2. Also, the stresses may not be exactly as they were estimated because of the end effects of the short cylinders. A flaw that begins on the inside surface of the specimen may propagate more slowly and not extend to complete fracture right away because of the stress gradient. The tensile stresses are lower ahead of the crack tip. On the other hand, once a critical stress is reached for a flaw on the outside surface, it is likely to extend all the way through the cross-section because the stress ahead of the crack is higher.

It is possible that these specimens were more susceptible to noise from non-structural sources than were the C-rings. The log duration versus amplitude plot were examined for each test and a Swansong Filter was applied to the data, which should have eliminated any noise from the filling of the hydraulic fluid or from the O-rings rubbing on the specimen. One possibility that was suggested

was that the ends of the specimens could have hit the steel plates of the test frame during loading times and cause noise that may be difficult to distinguish from genuine AE data. However, this is not borne out by the load hold data, which has a similar pattern to the loading data. During load holds, this possible source of emission will not be present.

5.4 LONG CYLINDER TEST RESULTS

The final two tests that were completed for this testing program were carried out on longer cylinders that were meant to mimic the actual SiC tubes that are used in industry. The two cylinders were a form of SiC similar to that of the first six short cylinder tests and had failure stresses between 25,000 and 26,000 psi according to previous test data. Both cylinders were uncoated material and were approximately 13 inches long. LT1 had a very smooth, almost machined surface while LT2 had a much rougher surface. As was mentioned in Section 5.1.2, in an attempt to simulate the actual proof test that may be used, these specimens would be loaded to only a pressure of 2700 psi at first. The value of 2700 psi was chosen because it was a pressure that was high enough to provide a substantial amount of data while hopefully not fracturing the specimen. All of the short cylinder tests reached this pressure level except ST3 and it was on the way up to this pressure when it failed. These specimens would be cycled to 2700 psi three times so that the AE results from each cycle could be compared. On the fourth cycle, the specimen would be taken all the way to failure so that the

maximum pressure could be recorded and compared to what the AE data had predicted from the previous cycles.

5.4.1 Strength and Fracture Results from the Long Cylinder Tests

The maximum pressures that were reached in the two long cylinder tests once again exhibited the size effect on the strength properties of this material. LT1 reached a maximum pressure of 3232 psi, while LT2 failed at a pressure of 2637 psi. Table 5.3 summarizes the strength and fracture results obtained from the long tube tests.

Specimen	Failure Pressure (psi)	Est. Maximum Stress (psi)	Max. Measured Hoop Strains (μin./in.)	Est. Max. Hoop Strain at internal surface (μin./in.)	Number of Failure Locations*
LT1	3232	8730	145.6	231.504	> 40
LT2	2637	7123	141.8	225.462	approx. 20

Table 5.3 Strength and fracture results from the long cylinder tests

Unfortunately, the experiment on LT2 did not proceed according to plan. There was a great deal of difficulty in holding the pressure during this test. It is much more difficult to machine the inside surface for these long specimens and their inside diameter appeared to be less circular to begin with. Since the pressure could not be controlled well, the specimen was taken to failure during the first load cycle. Therefore, the emission results from following cycles could not be studied. This specimen attained a pressure of only 2637 psi in any case.

Specimen LT1 could be cycled to 2700 psi three times as was planned and the results from this test were quite interesting.

The maximum hoop strains of 145.6 and 141.8 μin./in. measured on the outside surface of these specimens would equate to maximum strains of 231.5 and 225.5 μin./in. on their inside surface. These values correlate well to the low maximum pressures that were reached by these two cylinders.

Both long cylinder specimens fractured into many sections. Figures 5.33 and 5.34 show the fractured specimens for LT1 and LT2 respectively. No attempt was made to align the failure sections along the axis of the cylinder for the pictures. Once again the trend of the stronger specimens having more fracture planes is true for these tests as well. It would be reasonable to assume that the failure process for these specimens would be essentially the same as the shorter cylinders. However, the longitudinal strips are not quite as prevalent as in the short cylinder tests. There are a number of long pieces from both cylinders, but many of them have pointed ends. The pointed ends may be a result of these sections being thrust out to hit the containment box and the test frame after the original fracture, but this is not known.

Figure 5.33 Fractured sections from LT1

Figure 5.34 Fractured sections from LT2

The axial strain results were closer to what would be expected from the cylinders due to Poisson's Effect. Since the applied axial stress is zero and the theoretical radial stress is also zero at the outside surface, the axial strain should come solely from the Poisson Effect from the hoop stress. The axial strain would slowly increase negatively as the hoop strains increased in tension. Figure 5.35 shows the measured axial strain from the first cycle of loading of LT1.

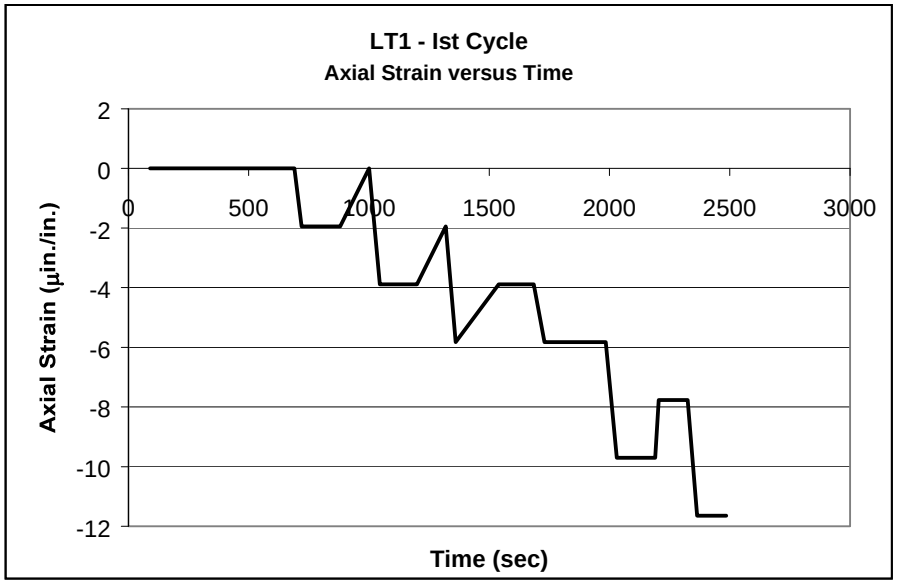

Figure 5.35 Axial strain versus time for the first load cycle of LT1

The reason that the data in this figure has such a block shape is due to the sensitivity of the equipment, as these strains were very low. The maximum axial strain of about 12 μin./in. is well below what would be expected from Poisson's ratio. A maximum hoop strain of 120.4 μin./in. was measured during this first cycle. Using a Poisson's ratio of 0.2 for this material, a maximum axial strain of

24 μin./in. is expected. Therefore, there still must be some effect of axial pulling from the friction of the plugs.

5.4.2 Acoustic Emission Results from the Long Cylinder Tests

The acoustic emission results were again separated into the data from the new load and reload conditions, and also the data from the load hold periods. This permitted a more in depth analysis. The AE data from LT1 was also compared between loading cycles to investigate for evidence of the Felicity Effect. Because of the inability to control the pressure for the test on LT2 and the fact that this specimen could not be cycled to 2700 psi, the AE results from this specimen will not be given much emphasis.

5.4.2.1 The AE Results from the First Long Cylinder Test

The cumulative signal strength versus time data for all four of the load cycles for LT1 are shown in Figure 5.36. The first cycle has a great deal of its emission early in the test and then goes quiet, a pattern that was observed in a number of the short cylinder tests. However, the total amount of emission detected for the first load cycle was relatively low compared to many of the short cylinder tests. The plot of the fourth cycle in Figure 5.36 shows the amount of emission that occurs when the new maximum pressure level is reached as the specimen was taken to 3000 psi. Failure occurred on the way to the next pressure step at 3232 psi.

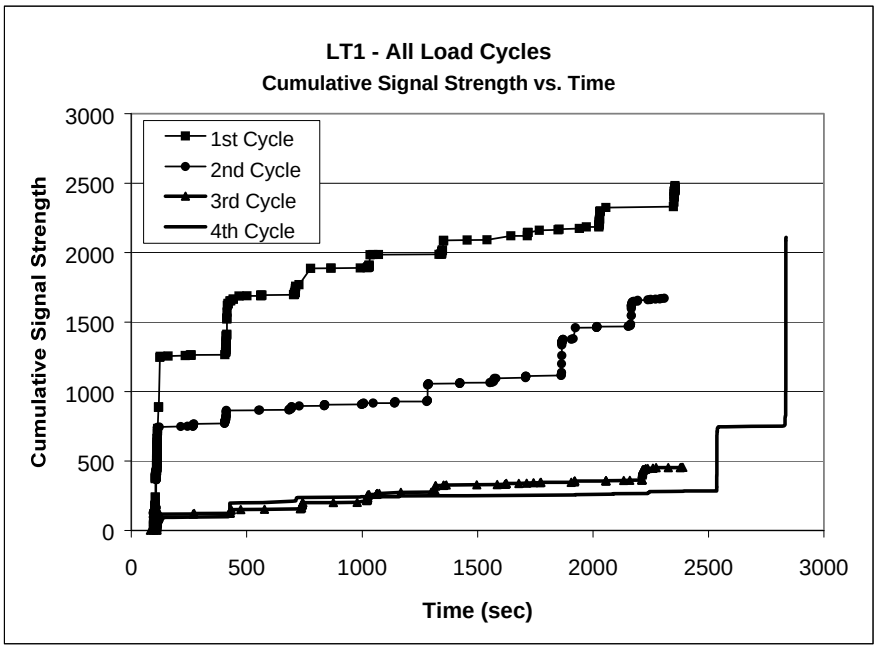

Figure 5.36 Cumulative signal strength versus time for LT1 – all four load cycles

Evidence of the Felicity Effect from the AE data from LT1 may have predicted that it was considerably damaged and would not sustain a very high maximum pressure. There is a significant amount of emission detected on the second cycle. The total emission of this cycle is about 65% of the total emission from the first cycle, which is a considerably high percentage. Even if the emission from the first pressure step of the second cycle is ignored, there was a great deal of emission generated at the last two pressure steps below 2700 psi. Significant emission is even generated on the third and fourth cycles before 2700 psi is reached. Table 5.4 shows the Felicity Ratio for each pressure cycle during the test on LT1. For the long cylinder tests, significant emission is defined as 100

total hits, a cumulative signal strength of 300, or a single hit with a amplitude of 60 dB or greater. Normally, this amount of emission on subsequent loadings and the low Felicity Ratios are an indication of a damaged specimen and would lead to the prediction of the fairly low maximum pressure that LT1 reached.

Cycle to 2700 psi	Felicity Ratio
1st	0.16
2nd	0.60
3rd	1.05

Table 5.4 Felicity Ratios for each cycle for LT1

Figure 5.37 is another way to look at these same data sets and shows the value of total cumulative signal strength that occurred for each cycle. A closer look at the hits that display the Felicity Effect during the second cycle of loading is shown in Figure 5.38, which is the amplitude versus time plot for the second cycle of load for LT1. This specimen provides some hope of using the Felicity Effect for determining the condition of a SiC cylinder, but the data are not conclusive.

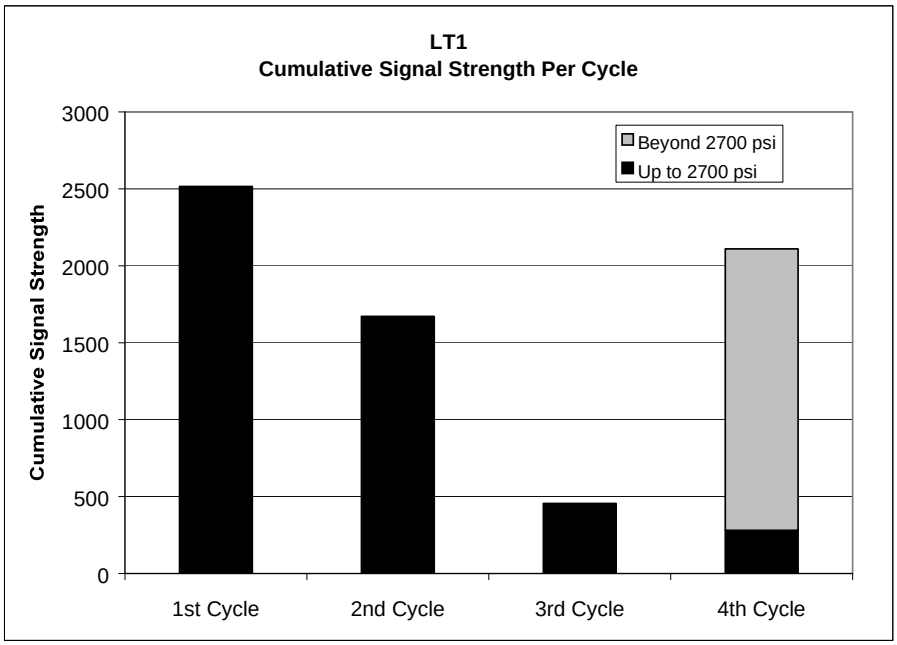

Figure 5.37 Cumulative signal strength totals for each load cycle for LT1

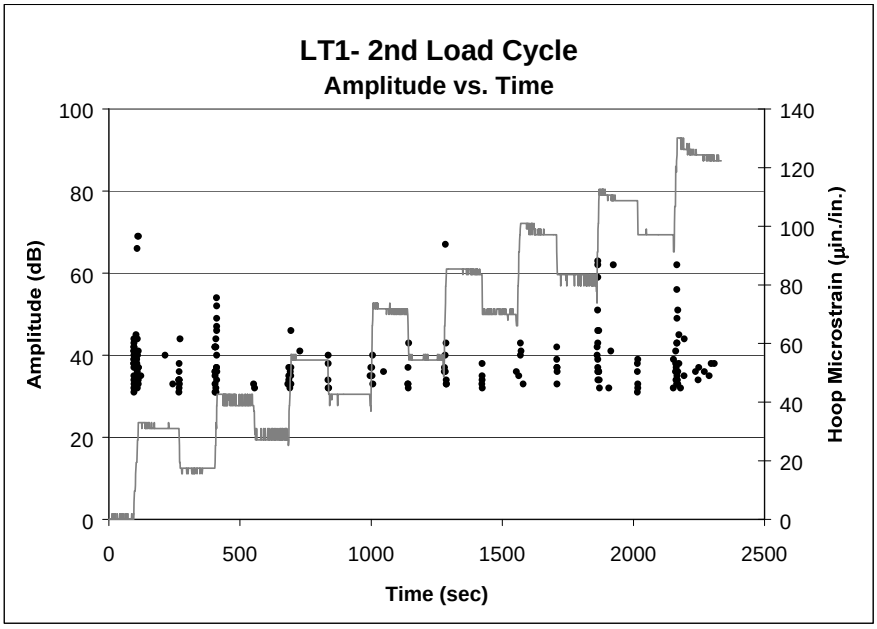

Figure 5.38 Amplitude versus time for the 2nd load cycle for LT1

5.4.2.1 The AE Results from the Second Long Cylinder Test

The cumulative signal strength versus time plot for specimen LT2 is shown as Figure 5.39. The difficulty in holding the applied pressure can be observed from the strain data in this plot. The pressures would decrease quickly during an attempted load hold during the first few load steps. From then on, an attempt was made to maintain the pressure by continuing to pump more hydraulic fluid into the cylinder. The AE cumulative signal strength plot shows a very irregular pattern of emission with a large increase in emission at the start of the

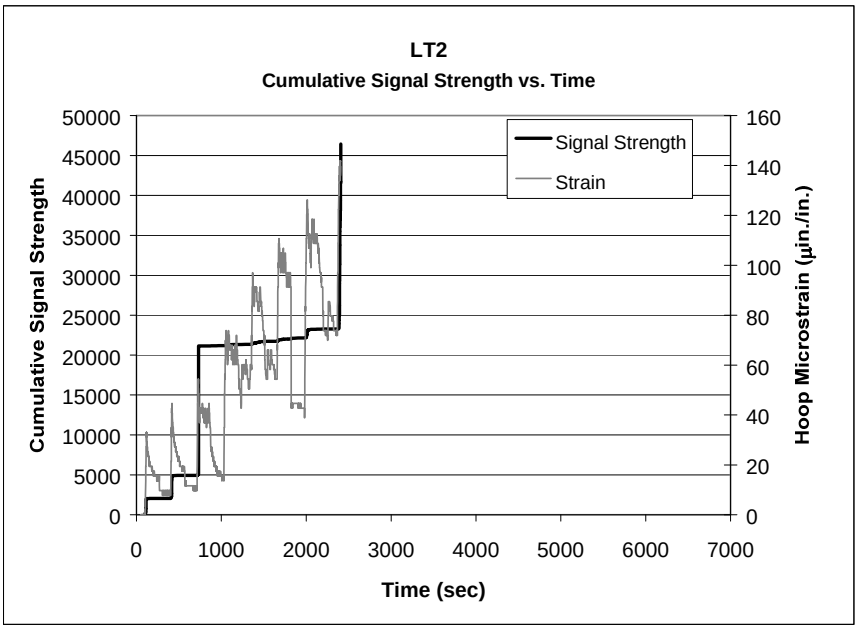

Figure 5.39 Cumulative signal strength versus time for LT2

of the third load hold attempt. The load hold data for each pressure step are shown in Figure 5.40. The large amount of emission during the third pressure step can be observed, but otherwise there is no real pattern. The irregularity of the emission with large emission jumps for LT2 is very similar to the result of ST5 from the short cylinder tests.

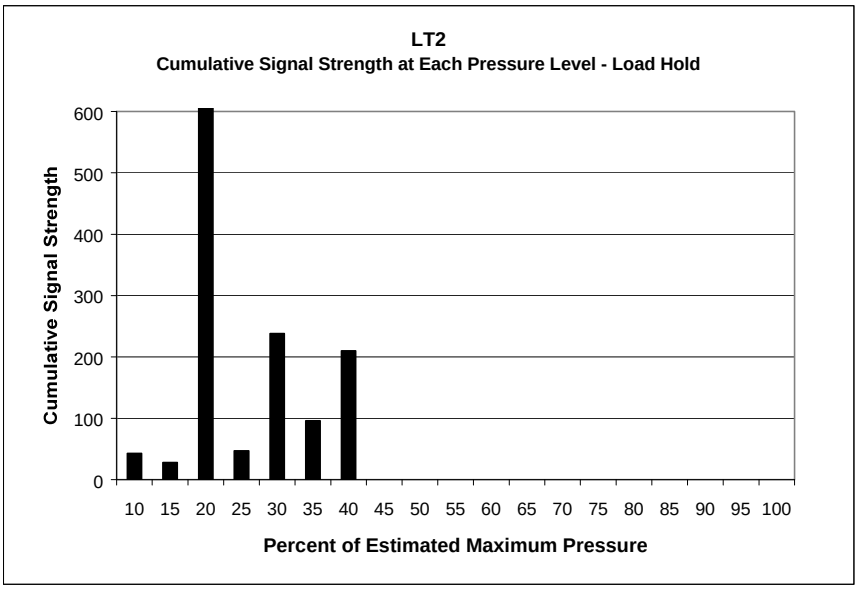

Figure 5.40 Cumulative signal strength at each pressure level during the load holds for LT2

5.5 SUMMARY AND CONCLUSIONS FROM THE CYLINDER TESTS

The internal pressure tests of the cylinders moved the testing program towards the type of test that would be necessary for the desired proof test. The range in failure stresses that was lacking from the C-ring tests was achieved in these tests as the maximum internal pressures to cause failure ranged from 2503

psi to 6179 psi (not including ST8 and ST11). This variation was as expected for a brittle material subjected entirely to tensile stresses.

The fractured sections of the cylinders once again provided some information as to the fracture process of this material. It is evident that as one cross-section would get fractured, the pressure would still be maintained and the stress would all get transferred to the cross-section 180° on the other side of the specimen. This cross-section would then become damaged and the stresses would get transferred again. This process produced the number of longitudinal strips observed from the fracture of the specimens. The whole process is instantaneous to the naked eye as the specimens shattered apart. The number of sections to which the cylinder breaks correlates with the maximum pressure attained by that specimen. The higher the stresses were throughout the general volume of the cylinder (higher energy built up), the more likely it was to have more fracture sections.

The acoustic emission data from the short cylinder tests provided some very interesting data. There were no general trends in this data as was observed for the C-ring tests. However, there were some groups of specimens that exhibited similar behavior. Unfortunately, there was no correlation between the strength of the specimens and those AE patterns. The specimens that exhibited each type of pattern had a wide variation of failure strengths. There was some evidence of the weakest or most defected specimens exhibiting lower amounts of total AE before final fracture. The Felicity Ratio was effective in predicting the failure strength for some of the specimens, but the data was not conclusive for all

the tests. The orientations and locations of the controlling flaws may be a factor in the variations in the acoustic emission data that was observed.

The strengths of the long cylinder specimens were quite low as can be expected due to the size effect of this material. These specimens also fractured into long strips, but many of the strips had pointed ends and were not complete down the entire length of the cylinder. Evidence of the Felicity Effect in the AE emission data from LT1 would normally serve as a warning that this specimen would not be very strong, but this was not a conclusive indication from the short tube tests. A significant amount of emission was detected in the later cycles after an internal pressure of 2700 psi had already been applied to the specimen. Unfortunately, due to an inability to maintain the pressure for specimen LT2 and because of the fact that it fractured on its first load cycle, very little valuable AE data were obtained from this test.

Chapter 6: Summary, Conclusions, and Recommendations

6.1 Summary of Research Program

From the study of earlier research, a substantial amount of valuable information was obtained which related to using acoustic emission as a method to proof test SiC tubes. The primary concern raised by the previous studies is whether AE can detect a warning of failure in this material or whether a significant defect will extend to failure without much warning from the AE until it is actually fracturing. If such a warning occurred, it could be expected to come from microcracking and coalescence of the microcracks in the highly stressed region around a defect.

There were some studies that reported a lack of warning from the AE when a substantial defect exists in the specimen. However, these tests utilized artificial defects that were usually located at a region of maximum stress and were often orientated perpendicular to the applied stress. It is likely that these artificial defects do not approximate natural flaws in the material in both size and geometry. The detection of microcracking preceding final fracture was investigated in a series of tests utilizing different specimen sizes and geometries and various methods for stressing those specimens.

Although the small flexural bars are the standard specimen type used for testing silicon carbide, they were not found to be suitable for this testing program. The small Pico sensors, which are resonant at 500 kHz, had to be used because of

the size of these specimens. Although the 500 kHz sensor is satisfactory for these small specimens, there would be too much attenuation encountered from this high frequency for the much larger SiC tubes. Without special equipment, problems were also encountered in being able to control the amount of load that was applied because these specimens fail under very low loads. Although some satisfactory preliminary data was recorded from two of the flexural bar tests, it was apparent that these specimens would not be suitable for this testing program.

The C-ring specimens proved to be a much more adequate specimen type to use for AE testing of SiC. A standard 150 kHz resonant sensor could be used and some very promising AE results were recorded in this set of tests. A warning of failure was evident in a majority of the tests from the cumulative signal strength increase that began at about 70% to 85% of the final fracture load. Also, hits with increasing amplitude and signal strength values were observed, as the stress was increases towards failure. There were a few of these specimens that did not behave typically and provided further important information. Specimens that were more significantly flawed showed the knee in the cumulative signal strength plot at a lower strain level than the other specimens. Also, hits with higher amplitudes and signal strengths occurred much earlier in the tests from these C-rings. However, most of the specimens failed within a narrow range of maximum failure loads. Therefore, the difference in the emission data from more severely flawed specimens was not conclusive.

The internal pressure tests on the SiC cylinders provided a greater variation in failure stresses. However, the acoustic emission data was not as

promising as it was for the C-ring data. A general trend in the AE data was not observed. There were, however, some groups of specimens that displayed similar emission patterns to one another.

A warning of failure was much more prevalent in the C-ring tests than the internal pressure tests on the cylinders. There are a number of possible reasons for this. The maximum tensile stress on the C-ring is concentrated on a very small volume of the specimen and thus the likelihood of a defect in that location is remote. Therefore, AE can detect the microcracking and coalescence in that area. There is also a very steep stress gradient in the C-rings that may also allow for more warning of failure. The stress gradient creates the opportunity for halting of the crack extension and slower crack growth. Finally, there may be AE detected from the compression area of the specimens where a more progressive damage process may be taking place.

This material may be too unstable under completely tensile stresses to develop a proof test in this manner. The uniform tensile stress is not essential because the actual stresses encountered in service are not like that. The actual stresses in SiC tubes are generated from a thermal gradient and thermal shock, which creates a more flexural phenomenon. The results of this testing program show that a bending test would produce more warning of failure from a defected specimen and the stresses would better approximate the actual stresses created in the tube while they are in service. However, the bending tests would have to be configured in such a manner that the entire tube gets stressed to a reasonable level or a significant defect may go undetected.

6.2 CONCLUSIONS AND RECOMMENDATIONS

This thesis reports the results of a comprehensive experimental program to evaluate the feasibility of using acoustic emission as a proof test of new and in-service silicon carbide tubes. The program involved testing small beams in bending, C-rings, and cylinders under internal pressure. The following conclusions and recommendations are based on this experimental data and a comprehensive literature search.

1. Additional research and development work to establish an acoustic emission based proof test for silicon carbide tubes is not recommended.

2. Silicon carbide generates significant emission under applied stress. The emission originates from microcrack and macrocrack growth.

3. In some situations, acoustic emission is unable to detect the presence of existing cracks. However, the technique will detect the development and growth of a new crack.

4. The sources of emission in a stressed SiC specimen are often unrelated to the ultimate failure of the specimen and thus its short-term strength.

5. As noted above, crack initiation and growth can be detected with acoustic emission. Based on this, a permanent monitor could be installed on the

silicon carbide tubes to detect initiation and development of cracks. Installation of a prototype in-service monitor may be justified.

6. It is difficult to envision a practical method of proof loading the SiC tubes that will simulate in-service thermal shocks.

7. The brittle nature of SiC can lead to rapid crack growth and sudden failure without warning. This is particularly true under an applied tensile stress. This is less of a problem under flexural stress conditions where cracks may be self-relieving.

8. Microcrack growth depends on a number of factors such as manufacturing process, service history, material type, and consistency.

9. The orientation of the defect to the stress field may significantly affect the nature of the emission. For example, a crack perpendicular to the principal tensile stress field may fail without precursor acoustic emission.

10. Acoustic emission monitoring of SiC can be a valuable tool in understanding the response of the material to the applied stress, and has applications for research.

References

American Society for Nondestructive Testing. (1999). "Recommended Practice for Acoustic Emission Evaluation of Fiber Reinforced Plastic (FRP) Tanks and Pressure Vessels." The Committee on Acoustic Emission from Reinforced Plastics, Draft I, October 1999, Columbus, Ohio.

American Society for Testing and Materials. (1994). "Standard Test Method for Flexural Strength of Advanced Ceramics at Ambient Temperature." C 1161 – 94, Philadelphia, PA.

American Society for Testing and Materials. (1993). "Standard Terminology for Nondestructive Examinations." E 1316 – 93b, Philadelphia, PA.

American Society of Mechanical Engineers. (1998). "Acoustic Emission Examination of Metallic Vessels During Pressure Testing." Section V, Article 12, Boiler and Pressure Vessel Code, New York, NY.

Association of American Railroads. (1999). "Procedure for Acoustic Emission Evaluation of Tank Cars and IM101 Tanks." Issue 8, October 1999, Washington, D.C.

Bray, D. E., and Stanley, R. K. (1997). "Nondestructive Evaluation: A Tool in Design, Manufacturing, and Service." Revised Edition, CRC Press, Inc., Boca Raton, FL, 181-213.

Ferber, M. K., Tennery, V. J., Waters, S. B., Ogle, J. (1986). "Fracture Strength Characterization of Tubular Ceramic Materials Using a Simple C-ring Geometry." Journal of Material Science, 21 (8), 2628 – 2632.

Fowler, T. J., Blessing, J. A., Conlisk, P. J., and Swanson, T. L. (1989). "The MONPAC System." Journal of Acoustic Emission, 8 (3).

Hamstad, M. A., Thompson, P. M., and Young, R. D. (1986). "Acoustic Emission Source Location During Four-Point Bend Tests of Alumina." Progress in Acoustic Emission III, Proceedings of The 8th International Acoustic Emission Symposium, Japanese Society for Non-Destructive Inspection, Tokyo, 26 – 33.

Jadaan, O. M., Lui, K. C., and Pih, H. (1993) "Fatigue Evaluation in Ceramic Materials By Acoustic Emission." Reliability, Stress Analysis, and Failure Prevention, DE – Vol. 55, Proceedings of the 10th Biennial Conference, Albuquerque, NM, 93 – 104.

Kahn, S., and Miller, D. (1979). "Acoustic Emission Detection: Part II – Detecting Ceramic Substrate Cracking During Thermocompression Bonding." Western Electric Engineer, New York, 15 – 19.

Lenain, J. C. (1979). "General Principles of Acoustic Emission." Technical Report DE 78-5. Dunegan/Endevco, San Juan Capistrano, CA.

Mori, Y., Nishino, M., Aoki, K., Kishi, T., Ueda, M., and Kitadate, K. (1988). "Acoustic Emission from Hot-Pressed Si_3N_4 with Artificial Defects." Progress in Acoustic Emission IV, Proceedings of The 9th International Acoustic Emission Symposium, Japanese Society for Non-Destructive Inspection, Tokyo, 615 – 620.

Shinke, N., Watanabe, Y., Nakagiri, A., and Yamano, T. (1988). "Fracture of Sintered Alumina with Artificial Defect." Progress in Acoustic Emission IV, Proceedings of The 9th International Acoustic Emission Symposium, Japanese Society for Non-Destructive Inspection, Tokyo, 621 – 626.

Timoshenko, S. (1930). "Strength of Materials: Part II Advanced Theory and Problems." Third Edition, D. Van Nostrand Company, Inc., Princeton, NJ, 205 – 210.

Timoshenko, S., and Goodier, J. N. (1970). "Theory of Elasticity." Third Edition, McGraw-Hill, New York, 83 – 86.

Wakayama, S., Koji, T., and Nishimura, H. (1990). "Microfracture Process During Bending Tests of Alumina Evaluated By Acoustic Emission." Progress in Acoustic Emission V, Proceedings of The 10th International Acoustic Emission Symposium, Japanese Society for Non-Destructive Inspection, Tokyo, 460 – 467.